

Orbital Functionals in Time-Dependent Density-Functional Theory

Von der Universität Bayreuth
zur Erlangung des Grades eines
Doktors der Naturwissenschaften (Dr. rer. nat)
genehmigte Abhandlung

von

Michael Mundt

aus Tübingen

1. Gutachter Prof. Dr. S. Kümmel
2. Gutachter Prof. Dr. Dr. h.c. P.-G. Reinhard
3. Gutachter Dr. R. van Leeuwen

Tag der Einreichung: 23. Mai 2007

Tag des Kolloquiums: 18. Juli 2007

Contents

1	Introduction	1
2	Density-functional theory (DFT)	5
2.1	Static density-functional theory	5
2.2	Time-dependent density-functional theory (TDDFT)	6
2.3	Kohn-Sham equations and related approximations	9
2.3.1	Static Kohn-Sham scheme	10
2.3.2	Time-dependent Kohn-Sham equations	12
2.3.3	Exchange-correlation (xc) approximations	14
3	DFT for fractional particle numbers	17
3.1	Ground-state theory	17
3.1.1	Formalism	17
3.1.2	Physical consequences	21
3.2	Time-dependent theory	25
3.2.1	Formalism	25
3.2.2	Physical consequences	27
3.3	Concluding remarks	30
4	The optimized effective potential (OEP)	31
4.1	Static OEP equation	31
4.1.1	Transformation to coupled differential equations	32
4.2	Time-dependent OEP equation	35
4.2.1	Transformation to coupled differential equations	36
4.2.2	Approximations to the time-dependent OEP	39
5	Numerical study of the OEP	43
5.1	Introductory remarks	43
5.2	Static OEP and Kohn-Sham equations	44
5.2.1	Solving the eigenvalue equation	45
5.2.2	Obtaining the orbital shifts	46
5.2.3	Evaluating the exchange-correlation potential	47

5.3	Time-dependent OEP and Kohn-Sham equations	49
5.3.1	Study of the coupled equations for the orbitals and orbital shifts	50
6	Exact properties of the xc potential	55
6.1	‘Harmonic-Potential theorem’	55
6.2	‘Zero-Force theorem’	58
6.3	Energy conservation and other constraints	64
7	Photoelectron spectra from Kohn-Sham DFT	67
7.1	Photoelectron spectroscopy in cluster physics	67
7.2	Theoretical background	68
7.3	Results for anionic sodium clusters	70
7.3.1	Photoelectron spectra from the exact-exchange OEP	70
7.3.2	Comparison between different theoretical approaches	72
8	Photoelectron spectra from TDDFT	77
8.1	Numerical details	78
8.2	Anionic sodium clusters	81
8.2.1	Technical aspects	81
8.2.2	Results for Na_3^-	82
8.2.3	Results for Na_5^- , Na_7^- , and Na_9^-	85
8.2.4	Conclusion	88
9	Summary and Conclusion	91
A	The density-response function on the Keldysh contour	95
B	The xc potential in terms of the orbitals and orbital shifts	99
C	Finite differencing scheme for the orbital shift’s equation-of-motion	101
	Bibliography	103
	Publications	113
	Acknowledgment	115

Abstract

The subject of this work are orbital functionals in density-functional theory (DFT). After a short introduction the basic ideas of static and time-dependent DFT are presented in Chap. 2. In this chapter the advantages and disadvantages of common approximations for the exchange-correlation (xc) functional are also discussed as well as the basic ideas behind orbital functionals.

In the first part of Chap. 3 the ground-state formalism of the DFT for fractional particle numbers is recapitulated. In the second part the concept of fractional particle numbers is extended to time-dependent situations and physical consequences are discussed. In particular, it is shown that under certain conditions the time-dependent xc potential must change discontinuously whenever the particle number crosses an integer number.

The subject of Chap. 4 is the static and time-dependent optimized effective potential equation. This integral equation must be solved to obtain the xc potential corresponding to an orbital-functional approximation for the xc functional. It is shown that the integral equation in the time-dependent case can be transformed into a set of coupled differential equations. Based on this set of differential equations an approximate solution for the xc potential is developed.

In Chap. 5 the set of coupled differential equations obtained in Chap. 4 is studied from a numerical point of view. It turns out that instabilities spoil the exact numerical solution, however, the approximation developed in Chap. 4 is found to be stable and can be used to go beyond the commonly used Krieger-Li-Iafrate (KLI) approximation.

Exact properties of the xc potential are studied in Chap. 6. In particular, it is shown that the widely used KLI approximation for the xc potential violates the ‘Zero-Force theorem’. As demonstrated in Chap. 6 this violation can render the whole approximate solution useless. In combination with the fact that the KLI approximation satisfies the ‘Harmonic-Potential theorem’ this observation also shows that the xc potential obtained from the KLI approximation is not a functional derivative of some xc functional.

In Chap. 7 and 8 the photoelectron spectra from small anionic sodium clusters are studied. In Chap. 7 the Kohn-Sham eigenvalues obtained from different approximations for the xc potential are compared to the experimental results. It is found that although the more weakly bound peaks are well reproduced in all approximations the more strongly bound peaks are not. In Chap. 8 the theoretical photoelectron spectra are extracted from the excitation energies of the clusters with one electron less. It is found that the general agreement between the experimental and theoretical spectra is considerably improved. Especially the more strongly bound parts of the spectra are reproduced much better. This result shows that even for sodium clusters effects beyond the independent-particle picture must be taken into account in the interpretation of photoelectron spectra.

Kurzfassung

Die vorliegende Arbeit beschäftigt sich mit Orbitalfunktionalen in der Dichtefunktionaltheorie (DFT). In Kap. 2 werden die Grundlagen der statischen und zeitabhängigen DFT präsentiert. Dieses Kapitel beinhaltet außerdem eine Diskussion der Vor- und Nachteile üblicher Näherungen für das Austausch-Korrelations(xc) Funktional. Des Weiteren wird in Kap. 2 die Grundidee von Orbitalfunktionalen vorgestellt.

Im ersten Teil von Kap. 3 wird das Konzept fraktionaler Teilchenzahlen in der zeitunabhängigen DFT vorgestellt. Im zweiten Teil wird das Konzept fraktionaler Teilchenzahlen auf den zeitabhängigen Fall erweitert und physikalische Konsequenzen diskutiert. Insbesondere wird gezeigt, dass unter gewissen Umständen das zeitabhängige xc Potential sich unstetig ändert, wenn die Teilchenzahl ganzzahlige Zahlen überschreitet.

Kap. 4 beschäftigt sich mit der ‘optimized effective potential’ Gleichung. Diese Integralgleichung muss gelöst werden, um das zu einem Orbitalfunktional gehörende xc Potential zu bestimmen. Es wird gezeigt, dass sich die Integralgleichung in ein gekoppeltes System von Differentialgleichungen transformieren lässt. Schließlich wird eine auf diesen Differentialgleichungen entwickelte Näherung präsentiert.

In Kap. 5 wird das in Kap. 4 hergeleitete Differentialgleichungssystem numerisch untersucht. Es stellt sich heraus, dass Instabilitäten auftreten, welche die exakte Lösung verhindern. Die in Kap. 4 entwickelte Näherung zeigt jedoch ein stabiles Verhalten und kann dazu benutzt werden, um einen Schritt weiter als die übliche Näherung von Krieger, Li und Iafrate (KLI) zu gehen.

Kap. 6 beschäftigt sich mit exakten Eigenschaften des xc Potentials. Insbesondere wird gezeigt, dass die viel genutzte KLI Näherung das ‘Zero-Force Theorem’ verletzt. Desweiteren wird gezeigt, dass dies dazu führen kann, dass die Näherung unbrauchbar wird. Die Beobachtung, dass die Näherung von KLI das ‘Harmonic-Potential Theorem’ erfüllt, jedoch das ‘Zero-Force Theorem’ verletzt, zeigt außerdem, dass das aus der KLI Näherung resultierende xc Potential keine Funktionalableitung eines xc Funktionals ist.

In Kap. 7 und 8 werden Photoelektronspektren von kleinen, anionischen Natriumclustern untersucht. In Kap. 7 werden die aus unterschiedlichen Näherungen für das xc Potential erhaltenen Kohn-Sham Eigenwerten mit den experimentellen Spektren verglichen. Es zeigt sich dabei, dass für alle Näherungen die schwächer gebundenen Peaks in den Photoelektronspektren gut reproduziert werden, die stärker gebundenen Peaks jedoch nicht. In Kap. 8 werden die theoretischen Photoelektronspektren aus den Anregungsenergien der Tochtercluster, d.h. der Cluster mit einem Elektron weniger, berechnet. Es zeigt sich dabei, dass die Übereinstimmung der theoretischen und experimentellen Spektren dadurch erheblich verbessert wird. Insbesondere die stärker gebundenen Peaks werden deutlich besser reproduziert. Dieses Ergebnis zeigt, dass es für die Interpretation von Photoelektronspektren selbst für Natriumcluster notwendig ist, Wechselwirkungseffekte mitzunehmen, die nicht durch das effektive Ein-Teilchenbild des Kohn-Sham Systems beschrieben werden.

Chapter 1

Introduction

Since the rigorous foundation by Hohenberg and Kohn in 1964 [Hoh64, Koh99] density-functional theory (DFT) has become one of the most important tools for calculating electronic properties of finite and infinite systems (see, e.g., Ref. [Dre90, Per92, Gro95]). As shown by Hohenberg and Kohn in their seminal work the electronic density of a many-particle system is sufficient for a complete description of the system, i.e., one can use the density, instead of the many-particle wavefunction, as a basic variable. In contrast to the high-dimensional wavefunction, the density depends only on three spatial coordinates. Due to this fact DFT offers access to large systems which are out of reach for wavefunction-based methods. Especially in the field of bio- and nanophysics in which large molecules consisting of several hundreds of atoms are of interest DFT offers a promising tool for theoretical investigations [Cha98, Ehr03, Ma03a].

Nowadays, typical quantities which can be reliably obtained from static DFT calculations are ground-state energies, densities, geometries, vibrational frequencies,...

Although, in principle, it is also possible to obtain excitation energies from static DFT, in practice these energies must be extracted from time-dependent DFT (see, e.g., Ref. [Gro96]). Based on the Runge-Gross theorem proved in 1984 [Run84] time-dependent DFT is a generalization of static DFT to the time domain, i.e., it allows to describe time-dependent processes in terms of the time-dependent density. In addition to being applicable to systems containing many electrons, time-dependent DFT also provides access to non-perturbative, non-linear effects like high-harmonic generation and above-threshold ionization on a first-principle basis [Gav92, Gro96, Poh03]. In general, the theoretical description of such effects requires the solution of the time-dependent, interacting Schrödinger equation. Since the solution of this equation is already beyond the capability of modern supercomputers for three electrons, time-dependent DFT is a natural candidate for the description of such phenomena.

The majority of DFT calculations is done in the Kohn-Sham scheme of DFT [Koh65]. In this scheme the interacting system is replaced by a system of non-interacting particles moving in a local potential. This potential is chosen in such a way that the density of

the non-interacting and the interacting system are identical. Commonly, this potential is separated into the external potential of the interacting system, the Hartree potential containing the classical electrostatic interaction, and the unknown exchange-correlation potential which contains all non-classical effects. Since the exact exchange-correlation potential is in general not known, approximations for it are required. In fact, having reliable approximations for this potential is of crucial importance for any Kohn-Sham DFT calculation and much research is devoted to this subject [Per98, Bec97, Gra00]. In particular, knowing as many exact properties of the true exchange-correlation potential as possible is extremely useful since this provides guidelines for the construction of approximate exchange-correlation potentials [Hes99, Per98].

At present, most approximations use the density and gradients thereof to construct approximations to the exchange-correlation potential. The best-known representatives of this class of approximations are the local-density approximation and the generalized-gradient approximation of Perdew *et al.* [Hoh64, Cep80, Per81, Per96]. Since these functionals suffer from several drawbacks, using a different class of functionals (named orbital functionals) is desirable [Gra00]. Instead of using the density and its gradients directly, these functionals use the Kohn-Sham orbitals, i.e., the orbitals from the non-interacting Kohn-Sham system, to construct approximations for the exchange-correlation potential. Since these orbitals are implicit functionals of the density, the resulting approximations are also legitimate density functionals. In static DFT orbital functionals have already been used successfully to calculate the static response of hydrogen chains to an electrical field [Kü04a]. The fact that functionals based directly on the density and its gradients fail completely in this situation clearly demonstrates how promising orbital functionals are.

In terms of applications DFT has been extensively used in the field of cluster physics, in particular for the description of sodium clusters (see, e.g., Ref. [Rei03] for an overview). Roughly speaking clusters are an aggregation of matter containing between a few and several thousand atoms or molecules. Of particular interest in cluster physics are the determination of the ionic structures of clusters which are governed by geometric and electronic finite size effects, e.g., electronic shell effects [Kni84]. In many cases the only method to reveal these structures is to combine photoelectron spectroscopy with theoretically predicted photoelectron spectra obtained from different ionic structures [Kie96, Kos07]. Clearly, this procedure crucially depends on the reliability of the theoretically obtainable photoelectron spectra. Since the overwhelming majority of clusters is too large to be described by quantum-chemical methods, density-functional theory is in many cases the only first-principle approach available. Therefore, developing methods for reliably extracting photoelectron spectra from a DFT calculation is highly desirable.

The present work deals with these aspects of DFT. Rather than being dedicated exclusively to one topic, it covers subjects ranging from fundamental considerations to applications in cluster physics, namely photoelectron spectra of anionic sodium clus-

ters. Roughly it can be divided into two parts; the first mainly covers fundamental aspects (Chap. 2 - Chap. 6) and the second discusses the results for anionic sodium clusters (Chap. 7 - Chap. 8). The two basic theorems, i.e., the Hohenberg-Kohn and the Runge-Gross theorem, are presented together with the Kohn-Sham scheme and the exchange-correlation potential in Chap. 2. As mentioned above this potential is of crucial importance for Kohn-Sham DFT and in general an exact expression for it is not known. Thus, it must be approximated. In Chap. 3 the influence of the particle number on the exact exchange-correlation potential is investigated in the framework of fractional particle-number DFT. Physical implications of the findings on systems with constant, integer particle number are also discussed in this chapter. In Chap. 4 the optimized effective potential equation is presented. This integral equation must be solved to obtain the exchange-correlation potential resulting from an orbital functional. As shown in Chap. 4 it is possible to transform this integral equation into a set of coupled differential equations. These equations offer a promising solution scheme for time-dependent situations in which solving the integral equation directly is out of reach at present. In Chap. 5 this solution scheme is investigated from a numerical point of view. After this chapter the first part is closed by Chap. 6. There, several properties of the exact exchange-correlation potential are presented. In addition, it is studied which approximations have these desired properties. In the last two chapters two different approaches to obtain photoelectron spectra from DFT calculations are investigated. Both approaches are compared to experimental photoelectron spectra of anionic sodium clusters and to each other. Finally, a summary and conclusion is provided in Chap. 9.

Chapter 2

Density-functional theory (DFT)

In this chapter the basic ideas of DFT are presented. It is pointed out that two things are crucial for a successful DFT description: a reliable approximation for the energy/action of a system in terms of the density *and* for the observables of interest. In addition, the Kohn-Sham scheme is presented which is the basis of orbital functionals. The latter are one of the main topics of this work.

2.1 Static density-functional theory

The original idea of DFT is to describe the electrons in a many-particle system in terms of the one-particle electron density $n(\mathbf{r})$ instead of a many-particle wavefunction. In static DFT this is possible due to the celebrated theorem proven by Hohenberg and Kohn in 1964 [Hoh64] for non-relativistic, spin-saturated systems with non-degenerate ground states (see, e.g., [Dre90] and references therein for extensions). This theorem, called the Hohenberg-Kohn theorem, states that for a given particle-particle interaction $W(\mathbf{r}, \mathbf{r}')$ a one-to-one mapping between the one-particle ground-state density and the local external potential $v(\mathbf{r})$ exists¹. In other words, a given ground-state density determines the external potential and, as a consequence, the Hamiltonian $\hat{H} = \hat{T} + \hat{W} + \hat{V}$ of the system (where $\hat{T} = \sum_j \frac{\hat{p}_j^2}{2m}$, $\hat{V} = \sum_j v(\hat{r}_j)$, $\hat{W} = \sum_{j \neq k} w(\hat{r}_j, \hat{r}_k)$, and the indices j, k run over all particles). Since, at least in principle, it is possible to extract any information about the system from its Hamiltonian via the stationary Schrödinger equation

$$\hat{H} |\psi_j\rangle = E_j |\psi_j\rangle, \quad (2.1)$$

the ground-state density itself provides access to all information. Thus, any observable is a functional of the density, in particular the ground state $|\psi_0\rangle = |\psi_0[n]\rangle$. Furthermore, Hohenberg and Kohn have proven that a universal functional $F[n] = \langle \psi_0 | \hat{T} + \hat{W} | \psi_0 \rangle$

¹To be precise the external potential is only determined up to a constant which has no physical consequences.

exists which via minimization of the total energy,

$$E[n] = F[n] + \int v(\mathbf{r}) n(\mathbf{r}) d^3r , \quad (2.2)$$

leads to the exact ground-state density corresponding to the given external potential $v(\mathbf{r})$. In other words, knowing the functional $F[n]$ allows one to obtain the ground-state density of a system via the variational equation

$$\frac{\delta E[n]}{\delta n(\mathbf{r})} = 0 . \quad (2.3)$$

The huge advantage of this method is obvious: instead of working with a wavefunction depending on 3^N coordinates, one only has to work with the density depending on three spatial coordinates. However, since the exact functional $F[n]$ is not known for an interacting N -particle system, the success of a DFT calculation crucially depends on the approximations available for $F[n]$. In Sec. 2.3 this aspect is discussed in detail.

2.2 Time-dependent density-functional theory (TDDFT)

The basis of time-dependent DFT is provided by the Runge-Gross theorem [Run84]. This theorem states that for a given initial state and particle-particle interaction $W(\mathbf{r}, \mathbf{r}')$, a one-to-one map between the one-particle density $n(\mathbf{r}, t)$ and the time-dependent external potential $v(\mathbf{r}, t)$ exists (this time up to a purely time-dependent function $c(t)$). Thus, in principle, every observable is known if one knows the exact time-dependent density and the initial state $|\psi(t_0)\rangle$ at time t_0 . As a consequence, any observable is not only a functional of the density as in static DFT, but also a functional of the initial state. Fortunately, the dependence on the initial state vanishes in many situations, namely those in which the initial state is a non-degenerated ground state. In this case the initial state itself is a functional of the density via the Hohenberg-Kohn theorem of static DFT. Thus, every observable is again a ‘pure’ density functional. A detailed discussion of this and other aspects of time-dependent DFT can be found in the review article of Gross *et al.* [Gro96].

In order to obtain a practical scheme for the description of time-dependent processes within DFT it is necessary to determine the correct density corresponding to a given time-dependent external potential without solving the time-dependent Schrödinger equation

$$i\hbar\partial_t |\psi(t)\rangle = \hat{H}(t) |\psi(t)\rangle \quad (2.4)$$

for the state $|\psi(t)\rangle$. In static DFT the density of interest can be calculated by approximating the functional $F[n]$ and subsequently minimizing the resulting energy expression. Since in a time-dependent case no energy minimization exists, one has to find a different

method to obtain the time-dependent density. One such method has been proposed by Runge and Gross [Run84]. They put forward the variational principle

$$\delta A = \delta \int_{t_0}^{t_1} \langle \psi[n](t) | i\hbar\partial_t - \hat{H}(t) | \psi[n](t) \rangle dt = 0 \quad (2.5)$$

to obtain the time-dependent density. However, this procedure suffers from serious problems as shown in [Lee98, Lee01] and explained in detail in the following.

To understand why the variational principle 2.5 cannot be used in the framework of time-dependent DFT one has to recall how the time-dependent Schrödinger equation can be derived from Eq. (2.5). Usually a partial integration is used to obtain

$$\delta A = \int_{t_0}^{t_1} \langle \delta\psi(t) | i\hbar\partial_t - \hat{H}(t) | \psi(t) \rangle + c.c. dt + [i\hbar \langle \psi(t) | \delta\psi(t) \rangle]_{t_0}^{t_1}. \quad (2.6)$$

Imposing the boundary condition $\delta\psi(t_1) = \delta\psi(t_0) = 0$ leads to

$$\delta A = 2 \operatorname{Re} \int_{t_0}^{t_1} \langle \delta\psi(t) | i\hbar\partial_t - \hat{H}(t) | \psi(t) \rangle dt. \quad (2.7)$$

Writing $\delta\psi = \delta\psi_1 + i\delta\psi_2$ (with $\delta\psi_j$ real-valued) and using $\operatorname{Re}(iz) = -\operatorname{Im}(z)$, one obtains

$$\begin{aligned} \delta A &= 2 \operatorname{Re} \int_{t_0}^{t_1} \langle \delta\psi_1(t) | i\hbar\partial_t - \hat{H}(t) | \psi(t) \rangle dt \\ &\quad - 2 \operatorname{Im} \int_{t_0}^{t_1} \langle \delta\psi_2(t) | i\hbar\partial_t - \hat{H}(t) | \psi(t) \rangle dt = 0. \end{aligned} \quad (2.8)$$

An independent variation of $\delta\psi_1$ and $\delta\psi_2$ shows that both the imaginary and the real part of $(i\hbar\partial_t - \hat{H}(t)) | \psi(t) \rangle$ must vanish, i.e., the time-dependent Schrödinger equation must hold.

In addition to this derivation a second way to obtain the time-dependent Schrödinger equation from the action principle 2.5 exists [Löw72]. Combining the general relation

$$\delta A = \int_{t_0}^{t_1} \langle \delta\psi(t) | i\hbar\partial_t - \hat{H}(t) | \psi(t) \rangle dt + \int_{t_0}^{t_1} \langle \psi(t) | i\hbar\partial_t - \hat{H}(t) | \delta\psi(t) \rangle dt = 0 \quad (2.9)$$

with the variations $\delta\psi(t) = \delta\phi(t)$ and $\delta\psi(t) = i\delta\phi(t)$, one obtains the equations

$$\delta A = \int_{t_0}^{t_1} \langle \delta\phi(t) | i\hbar\partial_t - \hat{H}(t) | \psi(t) \rangle dt + \int_{t_0}^{t_1} \langle \psi(t) | i\hbar\partial_t - \hat{H}(t) | \delta\phi(t) \rangle dt = 0 \quad (2.10)$$

and

$$\delta A = -i \int_{t_0}^{t_1} \langle \delta\phi(t) | i\hbar\partial_t - \hat{H}(t) | \psi(t) \rangle dt + i \int_{t_0}^{t_1} \langle \psi(t) | i\hbar\partial_t - \hat{H}(t) | \delta\phi(t) \rangle dt = 0. \quad (2.11)$$

From these equations one obtains

$$\int_{t_0}^{t_1} \langle \delta\phi(t) | i\hbar\partial_t - \hat{H}(t) | \psi(t) \rangle dt = 0 \quad (2.12)$$

and thus the time-dependent Schrödinger equation

$$(i\hbar\partial_t - \hat{H}(t)) |\psi(t)\rangle = 0. \quad (2.13)$$

In the framework of time-dependent DFT both methods are not applicable since the allowed density variations are restricted to ‘ v -representable’ densities, i.e., densities obtained from wavefunctions satisfying the time-dependent Schrödinger equation. In other words, all variations δn must be obtained from variations $\delta\psi$ satisfying the time-dependent Schrödinger equation. For such variations the second boundary term cannot vanish if the first one is zero. This is a direct consequence of the fact that the time-dependent Schrödinger equation is of first order in time. Additionally, shifting the second boundary to infinity and introducing a convergence factor $\lim_{\eta \rightarrow 0^+} \exp(-\eta(t - t_0))$ does not cure the problem since this leads to an additional term of the form

$$\lim_{\eta \rightarrow 0^+} \eta \int_{t_0}^{\infty} \exp(-\eta(t - t_0)) \langle \psi(t) | \delta\psi(t) \rangle dt \quad (2.14)$$

which generally does not need to vanish. Therefore, the first method to obtain the time-dependent Schrödinger equation from Eq. (2.5) does not work in the framework of time-dependent DFT. The second method to obtain the time-dependent Schrödinger equation also does not work since the variation $i\delta\psi$ can only be produced by a potential change $i\delta v$. Here, δv is the potential change that leads to $\delta\psi$. However, the potential variation $i\delta v$ is not allowed since the potential must be real. Thus, both ways to obtain the time-dependent Schrödinger equation from the Runge-Gross action, Eq. (2.5), are not applicable in the framework of DFT and, as a consequence, the Runge-Gross action cannot be used to obtain the time-dependent density in a DFT calculation.

To avoid the problems in conjunction with the Runge-Gross action a different action functional has been proposed by van Leeuwen [Lee98]. This functional is defined on the Keldysh contour which is known from the theory of non-equilibrium Green’s functions [Kel65, Dan84]. For the present work only the main idea behind the Keldysh formalism is important, namely the parameterization of the physical time t by a parameter τ which is called pseudotime. This parameterization is done in such a way that for τ running from τ_i to τ_f the physical time t runs from t_0 to \tilde{t} and back to t_0 . The detailed parameterization is not important since all physical results are independent of it. The only requirement is that \tilde{t} must be chosen later than any time t at which physical quantities are calculated. The equation-of-motion for any state on the Keldysh contour is given by

$$i\hbar t'(\tau)^{-1} \partial_\tau |\psi(\tau)\rangle = \hat{H}(\tau) |\psi(\tau)\rangle \quad (2.15)$$

with $\hat{H}(\tau) = \hat{T} + \hat{W} + \hat{v}(\tau)$ being the Hamiltonian consisting of the kinetic part, the particle-particle interaction and the time-dependent local external potential on the contour. The van Leeuwen action functional is defined as

$$A[n] = -\tilde{A}[v] + \int \int_C n(\mathbf{r}, \tau) v(\mathbf{r}, \tau) dt d^3r \quad (2.16)$$

where $\tilde{A}[v] = i\hbar \ln [\langle \psi_0 | T_C \exp(-i \int_C \hat{H}(\tau) dt / \hbar) | \psi_0 \rangle]$ and $\int_C dt = \int_{\tau_i}^{\tau_f} t'(\tau) d\tau$ (with $t'(\tau) = dt(\tau)/d\tau$) denoting integration on the Keldysh time contour [Lee98, Lee05]. T_C is the time-ordering operator on this contour. In the context of DFT one of the main advantages of the Keldysh formalism is that it allows to construct causal response functions from functional derivatives which are not causal (see Appendix A) and that the relation

$$\frac{\delta A[n]}{\delta n(\mathbf{r}, \tau)} = v(\mathbf{r}, \tau) \quad (2.17)$$

holds [Lee01]. This relation plays a crucial role in the next section where it is used to construct a practical scheme to compute the time-dependent density from the action (2.16).

2.3 Kohn-Sham equations and related approximations

The previous section shows that two ingredients are necessary to have a practical advantage from using DFT. First, a good approximation for the functional $F[n]$ (or $A[n]$) is needed to obtain an accurate density. Second, a good approximation for the functional connecting the density to the observables of interest must be found. It is clear that the first problem is of crucial importance for the second since it determines the density which must be used in the functional for the observable of interest. One way to approximate the functional $F[n]$ is based on a direct approximation of $\langle \psi_0 | \hat{T} + \hat{W} | \psi_0 \rangle$ in terms of the density. The Thomas-Fermi model is an example for this approach (other examples can be found in, e.g., [Dre90]). The most appealing feature of this approach is that it is independent of the particle number, i.e., one has to solve the same equations no matter how many particles are in the system. Unfortunately, this approach has a serious drawback: approximating $\langle \psi_0 | \hat{T} + \hat{W} | \psi_0 \rangle$ accurately in terms of the density is highly non-trivial [Koh65, Dre90]. In particular, approximating the kinetic energy part is extremely difficult.

In most DFT calculations this problem is circumvented by using the Kohn-Sham equations [Koh65] which are presented in the following subsections. The main idea behind the Kohn-Sham scheme is to use the kinetic energy expression for non-interacting particles and absorb the difference between the non-interacting and the interacting kinetic energy in an additional external potential. This procedure corresponds to replacing the interacting system by a system of non-interacting particles which move in an effective potential. This effective potential is chosen in such a way that the resulting density

is the *same* density as in the interacting system. One advantage of this approach is its capability to reproduce the atomic shell structure (due to the explicit treatment of the kinetic energy) [Koh65] which is missing in the Thomas-Fermi model. Furthermore, the Kohn-Sham scheme provides a starting point for perturbation expansions of the exact energy [Gör93, Lee96, Gör97, Bon01, Gra02, Ba05b]. For later applications the following equations will be formulated for spin-polarized systems [Bar72, Dre90]. The basic variables in this case are the two spin densities n_σ ($\sigma = \uparrow, \downarrow$). For notational simplicity functionals will nevertheless be written in the form $O[n]$ instead $O[n_\uparrow, n_\downarrow]$.

2.3.1 Static Kohn-Sham scheme

As mentioned above the main idea behind the Kohn-Sham method is to replace the interacting kinetic energy by the kinetic energy expression for non-interacting particles. Additionally, the classical electrostatic energy of the density is used in the energy functional, i.e., the total energy is written in the form

$$E[n] = T_S[n] + \underbrace{\int n(\mathbf{r}) v(\mathbf{r}) d^3r}_{E_{\text{ext}}} + \underbrace{\frac{1}{2} \int \int n(\mathbf{r}) W(\mathbf{r}, \mathbf{r}') n(\mathbf{r}') d^3r' d^3r}_{E_H} + E_{\text{xc}}[n]. \quad (2.18)$$

Here, E_{ext} is the energy contribution from the external potential and E_H , called the Hartree energy, is the classical electrostatic energy. T_S is the kinetic energy of a non-interacting system with the density n . Combining Eq. (2.18) and Eq. (2.2) shows that the energy contribution $E_{\text{xc}}[n]$, called the exchange-correlation energy, is *defined* as

$$E_{\text{xc}}[n] := F[n] - \frac{1}{2} \int \int n(\mathbf{r}) W(\mathbf{r}, \mathbf{r}') n(\mathbf{r}') d^3r' d^3r - T_S[n]. \quad (2.19)$$

This definition explicitly shows that the main problem of a DFT calculation, namely the missing knowledge of the functional $F[n]$, is not solved in Eq. (2.18), but shifted to the unknown functional $E_{\text{xc}}[n]$. However, since for many systems $T_S + E_H + E_{\text{ext}}$ is already a reasonable approximation for the total energy of the system, the splitting in Eq. (2.18) provides a good starting point for constructing accurate approximations for the total energy. As shown below neglecting $E_{\text{xc}}[n]$ completely leads to the well-known Hartree theory. Thus, even the most simple approximation based on Eq. (2.18) leads to results which are significantly superior to the results known from direct approximations of the functional $F[n]$, e.g., the Thomas-Fermi approximation.

In connection with Eq. (2.18) the question arises how T_S can be calculated. As mentioned previously T_S is the kinetic energy of a non-interacting N -particle system ($N = N_\uparrow + N_\downarrow$) which has the same ground-state density as the interacting N -particle system. Supposing the external potential v_S which leads to the ground-state density n in the non-interacting system exists [Dre90, Lee03], the kinetic energy T_S can be obtained

from

$$T_S[n] = \sum_{\substack{j=1 \\ \sigma=\uparrow,\downarrow}}^{N_\sigma} \int \varphi_{j\sigma}^*(\mathbf{r}) \left(-\frac{\hbar^2}{2m} \nabla^2 \right) \varphi_{j\sigma}(\mathbf{r}) d^3r \quad (2.20)$$

where the orbitals $\varphi_{j\sigma}$, known as the Kohn-Sham orbitals, are the N_σ lowest eigenfunctions of the one-particle Kohn-Sham Hamiltonian

$$\left(\underbrace{-\frac{\hbar^2}{2m} \nabla^2 + v_{S\sigma}(\mathbf{r})}_{h_{S\sigma}(\mathbf{r})} \right) \varphi_{j\sigma}(\mathbf{r}) = \epsilon_{j\sigma} \varphi_{j\sigma}(\mathbf{r}) \quad , \quad j = 1, \dots, N_\sigma . \quad (2.21)$$

The density of the system is given by

$$n_\sigma(\mathbf{r}) = \sum_{j=1}^{N_\sigma} |\varphi_{j\sigma}(\mathbf{r})|^2 \quad \text{and} \quad n(\mathbf{r}) = \sum_{\sigma=\uparrow,\downarrow} n_\sigma(\mathbf{r}) . \quad (2.22)$$

Thus, knowing the potential v_S , called the Kohn-Sham potential, allows one to calculate the ground-state density n and the kinetic energy T_S in a straightforward manner. It is important to note that since the Hohenberg-Kohn theorem also holds for a non-interacting system, the Kohn-Sham potential is uniquely defined up to an irrelevant constant. In other words, a one-to-one map between the density and the Kohn-Sham potential exists. Consequently, the Kohn-Sham orbitals are also determined by the density because they are uniquely connected to the Kohn-Sham potential via the Kohn-Sham equations. Thus, the Kohn-Sham orbitals are functionals of the density, i.e., $\varphi_{j\sigma} = \varphi_{j\sigma}[n]$. This fact shows that $T_S[n]$ is a legitimate density functional. Furthermore, this observation is the basis for the concept of orbital functionals (see below).

To obtain the Kohn-Sham potential the functional derivative of Eq. (2.18) with respect to the density n_σ is calculated. The result is

$$\frac{\delta E}{\delta n_\sigma(\mathbf{r})} = \frac{\delta T_S}{\delta n_\sigma(\mathbf{r})} + v(\mathbf{r}) + \underbrace{\int W(\mathbf{r}, \mathbf{r}') n(\mathbf{r}') d^3r'}_{v_H(\mathbf{r})} + \underbrace{\frac{\delta E_{xc}}{\delta n_\sigma(\mathbf{r})}}_{v_{xc\sigma}(\mathbf{r})} . \quad (2.23)$$

The functional derivative $\delta T_S / \delta n_\sigma$ can be calculated via

$$\begin{aligned} \delta T_S &= \sum_{j=1}^{N_\sigma} \int \delta \varphi_{j\sigma}^*(\mathbf{r}) \left(-\frac{\hbar^2}{2m} \nabla^2 \right) \varphi_{j\sigma}(\mathbf{r}) + c.c. d^3r \\ &= \sum_{j=1}^{N_\sigma} \int \delta \varphi_{j\sigma}^*(\mathbf{r}) (\epsilon_{j\sigma} - v_S(\mathbf{r})) \varphi_{j\sigma}(\mathbf{r}) + c.c. d^3r \\ &= \sum_{j=1}^{N_\sigma} \epsilon_{j\sigma} \int \delta \varphi_{j\sigma}^*(\mathbf{r}) \varphi_{j\sigma}(\mathbf{r}) + c.c. d^3r - \int v_S(\mathbf{r}) \delta n_\sigma(\mathbf{r}) d^3r . \end{aligned} \quad (2.24)$$

For norm-conserving variations the first term vanishes and Eq. (2.23) in combination with Eq. (2.3) shows that

$$v_{S\sigma}(\mathbf{r}) = v_H(\mathbf{r}) + v(\mathbf{r}) + v_{xc\sigma}(\mathbf{r}) . \quad (2.25)$$

must hold. This expression shows that the Kohn-Sham potential v_S depends on the density. On the other hand, the density depends on the Kohn-Sham potential via the Kohn-Sham equations, Eqs. (2.21). As a consequence, the ground-state density must be determined in a self-consistent way from Eq. (2.25) and Eqs. (2.21). This can be done in an iterative procedure. After an initial guess for the density one constructs the Kohn-Sham potential via Eq. (2.25). With this potential a new density is obtained from the solutions of the Kohn-Sham equations. Then a new potential is constructed which leads to a new density. These steps are repeated until convergence is achieved. Since the Kohn-Sham equations are one-particle equations, i.e., they only depend on three space coordinates, this procedure can be carried out very efficiently on a computer.

Finally, one last aspect of the Kohn-Sham scheme must be discussed. From Eq. (2.18) it is clear that the unknown functional $E_{xc}[n]$ is the central quantity in any Kohn-Sham calculation. Neglecting this energy contribution leads to the well-known Hartree theory as one can see from Eq. (2.25). Thus, in order to go beyond the Hartree theory it is crucial to have good approximations for $E_{xc}[n]$. Due to the outstanding importance of $E_{xc}[n]$ for all static Kohn-Sham DFT calculations the last subsection of this chapter is devoted to discussing approximations for this functional.

2.3.2 Time-dependent Kohn-Sham equations

The Kohn-Sham formalism for time-dependent systems is based on the same idea as in static DFT: the interacting system is replaced by a fictitious system of non-interacting particles moving in a, now time-dependent, Kohn-Sham potential $v_{S\sigma}(\mathbf{r}, t)$. This potential is again determined by the requirement that both systems, the interacting and the non-interacting one, have the same density. The existence of such a potential can be proved under mild restrictions [Lee99]. The time evolution of the non-interacting system is determined by the time-dependent Schrödinger equation

$$i\hbar\partial_t \varphi_{j\sigma}(\mathbf{r}, t) = h_{S\sigma}(\mathbf{r}, t) \varphi_{j\sigma}(\mathbf{r}, t) \quad , \quad j = 1, \dots, N_\sigma . \quad (2.26)$$

The time-dependent density is obtained via Eq. (2.22), but with time-dependent orbitals. As in the static case the Kohn-Sham potential and all Kohn-Sham orbitals are unique functionals of the density (this time due to the Runge-Gross theorem).

To derive an expression for the Kohn-Sham potential one defines the action of the non-interacting Kohn-Sham system. In analogy to Eq. (2.16) one obtains

$$A_S[n] = -\tilde{A}_S[v_S] + \sum_{\sigma=\uparrow,\downarrow} \int \int_C n_\sigma(\mathbf{r}, \tau) v_{S\sigma}(\mathbf{r}, \tau) dt d^3r \quad (2.27)$$

where

$$\tilde{A}_S[v_S] = i\hbar \ln [\langle \Phi_0 | U(\tau_f, \tau_i) | \Phi_0 \rangle] \quad (2.28)$$

and

$$\begin{aligned} U(\tau_f, \tau_i) &= T_C \exp \left(-i \int_C \hat{h}_S(\tau) dt / \hbar \right) \\ \hat{h}_S(\tau) &= \hat{T} + \hat{v}_S(\tau) \end{aligned}$$

is used. $|\Phi_0\rangle$ is the initial Kohn-Sham Slater determinant. Based on these quantities one can define the exchange-correlation part $A_{xc}[n]$ by

$$A[n] = A_S[n] - A_{xc}[n] - \frac{1}{2} \int \int \int_C n(\mathbf{r}, \tau) W(\mathbf{r}, \mathbf{r}') n(\mathbf{r}', \tau) dt d^3 r' d^3 r . \quad (2.29)$$

Taking the functional derivative of this expression one obtains

$$v(\mathbf{r}, \tau) = v_{S\sigma}(\mathbf{r}, \tau) - v_{xc\sigma}(\mathbf{r}, \tau) - v_H(\mathbf{r}, \tau) \quad (2.30)$$

where Eq. (2.17) has been applied to the action of the interacting and non-interacting system. $v_{xc\sigma}(\mathbf{r}, \tau) = \delta A_{xc} / \delta n_\sigma(\mathbf{r}, \tau)$ is the exchange-correlation potential and

$$v_H(\mathbf{r}, \tau) = \int W(\mathbf{r}, \mathbf{r}') n(\mathbf{r}', \tau) d^3 r' \quad (2.31)$$

is the Hartree potential. Thus, by construction, the Kohn-Sham potential reproduces the density of the interacting system if $v_{S\sigma}(\mathbf{r}, \tau) = v_H(\mathbf{r}, \tau) + v(\mathbf{r}, \tau) + v_{xc\sigma}(\mathbf{r}, \tau)$ holds. Taking the derivatives at the physical time-dependent density, one can transform to physical time and one obtains the time-dependent Kohn-Sham equations with the Hamiltonian

$$h_{S\sigma}(\mathbf{r}, t) = -\frac{\hbar^2}{2m} \nabla^2 + v_H(\mathbf{r}, t) + v(\mathbf{r}, t) + v_{xc\sigma}(\mathbf{r}, t) . \quad (2.32)$$

As in static Kohn-Sham DFT only the exchange-correlation part of the action functional must be approximated. Existing approximations for it are discussed below together with approximations for $E_{xc}[n]$.

At this point it is worth noting that, in principle, it is not necessary to introduce any action functional or variational principle for the exchange-correlation potential. The Kohn-Sham potential is uniquely defined by the condition that the non-interacting system has the same density as the interacting system. Subtracting from the Kohn-Sham potential the Hartree potential and the external potential of the interacting system leads to the exchange-correlation potential without invoking any action functional or variational principle. Nevertheless it is useful to work with an action principle for, at least, two reasons. First, as one can see from this section, the action principle provides an elegant derivation of the Kohn-Sham equations. Second and more important, it provides a systematic way to derive approximations for $v_{xc\sigma}(\mathbf{r}, t)$ [Lee96, Lee98]. Especially, approximating the action functional offers an elegant way to construct exchange-correlation

potentials which satisfy many exact constraints and fundamental conservation laws. For instance, momentum conservation is guaranteed if the exchange-correlation potential is derived from an action functional which is invariant under space translations. This is discussed in detail in Chap. 6. Moreover, Chap. 6 contains an example for an exchange-correlation potential which is not the functional derivative of some action functional, namely the time-dependent Krieger-Li-Iafrate potential.

2.3.3 Exchange-correlation (xc) approximations

Having established the basic formalism of Kohn-Sham DFT, it is now necessary to discuss approximations for the exchange-correlation functionals E_{xc} and A_{xc} . The oldest approximations for the exchange-correlation energy are explicit functionals of the density, i.e., only the density is used in these approximations. The most well-known example for such an explicit density functional is the local-density approximation (LDA) which is based on the homogenous electron gas [Koh65]. For this system the ground-state energy density $e^{\text{hom}}(n)$ can be obtained with high accuracy as a function of the constant density n [Cep80]. To approximate E_{xc} for an arbitrary system the resulting function is used in combination with a spatially varying density $n(\mathbf{r})$, i.e., $e^{\text{LDA}}[n(\mathbf{r})] := e^{\text{hom}}(n)|_{n \rightarrow n(\mathbf{r})}$. This approximation works surprisingly well even for non-homogenous systems as discussed, e.g., in [Dre90]. Improvements can be obtained by the inclusion of gradient terms of the density. This leads to the ‘generalized gradient approximations’ (GGAs) which are explicit functionals of the density and the gradients thereof [Pe85a, Bec88, Lee88, Per96, Per98]. For completeness, another class of functionals should be mentioned, namely ‘hybrid’ functionals. These functionals are outside the Kohn-Sham scheme since they mix a fractional amount of the Hartree-Fock exact-exchange energy to the total energy of the system [Bec92, Bec97].

For time-dependent DFT the most frequently used approximation is the adiabatic LDA/GGA [And77, Peu78, Zan80]. This approximation is obtained by using the static LDA/GGA functional in combination with the time-dependent density. Thus, these approximations are also explicit density functionals. The action is given in this case by

$$A_{xc}^{\text{LDA/GGA}} = \int_C E_{xc}^{\text{LDA/GGA}}[n(\mathbf{r}, \tau)] dt . \quad (2.33)$$

In addition to the approximations already present in the static case the adiabatic LDA also neglects any memory effects, i.e., the exchange-correlation potential $v_{xc}(\mathbf{r}, t)$ resulting from Eq. (2.33) depends only on the density at time t and not at prior times $t' < t$. This is in contrast to the exact exchange-correlation potential which depends on the density at all former times [Ma02a].

In general, the main advantages of the static and time-dependent LDA/GGA are its extreme efficiency (systems with up to 600 electrons can be treated [Kro06]) and the satisfaction of many constraints of the exact exchange-correlation potential (see Chap. 6). However, the LDA/GGA also has serious problems:

- The Hartree energy contains a contribution coming from the interaction of each electron with itself. This self-interaction contribution is canceled by the exact exchange-correlation energy, but not by the LDA/GGA exchange-correlation energy. This can be most easily seen in the case of a hydrogen atom in which the exact exchange-correlation potential must be equal to the Hartree potential. In general, the self-interaction error is particularly problematic in situations involving strongly localized electrons since it prevents a strong localization. This can lead to a completely wrong description of a system, e.g., an insulator predicted to be metallic [Sva90].
- Instead of the $-1/r$ asymptotic behavior of the exact exchange-correlation potential [Alm85], the LDA/GGA potential falls off exponentially. As a result ionization potentials and ionization dynamics are wrong, no Rydberg series are observed, . . .
- Charge-transfer excitations are severely underestimated [Toz03].
- The adiabatic LDA yields only single excitations due to the missing memory effects, i.e., the missing dependence on the density at former times. Excited states with double excitation character cannot be obtained without including memory effects [Mai04].
- In the framework of fractional particle-number DFT (Chap. 3) the LDA/GGA exchange-correlation potential does not show a discontinuous behavior with particle number changes [Pe82a]. This can lead, e.g., to non-integer particle numbers for two atoms separated by a large distance.

In order to solve these problems orbital functionals are a promising concept. In this class of functionals the quantity of interest is not expressed explicitly in terms of the density and the gradients thereof, but in terms of the Kohn-Sham orbitals. Since these orbitals, as discussed above, are themselves functionals of the density, any explicit functional of the Kohn-Sham orbitals is an implicit density functional. The most simple orbital functional for the exchange-correlation energy is the exact-exchange functional

$$E_x[\{\varphi_{i\tau}[n]\}] = -\frac{e^2}{2} \sum_{\substack{j,k=1 \\ \sigma=\uparrow,\downarrow}}^{N_\sigma} \int \int \frac{\varphi_{j\sigma}^*(\mathbf{r})\varphi_{j\sigma}(\mathbf{r}')\varphi_{k\sigma}^*(\mathbf{r}')\varphi_{k\sigma}(\mathbf{r})}{|\mathbf{r}-\mathbf{r}'|} d^3r' d^3r. \quad (2.34)$$

It is important to note that the orbitals in this expression are the Kohn-Sham orbitals and *not* the Hartree-Fock orbitals. In contrast to the Hartree-Fock orbitals, the Kohn-Sham orbitals must be obtained from the local and orbital-independent Kohn-Sham potential. The main advantages of orbital functionals are:

- Using the exact-exchange functional cures the Hartree self-interaction error and thus, one of the main deficiencies of explicit density functionals.

- The exchange potential resulting from the exact-exchange functional, Eq. (2.34), has the correct $-1/r$ asymptotic behavior [Tal76]. As a consequence, much improved ionization potentials and Rydberg series are found.
- Since the Kohn-Sham orbitals at time t depend on the densities at all prior times $t' \leq t$ [Ma02a], orbital functionals include memory effects.
- Perturbation expansions of the exact energy in terms of the Kohn-Sham orbitals exist [Gör94, Lee96, Lee98].
- The exchange-correlation potential resulting from an orbital functional can show a discontinuous behavior under particle number changes [Kr92a, Mun05].

However, orbital functionals also have a serious drawback. For these functionals the construction of the Kohn-Sham potential is much more involved than for explicit density functionals since $\delta E_{xc}/\delta n$ cannot be evaluated analytically. Instead, one has to solve an integral equation for the potential [Sha53, Ull95]. As shown in Chap. 4 solving this equation (called the optimized effective potential equation) is not a trivial task.

Chapter 3

DFT for fractional particle numbers

In Chap. 2 the importance of the exchange-correlation potential v_{xc} for the success of any DFT calculation has been pointed out. Although ever more refined approximations have been developed and tested [Mar01], the existing approximations can still fail dramatically in some situations [Pet99, Gis99, Gri00]. Thus, it is necessary to construct better exchange-correlation potentials. In order to do this it is important to include as many properties of the exact potential as possible into the approximate potential. This chapter deals with such an exact property, namely the influence of the particle number on the exchange-correlation potential. Since the static case is crucial to understand the time-dependent one, a thorough discussion of the ground-state case is given first.

3.1 Ground-state theory

3.1.1 Formalism

In the original proof of the Hohenberg-Kohn theorem an integer number of electrons in a closed system is assumed. As a consequence, the functional $F_N[n]$ is defined only for integer particle numbers N in the Hohenberg-Kohn formulation. Here, $F_N[n]$ is used instead of $F[n]$ to point out explicitly the dependence on the particle number N . Although fractional particle numbers do not exist in nature, it is desirable to extend the definition of the functional $F_N[n]$ to non-integer particle numbers. In the statistical description of open systems, for instance, fractional particle numbers are an extremely useful concept. In addition, using an unrestricted density variation in combination with imposing the subsidiary condition $\int n(\mathbf{r}) d^3r = N$ via the Lagrange multiplier $\tilde{\mu}$, i.e.,

$$\frac{\delta}{\delta n} \{E_N[n] - \tilde{\mu} \int n(\mathbf{r}) d^3r\} = 0 , \quad (3.1)$$

requires a definition of $E_N[n]$ for arbitrary particle numbers.

The most natural way to include non-integral particle numbers into static DFT is via Mermin's generalization of the Hohenberg-Kohn theorem to systems in equilibrium with a reservoir [Mer65, Pe85b]. In the zero-temperature limit the 'constraint search' concept [Lev79, Val80, Dre90] leads to the expression

$$E_N[n] = F_{\text{frac}}[n] + \int n(\mathbf{r}) v(\mathbf{r}) d^3r \quad (3.2)$$

with

$$F_{\text{frac}}[n] := \min_{\hat{\rho} \rightarrow n} \text{tr}\{\hat{\rho}(\hat{T} + \hat{W})\} \quad (3.3)$$

$$\hat{\rho} = (1-\omega)|\psi^M\rangle\langle\psi^M| + \omega|\psi^{M+1}\rangle\langle\psi^{M+1}|$$

for the energy functional $E_N[n]$ of a system with $N = M + \omega$ particles (M : integer, $0 < \omega < 1$) [Pe82a]. In Eq. (3.3) the search for the minimum runs over all ensembles which consist of an M - and an $(M + 1)$ -particle function and which yield the given density n . With the above expressions the variational principle is well defined and Eq. (3.1) results in

$$\frac{\delta E_N[n]}{\delta n(\mathbf{r})} = \tilde{\mu} . \quad (3.4)$$

The physical meaning of the Lagrange multiplier $\tilde{\mu}$ for a given particle number N is revealed by the relation

$$E_{N+\epsilon} - E_N = \int \left. \frac{\delta E_N[n]}{\delta n(\mathbf{r})} \right|_{n_N} (n_{N+\epsilon}(\mathbf{r}) - n_N(\mathbf{r})) d^3r . \quad (3.5)$$

Combining this equation with Eq. (3.4) shows that $\tilde{\mu}$ is equal to the chemical potential μ because

$$E_{N+\epsilon} - E_N = \int \tilde{\mu} (n_{N+\epsilon}(\mathbf{r}) - n_N(\mathbf{r})) d^3r = \tilde{\mu} \epsilon \quad (3.6)$$

and thus,

$$\tilde{\mu} = \frac{\partial E_N}{\partial N} = \mu(N) \quad (3.7)$$

in the limit $\epsilon \rightarrow 0$.

From Eq. (3.2) it follows that the ground-state energy of the system consisting of $M + \omega$ particles is given by [Pe82a]

$$E_{M+\omega} = (1 - \omega) E_M + \omega E_{M+1} \quad (3.8)$$

where E_M is the ground-state energy of the M -particle system. Thus, for a finite system with electron affinity A and ionization potential I the energy as a function of ω looks as in Fig. 3.1. Obviously, $\mu(N) = \partial E_N / \partial N$ changes discontinuously at $\omega = 0$. In

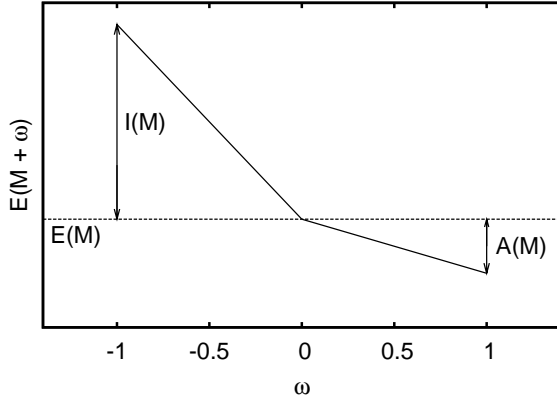


Figure 3.1: Ground-state energy of a finite $(M + \omega)$ -particle system. $I(M)$ is the ionization potential and $A(M)$ the electron affinity of the system with integer particle number M . By construction the curve is a continuous series of straight-line segments with possible discontinuous derivatives at integer M .

other words, the energy E_N as a function of the particle number N has a derivative discontinuity at integer particle numbers. The value of the derivative discontinuity is

$$\begin{aligned} \Delta &:= I(M) - A(M) \\ &= \lim_{\omega \rightarrow 0} \{ \mu(M + \omega) - \mu(M - \omega) \} \\ &= \lim_{\omega \rightarrow 0} \left\{ \left. \frac{\delta E[n]}{\delta n(\mathbf{r})} \right|_{M+\omega} - \left. \frac{\delta E[n]}{\delta n(\mathbf{r})} \right|_{M-\omega} \right\}, \end{aligned} \quad (3.9)$$

where $|_{M+\omega}$ denotes ‘taken at the correct (i.e., minimizing) density of the $(M + \omega)$ -particle system’. $I(M)$ and $A(M)$ are the ionization potential and the electron affinity of the system containing M electrons, respectively.

In the Kohn-Sham scheme the derivative discontinuity can be expressed in terms of the functional derivatives of the exchange-correlation energy E_{xc} and the kinetic energy of the Kohn-Sham system. This is possible since neither the functional derivative of the external-energy contribution, i.e., the external potential, nor the functional derivative of the Hartree energy (i.e., the Hartree potential) changes discontinuously with the particle number. Thus, the contributions of these two energies to the derivative discontinuity vanish and one obtains

$$\begin{aligned} \Delta &= \lim_{\omega \rightarrow 0} \left\{ \left. \frac{\delta T_S[n]}{\delta n(\mathbf{r})} \right|_{M+\omega} - \left. \frac{\delta T_S[n]}{\delta n(\mathbf{r})} \right|_{M-\omega} \right\} \\ &+ \lim_{\omega \rightarrow 0} \left\{ \left. \frac{\delta E_{xc}[n]}{\delta n(\mathbf{r})} \right|_{M+\omega} - \left. \frac{\delta E_{xc}[n]}{\delta n(\mathbf{r})} \right|_{M-\omega} \right\}. \end{aligned} \quad (3.10)$$

The first summand can be written as

$$\begin{aligned} \lim_{\omega \rightarrow 0} \left\{ \left. \frac{\delta T_S[n]}{\delta n(\mathbf{r})} \right|_{M+\omega} - \left. \frac{\delta T_S[n]}{\delta n(\mathbf{r})} \right|_{M-\omega} \right\} &= \lim_{\omega \rightarrow 0} \{ \epsilon_{M+1}(M + \omega) - v_S(\mathbf{r})|_{M+\omega} \\ &- \epsilon_M(M - \omega) + v_S(\mathbf{r})|_{M-\omega} \} \end{aligned} \quad (3.11)$$

where $\epsilon_j(N)$ is the j -th Kohn-Sham eigenvalue of the N -particle system. Furthermore, in the limit $\omega \rightarrow 0$ the Kohn-Sham potential $v_S(\mathbf{r})|_{M+\omega}$ and the potential $v_S(\mathbf{r})|_{M-\omega}$ can only differ by some constant c since the difference between the densities vanishes,

i.e., $\lim_{\omega \rightarrow 0} \{v_S(\mathbf{r})|_{M+\omega}\} = \lim_{\omega \rightarrow 0} \{v_S(\mathbf{r})|_{M-\omega} + c\}$ holds. As a consequence, the Kohn-Sham eigenvalues $\epsilon_{M+1}(M + \omega)$ and $\epsilon_{M+1}(M - \omega)$ can also differ only by the same constant in the limit $\omega \rightarrow 0$, i.e., $\lim_{\omega \rightarrow 0} \epsilon_{M+1}(M + \omega) = \lim_{\omega \rightarrow 0} \epsilon_{M+1}(M - \omega) + c$ holds. Thus, one can write

$$\lim_{\omega \rightarrow 0} \left\{ \left. \frac{\delta T_S[n]}{\delta n(\mathbf{r})} \right|_{M+\omega} - \left. \frac{\delta T_S[n]}{\delta n(\mathbf{r})} \right|_{M-\omega} \right\} = \lim_{\omega \rightarrow 0} \underbrace{\{\epsilon_{M+1}(M - \omega) - \epsilon_M(M - \omega)\}}_{=: \Delta_{\text{nonint}}} \quad (3.12)$$

For open-shell systems the eigenvalues $\epsilon_{M+1}(M - \omega)$ and $\epsilon_M(M - \omega)$ are equal and thus, according to Eq. (3.10), the exchange-correlation potentials for a system with $M + \omega$ and one with $M - \omega$ particles must differ by the constant $\Delta = I(M) - A(M)$ in the limit $\omega \rightarrow 0$.

At first sight this result seems to be a contradiction to the fact that the Kohn-Sham potential vanishes at infinity for all particle numbers, i.e.,

$$\lim_{r \rightarrow \infty} \{v_{xc}(\mathbf{r})|_{M+\omega} - v_{xc}(\mathbf{r})|_{M-\omega}\} = 0. \quad (3.13)$$

Indeed, if the limit $r \rightarrow \infty$ is taken first, as done by Zahariev and Wang [Zah04], the difference between $v_{xc}(\mathbf{r})|_{M+\omega}$ and $v_{xc}(\mathbf{r})|_{M-\omega}$ vanishes in the limit $\omega \rightarrow 0$ [Pe85b]. This is, however, no contradiction to the above result since for any arbitrarily small, but finite, ω , the difference between the exchange-correlation potentials is

$$v_{xc}(\mathbf{r})|_{M+\omega} - v_{xc}(\mathbf{r})|_{M-\omega} = f(\mathbf{r}) \neq \text{const.} \quad (3.14)$$

Similar to the Fermi function for low temperatures the function $f(\mathbf{r})$ is constant in a region $r < r_c$ and goes to zero for $r > r_c$ [Pe85b, Per97]. For $\omega \rightarrow 0$ the radius r_c increases and approaches infinity. As a consequence, different results are obtained for a different order of the two limits and thus, Eq. (3.13) is no contradiction to $\lim_{\omega \rightarrow 0} \{v_{xc}(\mathbf{r})|_{M+\omega} - v_{xc}(\mathbf{r})|_{M-\omega}\} = \text{const.}$

Before discussing the physical implications of the discontinuities, two final remarks should be made. First, it is important for the time-dependent case, Sec. 3.2, that the same results can be obtained with the definition

$$\tilde{F}_{\text{frac}}[n] := \min_{\hat{\rho} \rightarrow n} \text{tr}\{\hat{\rho}(\hat{T} + \hat{W})\} \quad (3.15)$$

$$\hat{\rho} = \sum_{j=1}^{\infty} p_j |\psi^j\rangle\langle\psi^j|$$

$$\sum_{j=1}^{\infty} p_j = 1$$

instead of Eq. (3.3). Here, the search runs over density matrices containing antisymmetric j -particle functions. Nevertheless the minimizing condition leads to exactly the same minimizing ensemble consisting of an M -particle and $(M + 1)$ -particle state as Eq. (3.3) [Pe82a]. In other words, the energy minimization establishes a one-to-one

mapping between the ensemble and the particle number which is independent of the particle reservoir¹.

The second remark is about existing approximations for the exchange-correlation functional. One may ask if any approximations with such discontinuities exist. The answer is yes. As Krieger, Li, and Iafrate have impressively demonstrated [Kr92a] orbital functionals, in contrast to the LDA/GGA functionals, have such a property. In addition to the advantages of orbital functionals discussed in Chap. 2 this is another reason why orbital functionals are a promising concept in DFT.

3.1.2 Physical consequences

The fact that virtually all DFT calculations deal with an integer particle number raises the question whether the discontinuities presented in the preceding subsection are of any practical importance. Following Perdew *et al.*, this can be answered by considering a system composed of two separated atoms, A and B , with nuclear charge Z_A and Z_B (Z_A, Z_B : integer). For the time being, any interactions between the atoms are neglected and the Hamiltonian of the system is approximated by

$$\hat{H} = \hat{H}^{(A)} \otimes \mathbb{1} + \mathbb{1} \otimes \hat{H}^{(B)} \quad (3.16)$$

where \otimes is the tensor product and $\hat{H}^{(A/B)}$ the Hamiltonian of atom A/B . Given the Hamiltonian (3.16) antisymmetrization of atom A 's states with the states of atom B is not required. In fact, it is even not allowed for the system defined by Eq. (3.16) since the Hamiltonian is not symmetric under particle exchange between the two atoms. The state of the complete system can be written in the form

$$|\psi\rangle = \sum_{J=0}^{Z_A+Z_B} \sum_{j,k} c_{j,k}(J) |\psi_j^{(A)}(J)\rangle |\psi_k^{(B)}((Z_A + Z_B) - J)\rangle \quad (3.17)$$

where $|\psi_j^{(A/B)}(J)\rangle$ is the j -th eigenstate of atom A/B with J electrons, i.e., (with \hat{N} being the particle-number operator)

$$\hat{H}^{(A)} |\psi_j^{(A)}(J)\rangle = E_j^{(A)}(J) |\psi_j^{(A)}(J)\rangle \quad (3.18)$$

$$\langle \psi_j^{(A)}(J) | \hat{N} | \psi_j^{(A)}(J) \rangle = J. \quad (3.19)$$

Since the smallest first ionization potential I in the periodic table is greater than the largest electron affinity A ($I_{\text{Cs}} = 3.89$ eV, $A_{\text{Cl}} = 3.62$ eV), the ground-state energy of the complete system is given by

$$E_0(Z_A + Z_B) = E_0^{(A)}(Z_A) + E_0^{(B)}(Z_B). \quad (3.20)$$

¹This statement requires the assumption that the energy as a function of the particle number M is upward convex for integer M [Pe82a]. Although this property is not generally proven, it seems to be satisfied for all systems with repulsive interactions [Pe82a, Dre90, Aye00].

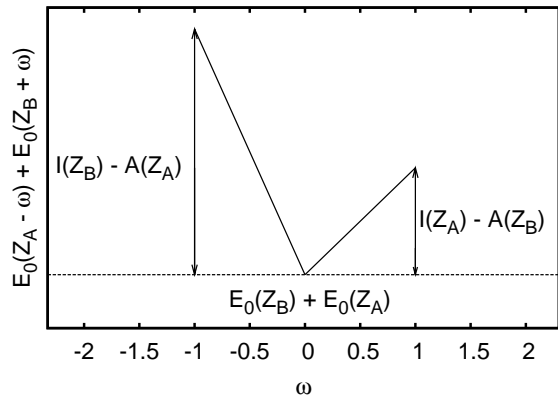


Figure 3.2: Energy of two widely separated atoms with nuclear charge Z_A and Z_B as a function of the electron shift from atom A to atom B . Clearly, the energy is minimized at zero net charge. $I(M)$ is the ionization potential and $A(Z)$ the electron affinity of an atom with nuclear charge Z .

The total ground-state density is the sum of the two ground-state densities $n_0^{(A)}(Z_A)$ and $n_0^{(B)}(Z_B)$, i.e.,

$$n_0(Z_A + Z_B) = n_0^{(A)}(Z_A) + n_0^{(B)}(Z_B). \quad (3.21)$$

As expected both atoms are neutral in the ground state, i.e., Z_A electrons are found in atom A and Z_B electrons in atom B .

In order to describe the closed $(Z_A + Z_B)$ -particle system in the framework of DFT, the fractional DFT formalism of the previous subsection can be used. Since the two atoms do not interact, the energy minimization of the $(Z_A + Z_B)$ -particle system can be replaced by two separate energy minimizations for atom A and atom B with fractional particle numbers. The possibility of fractional particle numbers is a result of the fact that arbitrary density variations are allowed in the closed $(Z_A + Z_B)$ -particle system. The only constraint in the closed system is $\int n(\mathbf{r}) d^3r = Z_A + Z_B$. As shown in Fig. 3.1 the exact ground-state energy of atom A as a function of the particle number is a series of straight lines (compare Eq. (3.8)). Combining this curve with the analogous result for atom B , one obtains the graph shown in Fig. 3.2. There, the minimal energy of the two separated atoms is shown as a function of the transferred particle number from atom A to B . As one can see the absolute minimum of the energy is zero, i.e., no fractional particle number is transferred. Thus, in accordance with reality, both atoms are also neutral in the *exact* DFT treatment with fractional particle numbers.

The situation changes dramatically, however, if one uses approximate energy functionals without a derivative discontinuity at integer particle number. In this case $\mu(N)$ is a continuous function of N and, as a consequence, the total energy of the system can be lowered by transferring some density from one atom to the other atom with lower μ . Thus, in clear contradiction to all experimental facts, two well-separated atoms are not neutral but slightly charged. As an example the missing derivative discontinuity in the LDA functional leads to the configuration $\text{Li}^{+0.25} \text{H}^{-0.25}$ for a Lithium and Hydrogen atom at large distances [Pe82a].

The example of the two separate atoms clearly demonstrates that, even for integer

particle numbers, any approximate energy functional without a derivative discontinuity can lead to wrong results. Without interactions between the two atoms one may argue that this is not a real problem since it can be easily circumvented by a separate energy minimization with integer particle numbers for the two atoms. However, with interactions between the atoms included this procedure does not work anymore. Thus, the question arises how interactions between the two atoms influence the arguments given above. As described in the following the first problem one observes in this situation is that the inclusion of the interactions makes impossible a rigorous definition of the particle numbers of the two atoms. Without interactions the potential part of the Hamiltonian as defined in Eq. (3.16) is

$$\hat{v} = \hat{v}^{(A)} \otimes \mathbb{1} + \mathbb{1} \otimes \hat{v}^{(B)}. \quad (3.22)$$

As mentioned above the antisymmetrization of the atoms' states is missing and one can define the particle number in the atoms via

$$\hat{N}^{(A)} = \hat{N} \otimes \mathbb{1}, \quad (3.23)$$

$$\hat{N}^{(B)} = \mathbb{1} \otimes \hat{N}. \quad (3.24)$$

In a more rigorous description of the two atoms the Hamiltonian must include an atom-atom interaction and it must be symmetric under particle exchange. For instance, the external potential part must have the form

$$\hat{v} = (\hat{v}^{(A)} + \hat{v}^{(B)}) \otimes \mathbb{1} + \mathbb{1} \otimes (\hat{v}^{(A)} + \hat{v}^{(B)}) \quad (3.25)$$

and the wavefunction must be antisymmetric. Consequently, the two operators $\hat{N}^{(A)}$ and $\hat{N}^{(B)}$ have the same expectation values and are useless to define a particle number of the single atoms. The missing rigorous definition of an atom's particle number is just a consequence of the fact that the wavefunctions of the two atoms have a non-zero overlap for any finite distances R_{A-B} between atom A and B . Nevertheless it is possible to define the observable

$$N_{\text{geom}}^{A/B} := \int_{V_{A/B}} n(\mathbf{r}) d^3r \quad (3.26)$$

where $V_{A/B}$ is a volume around the nucleus of atom A/B and n is the density of the total system. In this definition V_A is assumed to have zero overlap with V_B and the sum of V_A and V_B constitutes the complete space. The ground-state energy of the complete system can be written as

$$E_0(M_A + M_B) = E_0^{(A)}(M_A) + E_0^{(B)}(M_B) + E_{A-B}. \quad (3.27)$$

Here, the interaction energy E_{A-B} is simply defined as the difference between the true ground-state energy $E_0(M_A + M_B)$ of the combined system and the sum of the two

ground-state energies $E_0^{(A)}(M_A)$ and $E_0^{(B)}(M_B)$ of the isolated atoms. The crucial observation now is that in the limit $R_{A-B} \rightarrow \infty$ the above quantities have the limits

$$E_{A-B} \rightarrow 0, \quad (3.28)$$

$$N_{\text{geom}}^A \rightarrow M_A, \quad (3.29)$$

$$N_{\text{geom}}^B \rightarrow M_B. \quad (3.30)$$

This can be proven by using a Heitler-London-type ansatz to calculate an upper bound for the ground-state energy as, e.g., done in [Sch93]. Thus, for sufficiently large distances R_{A-B} the difference between the results from a DFT calculation with fractional particle numbers (possibly approximating the interaction between the atoms via the electrostatic expression $-e^2\omega^2/R_{A-B}$ where ω is the transferred charge) and the results of a DFT calculation with integer particle number must be arbitrary small. For approximations of the total energy which do not have a derivative discontinuity with respect to the particle number this observation is clearly not reproduced. In other words, given an approximation for the energy functional of a system with arbitrary particle number and without a derivative discontinuity, one can construct a situation in which the results of a DFT calculation with fractional particle number differ significantly from the results of a DFT calculation with integer particle number although the results should be almost equal.

The previous discussion also shows that in the ‘integer particle DFT’, e.g., the Hohenberg-Kohn formulation, $F[n]$ must have a property that guarantees particle numbers N_{geom} almost identical to an integer for distant atoms². In the limit $R_{A-B} \rightarrow \infty$ this property of $F[n]$ has exactly the same consequences as the derivative discontinuity in the DFT for fractional particle numbers. Consequently, the Kohn-Sham potential must also have a feature that guarantees integer particle numbers for large enough distances. Since neither the Hartree potential nor the external potential provide such a feature, the exchange-correlation potential must include a property that leads to integer particle numbers in the situation described above. Clearly, this property becomes especially important if processes involving well-separated subsystems are of interest. The response of molecular chains like poly-acetylene to electric fields is just one, but technologically very relevant [Kan94], example for such a process. Other examples are the adiabatic dissociation of a molecule and charge-transfer processes in extended systems.

Since neither the LDA nor the GGA exchange-correlation potential has a property that guarantees integer particle numbers for distant atoms, it is hardly surprising from the previous discussion that these approximations fail dramatically (in some cases by orders of magnitude) in the description of the just mentioned processes. For instance,

²Using the same electrostatic approximation for the interaction energy as above, the minimum distance for which neutral atoms can be expected is approximately given by $R_{A-B} \approx e^2/(I_A - A_B)$. In this estimate it is assumed that $I_A - A_B < I_B - A_A$ holds.

the energy required for a charge transfer between two separated systems is predicted significantly too low in an LDA or GGA calculation [Toz03]. Also, the static longitudinal linear and non-linear polarizabilities of different molecular chains are extremely overestimated by DFT calculations using the LDA or GGA functional [Cha98]. In contrast to the LDA or GGA exchange-correlation potential, the exact-exchange potential obtained from the exact-exchange orbital functional shows, like the *true* exchange-correlation potential, a field-counteracting behavior when the external field is applied to the molecular chain [Gis99, Kü04a]. As a consequence, the static linear and non-linear polarizabilities are reduced tremendously. For hydrogen chains highly accurate Møller-Plesset results are available and the exact-exchange results are in good agreement with them [Kü04a]. A thorough study of the field-counteracting effect [Kör06] shows that its origin is in the same term of the exchange-correlation potential which is also responsible for the derivative discontinuity in the case of fractional particle numbers. This observation, discussed in Chap. 4 in more detail, demonstrates the close relationship between features of the exchange-correlation potential for a system with integer particle number and the discontinuous behavior of the exchange-correlation potential found in the DFT for fractional particle numbers.

Before closing this subsection, it should also be mentioned that the jump of the exchange-correlation potential at integer particle number is of crucial importance if the band gap of a solid is extracted in the standard way, i.e., from the Kohn-Sham band-structure [Per83, Sha83, Pe85b, Dre90]. The reason for this is that the Kohn-Sham band gap Δ_{nonint} is not equal to the true band gap Δ , but differs by the jump in the exchange-correlation potential as can be seen from Eq. (3.12) and Eq. (3.10).

3.2 Time-dependent theory

3.2.1 Formalism

The natural way to include non-integral particle numbers into time-dependent DFT is via statistical ensembles in analogy to static DFT [Mun05]. This method relies on an extension of the Runge-Gross theorem to time-dependent ensembles [Li85]. The central statement of this extension is that for a given initial state a one-to-one map between an ensemble v -representable density and an external potential $v(\mathbf{r}, t)$ (up to an additive purely time-dependent function) exists. In other words, the ensemble density operator with probabilities p_j ,

$$\hat{\rho}(t) = \sum_j p_j |\psi^j(t)\rangle\langle\psi^j(t)| \quad (3.31)$$

is a functional of the density $n(\mathbf{r}, t)$ and, as in the standard Runge-Gross theorem and in contrast to static DFT, a functional of the initial state, i.e. $\hat{\rho}(t) = \hat{\rho}[n, \hat{\rho}_0]$. Thus, the expectation value of any observable $\bar{O} = \text{Tr}(\hat{\rho}\hat{O})$ is a functional of the density and the

initial state. Varying the particle number for a fixed external potential and asking how such a functional changes at the correct time-dependent density immediately reveals a problem: a given fractional particle number can be associated with infinitely many different ensembles via Eq. (3.31). As described above in the static case the condition that the energy be minimized ensures that just one specific ensemble – the minimizing one – is associated with a given fractional particle number. But in a time-dependent theory, *a priori* no such minimizing criterion exists. Thus, without an additional prescription of how to choose the ensemble no statement can be made on how functionals change with particle number.

This ambiguity is resolved when the initial state at time t_0 in the time-dependent theory is chosen to be the ground state. Although a special case, this is the typical physical situation and therefore of great practical importance. As already mentioned in Chap. 2 for a non-degenerate ground state the functional becomes a pure density functional via the Hohenberg-Kohn theorem. In contrast to the general time-dependent case, the density operator is now uniquely determined at all times by just the total particle number: for the $(M + \omega)$ -particle system the initial condition

$$\hat{\rho}(t_0) = (1 - \omega) |\psi_0^M\rangle\langle\psi_0^M| + \omega |\psi_0^{M+1}\rangle\langle\psi_0^{M+1}|, \quad (3.32)$$

fixes the ensemble once and for all since the propagation does not affect the weights. Again, M is integer, $0 < \omega < 1$, and $|\psi_0^M\rangle$ denotes the ground state of the system with M particles. As in the static case the expectation values of all observables are now given by linear interpolation between the neighboring systems with integer particle numbers. As a consequence, any observable's expectation value $O[n]$ at the correct time-dependent density changes continuously with varying particle number, but its functional derivative needs not. The corresponding time-dependent derivative discontinuity is defined by

$$\Delta_O(t) := \lim_{\omega \rightarrow 0} \left\{ \left. \frac{\delta O[n]}{\delta n(\mathbf{r}, t)} \right|_{M+\omega} - \left. \frac{\delta O[n]}{\delta n(\mathbf{r}, t)} \right|_{M-\omega} \right\}, \quad (3.33)$$

where $|_{M+\omega}$ denotes ‘taken at the true (physical) time-dependent density of the $(M + \omega)$ -particle system corresponding to the given external potential’.

It follows from the considerations in the static case that the time-dependent energy functional $E(t) = \text{Tr}(\hat{\rho}(t) \hat{H}(t))$ at the initial time t_0 has a derivative discontinuity. Since the system evolves in time in a continuous manner for $t > t_0$, the derivative discontinuity must also exist in the time-dependent system, at least for times close to t_0 . The question whether this initial discontinuity will persist for *all* later times is not easy to answer for interacting systems. For non-interacting particles it seems possible to make Δ_E vanish at later times by switching adiabatically from an external potential without degenerate highest-occupied orbital to a potential with degenerate highest-occupied orbital.

An elegant way to study the influence of derivative discontinuities on the time evolution of the density is via the action functional (2.16) presented in the previous chapter,

i.e.,

$$A[n] = -\tilde{A}[v] + \int \int_C n(\mathbf{r}, \tau) v(\mathbf{r}, \tau) dt d^3r . \quad (3.34)$$

Taking the derivative of the action of the interacting system with respect to the density and evaluating this derivative at the physical time-dependent density, one obtains (see Chap. 2)

$$\left. \frac{\delta A}{\delta n(\mathbf{r}, \tau)} \right|_{n(\mathbf{r}, t)} = v(\mathbf{r}, t) . \quad (3.35)$$

Since the external potential $v(\mathbf{r}, t)$ is kept fixed the action of the interacting system has no derivative discontinuity. Carrying out the same calculation for the action of the Kohn-Sham system A_S one obtains $\delta A_S / \delta n(\mathbf{r}, \tau) |_{n(\mathbf{r}, t)} = v_S(\mathbf{r}, t)$. As pointed out above the Kohn-Sham potential $v_S(\mathbf{r}, t)$ changes discontinuously when the number of particles crosses an integer and thus, in analogy to the arguments given for the time-dependent energy, one obtains the result that the action of the Kohn-Sham system A_S has a derivative discontinuity in the A_{xc} part.

3.2.2 Physical consequences

In the ground-state theory of Sec. 3.1 the example of the two well-separated atoms shows that the static exchange-correlation potential must have a property that guarantees integer particle numbers at each atom. Since such a situation can evolve from an adiabatic time-dependent process, it is clear that the time-dependent exchange-correlation potential must also have such a property. However, the question how this property is related to the derivative discontinuities discussed in the previous subsection is considerably more involved in the time-dependent case than in the ground-state situation of Sec. 3.1. There, combining arbitrary density variations with the fact that for large distances $E_{\text{tot}} = E_A + E_B$ holds provides a connection between the derivative discontinuities in the ‘fractional particle DFT’ and the properties of the exchange-correlation potential in the ‘integer particle DFT’.

In the time-dependent case the connection between the ‘fractional-particle formalism’ and the integer particle-number treatment is mainly complicated by the fact that the time-dependent density is not obtained from any minimization with arbitrary density variations. Instead, the density at some instant t_1 evolves from the densities at former times $t < t_1$. In other words, the time evolution depends on the system’s past, i.e., memory effects or, equivalently, initial state dependencies exist [Ma02a]. Thus, it is generally not possible to switch from a pure state description to an ensemble description with fractional particle numbers. Especially, going over from a pure state to an ensemble description by calculating the partial trace in one subsystem does not allow one to connect the fractional and integer particle-number descriptions since the resulting density operator for the subsystem has time-dependent weights $p_j = p_j(t)$ and its time evolution is thus no longer given by the von Neumann equation (see, e.g., [Coh99]).

Despite the just discussed problems situations exist in which the time-dependent exchange-correlation potential of a system with integer particle number can be expected to be almost identical to the potential from a fractional particle-number calculation. One such situation is long after an ionization process in which only the weakest-bound electron can be ionized. In the beginning of such a process the atom consists of $M + 1$ electrons. After some time t_I the density around the nucleus integrates to $M + \omega$ with $\omega \ll 1$. Under the reasonable assumption that memory effects and the small additional amount of density do not influence the time evolution of the remaining atom significantly, the exchange-correlation potential around the nucleus must be almost identical to the potential from a $M + \omega$ -particle calculation for $t > t_I$. This potential in turn can be expected to differ from the M -particle potential by just the constant shift of the derivative discontinuity in the exchange-correlation potential.

In order to support these arguments an ionization process of a one-dimensional Li atom is numerically studied in the following. For this purpose the exact-exchange action functional

$$A_x[n] = -\frac{1}{2} \sum_{\substack{j,k=1 \\ \sigma=\uparrow,\downarrow}}^{N_\sigma} \int \int \int_C \frac{\varphi_{j\sigma}^*(\mathbf{r}', \tau) \varphi_{k\sigma}(\mathbf{r}', \tau) \varphi_{j\sigma}(\mathbf{r}, \tau) \varphi_{k\sigma}^*(\mathbf{r}, \tau)}{|\mathbf{r} - \mathbf{r}'|} dt d^3 r' d^3 r . \quad (3.36)$$

is used. The resulting exchange potential in the KLI approximation is (a detailed discussion can be found in Chap. 4)

$$v_{x\sigma}^{\text{KLI}}(\mathbf{r}, t) = \frac{1}{2n_\sigma(\mathbf{r}, t)} \sum_{j=1}^{N_\sigma} |\varphi_{j\sigma}(\mathbf{r}, t)|^2 [u_{xj\sigma}(\mathbf{r}, t) + (\bar{v}_{xj\sigma}^{\text{KLI}}(t) - \bar{u}_{xj\sigma}(t))] + c. c. \quad (3.37)$$

where $n_\sigma(\mathbf{r}, t)$ is the total spin density,

$$u_{xj\sigma}(\mathbf{r}, t) = \frac{1}{\varphi_{j\sigma}^*(\mathbf{r}, t)} \frac{\delta A_x}{\delta \varphi_{j\sigma}(\mathbf{r}, t)} \quad (3.38)$$

and bars denote orbital averages, e.g., $\bar{v}_{xj\sigma}^{\text{KLI}}(t) = \int |\varphi_{j\sigma}(\mathbf{r}, t)|^2 v_{x\sigma}^{\text{KLI}}(\mathbf{r}, t) d^3 r$. The condition that $v_{x\sigma}(\mathbf{r}, t)$ must go to zero for $|\mathbf{r}| \rightarrow \infty$ is fulfilled by enforcing

$$\bar{v}_{xN\sigma}^{\text{KLI}}(t) = \bar{u}_{xN\sigma}(t) . \quad (3.39)$$

Although this potential is not the *exact* exchange-correlation potential, it can be expected to be qualitatively close to the true potential for atoms [Ull95]. In the simulation the $(-1/r)$ Coulomb interaction is replaced by $(-1/\sqrt{z^2 + 0.3})$ (see Chap. 5 for details). Initially, the atom is in its ground state. At $t = 0$ a homogenous external field (pulling density to the left) is linearly switched on over a time period of 40 a.u. As commonly done in strong-field calculations the field is cut off at some large distance (here, 20 a.u.) to avoid problems with strongly accelerated electrons. The Kohn-Sham orbitals are propagated on a real-space grid in real time with a Crank-Nicolson algorithm [Pre92]

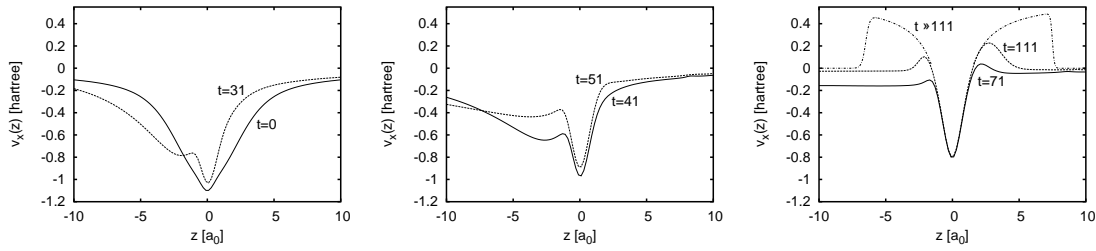


Figure 3.3: Li atom in one dimension subjected to a strong, ionizing external field $F=0.06$ a.u. In each figure the exchange potential of the two spin-up electrons at different times (as labeled) is shown. At time $t = 0$ the atom is in its ground state. Then the external field is linearly ramped up over 40 a.u. and finally held constant. One can clearly see the escape of density to the left and the buildup of the steplike structure. $t \gg 111$ denotes an extrapolation to very large times.

and a time step of 0.025 a.u. A large grid is used, 1500 points with a spacing of 0.2 a.u., to guarantee that no density reaches the boundary of the numerical box over the whole simulation time. The field strength (0.06 a.u.) is chosen such that only the highest occupied Kohn-Sham orbital is ionized.

Fig. 3.3 shows the exchange potential of the two spin-up electrons during the ionization process. In the left part the ground-state potential and the potential at time $t = 31$ a.u. are plotted. One clearly sees how the potential is lowered on the left-hand side due to the outgoing density. At later times (middle part of Fig. 3.3) ‘humps’ or ‘steps’ start to build up at the edges of the remaining Li^+ ion. Finally (right part), the potential in the area around the nucleus remains almost unchanged, but the humps on both flanks keep growing and move outwards. The dotted line marked $t \gg 111$ indicates what the potential would qualitatively look like if one continued the simulation further to times close to ‘infinity’. The humps would turn more and more steplike and continue to move outwards. When all of the 2s orbital-density would have escaped to ‘infinity’, the steps would reach ‘infinity’.

To demonstrate the relationship between the exchange potential of the Li atom and the potential from the Li^+ ion one can do a second simulation, subjecting a Li^+ ion to exactly the same field as the Li atom. The exchange potential for both systems after a time of 111 a.u. is shown in Fig. 3.4. The chosen field strength is too small to ionize the more strongly bound 1s electrons, but the orbital density of the Li atom’s 2s electron has nearly completely been removed from the core region. Therefore, in both systems the core region (shown in Fig. 3.4) basically corresponds to a Li^+ ion with slightly polarized 1s orbital densities. However, in the simulation where one starts from a Li atom and then explicitly ionizes it, one is effectively looking at a 1s core with a tiny additional fractional charge still left over from the 2s electron. As predicted above this tiny fractional charge has no recognizable influence on the shape of the potential (the two curves are perfectly

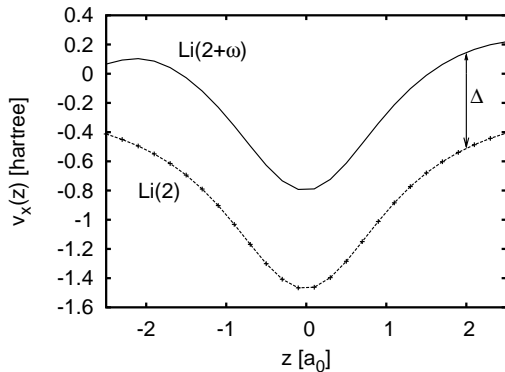


Figure 3.4: Snapshot at $t=111$ a.u. of the TD spin-up exchange potential of a Li atom (labeled $\text{Li}(2+\omega)$) and a Li^+ ion (labeled $\text{Li}(2)$). Both were subjected to the electrical field of Fig. 3.3. The Li 2s electron has been nearly completely ionized, so both systems are basically Li^+ cores. But for the system that started as a Li atom the minute fractional 2s electron charge around the core leads to a constant upward shift Δ .

parallel between -2 and 2), but it leads to a constant upward shift in the potential.

Mathematically, the shift comes in via Eq. (3.39): to guarantee that $v_x(\mathbf{r}, t)$ vanishes at infinity $\bar{v}_{xN\sigma}^{\text{KLI}}(t) - \bar{u}_{xN\sigma}(t)$ must be chosen to vanish for $N = 1$ in the Li^+ case and $N = 2$ in the Li case. This leads to a constant difference between the potentials in the non-asymptotic region. The ‘steps’ appear in those regions where the Li potential goes over from the non-asymptotic to the asymptotic form that decays to zero, i.e., the regions in which the highest-occupied orbital starts to dominate the total density. With progressing ionization, this region moves further away from the core towards ‘infinity’.

In the fractional particle-number treatment the main difference between the Li^+ ion’s exchange potential and the $(2 + \omega)$ -particle exchange potential is again that the term $\bar{v}_{xN\sigma}^{\text{KLI}}(t) - \bar{u}_{xN\sigma}(t)$ must be zero for $N = 1$ and, respectively, $N = 2$. Since for very small ω the tiny additional density has practically no influence in the core region, both potentials have again a similar shape there, but differ by a constant. Thus, in the above situation the exchange potential from the integer particle-number calculation and the exchange potential from the fractional particle-number treatment are practically identical.

3.3 Concluding remarks

Before closing this chapter, it should be mentioned again that fractional particle numbers are not essentially necessary for a DFT description of systems at zero temperature. However, the previous sections show that the concept of fractional particle numbers can be useful to understand the properties of functionals even in situations involving integer particle numbers. In particular, the present chapter clearly shows that any given approximation for the exchange-correlation energy of the form $E_{\text{xc}}[n] = \int f(n(\mathbf{r})) d^3r$, with $f(x)$ being a smooth function with finite derivatives must fail in situations involving well-separated subsystems. In addition, the discrepancy between the Kohn-Sham band gap and the true band gap demonstrates the importance of the discontinuities in the DFT for fractional particle numbers. Having these facts in mind, there is no doubt that the generalization to fractional particle numbers is a useful concept even in the zero temperature case.

Chapter 4

The optimized effective potential (OEP)

As pointed out in the previous two chapters several reasons exist why orbital functionals are a promising concept for the construction of accurate exchange-correlation potentials. However, orbital functionals also have a serious drawback: one has to solve a complicated integral equation to get the exchange-correlation potential. This equation, called the optimized effective potential (OEP) equation, is the subject of this chapter. Since the derivation and the final form of the equation differ considerably in the static and time-dependent theory, both cases are discussed in separate sections.

4.1 Static OEP equation

As mentioned in Chap. 2 the starting point in static Kohn-Sham DFT is an approximation for the exchange-correlation part E_{xc} of the energy. The corresponding exchange-correlation potential is then given by the functional derivative of E_{xc} with respect to the spin density n_σ , i.e.,

$$v_{xc\sigma}(\mathbf{r}) = \frac{\delta E_{xc}[n]}{\delta n_\sigma(\mathbf{r})}. \quad (4.1)$$

This equation immediately reveals the problem caused by orbital functionals: for them $E_{xc}[n]$ is not known explicitly but just implicitly via the orbitals, i.e., $E_{xc}[\{\varphi_{i\tau}[n]\}]$ ¹. As a consequence, the derivative must be calculated by applying the functional chain rule twice [Sha93, Gör94]. This leads to the expression

$$v_{xc\sigma}(\mathbf{r}) = \sum_{\alpha,\beta=\uparrow,\downarrow} \sum_{j=1}^{N_\alpha} \int \int \left(\frac{\delta E_{xc}[\{\varphi_{i\tau}\}]}{\delta \varphi_{j\alpha}(\mathbf{r}')} \frac{\delta \varphi_{j\alpha}(\mathbf{r}')}{\delta n_\sigma(\mathbf{r})} + c.c. \right) \frac{\delta v_{S\beta}(\mathbf{r}'')}{\delta n_\sigma(\mathbf{r})} d^3 r'' d^3 r'. \quad (4.2)$$

¹In the following it is assumed that E_{xc} and A_{xc} only depend on occupied orbitals. In Appendix A the general case involving also unoccupied orbitals is discussed.

The last term on the right side is the inverse of the static density-response function $\chi_{S\alpha,\beta}(\mathbf{r}, \mathbf{r}') = \delta n_\alpha(\mathbf{r}) / \delta v_{S\beta}(\mathbf{r}')$ of the Kohn-Sham system. Since this function is diagonal with respect to the spin variables, the sum over β breaks down and just the sum over α remains. With the help of first-order perturbation theory the expression

$$\frac{\delta \varphi_{j\alpha}(\mathbf{r})}{\delta v_{S\beta}(\mathbf{r}')} = \delta_{\alpha,\beta} \sum_{\substack{k=1 \\ k \neq j}}^{\infty} \frac{\varphi_{k\alpha}(\mathbf{r}) \varphi_{k\alpha}^*(\mathbf{r}')}{\epsilon_{j\alpha} - \epsilon_{k\alpha}} \varphi_{j\alpha}(\mathbf{r}') \quad (4.3)$$

is calculated under the assumption of non-degenerate states. If degenerate states exist the sum is restricted to all states with $\epsilon_{k\alpha} \neq \epsilon_{j\alpha}$ [Kr92a]. Given Eq. (4.3) the response function can be written in the form

$$\begin{aligned} \chi_{S\alpha,\beta}(\mathbf{r}, \mathbf{r}') &= \frac{\delta}{\delta v_{S\beta}(\mathbf{r}')} \left(\sum_{j=1}^{N_\alpha} \varphi_{j\alpha}^*(\mathbf{r}) \varphi_{j\alpha}(\mathbf{r}') \right) \\ &= \delta_{\alpha,\beta} \sum_{j=1}^{N_\alpha} \sum_{\substack{k=1 \\ k \neq j}}^{\infty} \frac{\varphi_{j\alpha}^*(\mathbf{r}) \varphi_{k\alpha}(\mathbf{r}) \varphi_{k\alpha}^*(\mathbf{r}') \varphi_{j\alpha}(\mathbf{r}')}{\epsilon_{j\alpha} - \epsilon_{k\alpha}} + c.c. \end{aligned} \quad (4.4)$$

Multiplying both sides of Eq. (4.2) with the response function and using Eq. (4.3) and Eq. (4.4), one obtains

$$\sum_{j=1}^{N_\sigma} \int (v_{xc\sigma}(\mathbf{r}') - u_{xcj\sigma}(\mathbf{r}')) \varphi_{j\sigma}^*(\mathbf{r}') \varphi_{j\sigma}(\mathbf{r}) \sum_{\substack{k=1 \\ k \neq j}}^{\infty} \frac{\varphi_{k\sigma}^*(\mathbf{r}) \varphi_{k\sigma}(\mathbf{r}')}{\epsilon_{j\sigma} - \epsilon_{k\sigma}} d^3 r' + c.c. = 0 \quad (4.5)$$

where

$$u_{xcj\sigma}(\mathbf{r}) = \frac{1}{\varphi_{j\sigma}^*(\mathbf{r})} \frac{\delta E_{xc}[\{\varphi_{i\tau}\}]}{\delta \varphi_{j\sigma}(\mathbf{r})}. \quad (4.6)$$

Eq. (4.5) is the optimized effective potential equation for the exchange-correlation potential. As one can expect from the Hohenberg-Kohn theorem this equation fixes the potential only up to a constant. At this point it is worth mentioning that the same result can be obtained by using $\delta E_v / \delta v_{S\sigma}(\mathbf{r}) = 0$ [Sha53, Tal76, Kr92a], i.e., by choosing the Kohn-Sham potential $v_{S\sigma}$ in such a way that the total energy E_v for a fixed external potential v is minimized. This is the historical reason for the name *optimized effective potential* [Sha53, Tal76].

4.1.1 Transformation to coupled differential equations

Eq. (4.5) is not very well suited for a numerical treatment in three dimensions because of the sum over all occupied and unoccupied Kohn-Sham orbitals. Nevertheless for spherical systems one can reduce the problem to solving a one-dimensional integral equation. For the exact-exchange functional this has been done for several atoms by Talman [Tal76] and Engel [Eng93, Eng94]. For solids Kotani has performed calculations

using the atomic-sphere approximation [Kot94, Ko95a, Ko95b, Kot96]. A review of all results for atomic systems can be found in [Gra00].

In order to construct the full three-dimensional optimized effective potential three possibilities exist. One is by brute force evaluation of the response function with the help of a basis set and a subsequent inversion of the response function [Stä97, Stä99, Gör94, Gör99, Iva99, Hir01, Del01, Ham02]. In the second method the Kohn-Sham potential is expanded in a set of basis functions. The expansion coefficients in this expansion are then determined in such a way that the total energy is minimized [Yan02]. The third method, which is discussed in the following, is based on auxiliary functions $\psi_{j\sigma}$, called orbital shifts [Kü03a, Kü03b]. Following Krieger, Li and Iafate [Kr92b], one defines the orbital shifts as

$$\psi_{j\sigma}(\mathbf{r}) := \sum_{\substack{k=1 \\ k \neq j}}^{\infty} \frac{\int \varphi_{k\sigma}^*(\mathbf{r}') (v_{xc\sigma}(\mathbf{r}') - u_{xcj\sigma}^*(\mathbf{r}')) \varphi_{j\sigma}(\mathbf{r}') d^3r'}{\epsilon_{j\sigma} - \epsilon_{k\sigma}} \varphi_{k\sigma}(\mathbf{r}) . \quad (4.7)$$

Actually, this is not exactly the function defined in [Kr92b]. There, $p_{j\sigma}(\mathbf{r}) = \psi_{j\sigma}(\mathbf{r})/\varphi_{j\sigma}(\mathbf{r})$ is used. Since $p_{j\sigma}$ becomes singular whenever the Kohn-Sham orbital $\varphi_{j\sigma}$ is zero, it is much better to work with the orbital shifts $\psi_{j\sigma}$. With this definition the integral equation (4.5) becomes

$$\sum_{j=1}^{N_\sigma} \psi_{j\sigma}^*(\mathbf{r}) \varphi_{j\sigma}(\mathbf{r}) + c.c. = 0 . \quad (4.8)$$

Since $\psi_{j\sigma}$ is the orbital shift of $\varphi_{j\sigma}$ induced by $(v_{xc\sigma} - u_{xcj\sigma}^*)$ in first-order perturbation theory, Eq. (4.8) states that the induced density change

$$\delta n_\sigma(\mathbf{r}) = \sum_{j=1}^{N_\sigma} |\varphi_{j\sigma}(\mathbf{r}) + \delta\varphi_{j\sigma}(\mathbf{r})|^2 - |\varphi_{j\sigma}(\mathbf{r})|^2 \quad (4.9)$$

must vanish to first order.

Up to here Eq. (4.5) has just been rewritten. The essential observation now is that an equation for the orbital shift $\psi_{j\sigma}$ exists which can be solved easily. Acting with the Kohn-Sham Hamiltonian and the Kohn-Sham eigenvalue on $\psi_{j\sigma}$, one obtains

$$(h_{S\sigma}(\mathbf{r}) - \epsilon_{j\sigma}) \psi_{j\sigma}(\mathbf{r}) = -(v_{xc\sigma}(\mathbf{r}) - u_{xcj\sigma}^*(\mathbf{r}) - (\bar{v}_{xcj\sigma} - \bar{u}_{xcj\sigma}^*)) \varphi_{j\sigma}(\mathbf{r}) \quad (4.10)$$

where

$$\bar{v}_{xcj\sigma} = \int \varphi_{j\sigma}^*(\mathbf{r}) v_{xc\sigma}(\mathbf{r}) \varphi_{j\sigma}(\mathbf{r}) d^3r \quad (4.11)$$

and

$$\bar{u}_{xcj\sigma} = \int \varphi_{j\sigma}^*(\mathbf{r}) u_{xcj\sigma}(\mathbf{r}) \varphi_{j\sigma}(\mathbf{r}) d^3r . \quad (4.12)$$

This equation is singular since to every solution the Kohn-Sham orbital $\varphi_{j\sigma}$ can be added. However, this ambiguity is resolved by the condition

$$\int \psi_{j\sigma}^*(\mathbf{r}) \varphi_{j\sigma}(\mathbf{r}) d^3r = 0 \quad (4.13)$$

which can be easily proven with the definition of $\psi_{j\sigma}$ (4.7). In the case of any degeneracies $\psi_{j\sigma}$ must be orthogonal to all orbitals $\varphi_{l\sigma}$ with $\epsilon_{l\sigma} = \epsilon_{j\sigma}$ [Kr92a].

To express the exchange-correlation potential in terms of the orbitals and orbital shifts one multiplies Eq. (4.8) with the exchange-correlation potential and replaces the term $v_{xc\sigma} \psi_{j\sigma}^*$ with the help of Eq. (4.10). Eq. (4.8) and the Kohn-Sham equations ($h_{S\sigma} - \epsilon_{j\sigma}) \varphi_{j\sigma}(\mathbf{r}) = 0$ can then be used to obtain

$$v_{xc\sigma}(\mathbf{r}) = \frac{1}{2n_{\sigma}(\mathbf{r})} \sum_{j=1}^{N_{\sigma}} \left\{ |\varphi_{j\sigma}(\mathbf{r})|^2 (u_{xcj\sigma}(\mathbf{r}) + (\bar{v}_{xcj\sigma} - \bar{u}_{xcj\sigma})) - \frac{\hbar^2}{m} \nabla \cdot (\psi_{j\sigma}^*(\mathbf{r}) \nabla \varphi_{j\sigma}(\mathbf{r})) \right\} + c.c. \quad (4.14)$$

Although still being an integral equation for the exchange-correlation potential, this equation can be solved semi-analytically [Kr92a]. Multiplying Eq. (4.14) by $|\varphi_{l\sigma}(\mathbf{r})|^2$ and integrating over space yields

$$\bar{v}_{xcl\sigma} = \bar{w}_{l\sigma} + \sum_{j=1}^{N_{\sigma}} M_{lj\sigma} (\bar{v}_{xcj\sigma} - \frac{1}{2}(\bar{u}_{xcj\sigma} + \bar{u}_{xcj\sigma}^*)) \quad (4.15)$$

where

$$\bar{w}_{l\sigma} = \int \frac{|\varphi_{l\sigma}(\mathbf{r})|^2}{n_{\sigma}(\mathbf{r})} \sum_{j=1}^{N_{\sigma}} \left\{ |\varphi_{j\sigma}(\mathbf{r})|^2 \frac{1}{2} (u_{xcj\sigma}(\mathbf{r}) + u_{xcj\sigma}^*(\mathbf{r})) - \frac{\hbar^2}{2m} \nabla \cdot (\psi_{j\sigma}^*(\mathbf{r}) \nabla \varphi_{j\sigma}(\mathbf{r}) + \psi_{j\sigma}(\mathbf{r}) \nabla \varphi_{j\sigma}^*(\mathbf{r})) \right\} d^3r \quad (4.16)$$

and

$$M_{lj\sigma} = \int \frac{|\varphi_{l\sigma}(\mathbf{r})|^2 |\varphi_{j\sigma}(\mathbf{r})|^2}{n_{\sigma}(\mathbf{r})} d^3r. \quad (4.17)$$

The matrix equation (4.15) determines the averaged terms $\bar{v}_{xcl\sigma}$. Again, the exchange-correlation potential is fixed only up to an additive constant. This is determined by the condition [Kr92b, Gra00]

$$\bar{v}_{xcN_{\sigma}\sigma} - \bar{u}_{xcN_{\sigma}\sigma} = 0. \quad (4.18)$$

This condition guarantees that the exchange-correlation potential vanishes at infinity for the regions dominated by the highest-occupied orbital. If this orbital has a nodal surface which extends out to infinity the potential does not vanish there and, as a consequence, the exchange-correlation potential goes to different asymptotic constants for

different spatial directions [Kr92b, Del02, Kü03b]. In a practical calculation Eq. (4.18) is simply enforced by restricting the sum in Eq. (4.15) to the first $N_\sigma - 1$ terms, i.e., by neglecting the term corresponding to the highest-occupied orbital φ_{N_σ} . The crucial point in Eq. (4.14) is that the exchange-correlation potential is expressed by just the occupied orbitals and their corresponding orbital shifts. Thus, in order to obtain the optimized effective potential only this equation and the ones for the orbital shifts and the orbitals must be solved self-consistently. This can be done in a straight-forward manner as discussed in Chap. 5 and [Kü03a, Kü03b].

Another advantage of replacing the integral equation (4.5) by the set of coupled differential equations is that one can easily construct an approximate solution to the exact optimized effective potential [Kr92a, Kr92b]. It is obtained by neglecting the terms involving the orbital shifts, i.e., neglecting the $\nabla \cdot (\dots)$ term. This approximation is called the KLI approximation [Kr92b, Gra00]. The exchange-correlation potential is given by

$$v_{xc\sigma}^{\text{KLI}}(\mathbf{r}) = \frac{1}{2n_\sigma(\mathbf{r})} \sum_{j=1}^{N_\sigma} |\varphi_{j\sigma}(\mathbf{r})|^2 (u_{xcj\sigma}(\mathbf{r}) + (\bar{v}_{xcj\sigma} - \bar{u}_{xcj\sigma})) + c.c. \quad (4.19)$$

Although this approximation gives excellent results for the energy and possesses many properties of the exact solution [Kr92a, Li93, Gra00], it can fail dramatically in some systems when response properties are calculated [Kü04a]. This is the reason for the importance of the exact solution scheme described above. In addition, this is also the reason why it is so desirable to have a solution scheme beyond the KLI approximation for the time-dependent equation derived in the next section.

4.2 Time-dependent OEP equation

In the original derivation of the time-dependent optimized effective potential equation [Ull95] Ullrich *et al.* have used the Runge-Gross action and required stationarity with respect to variations of the Kohn-Sham potential. Although this procedure leads to the correct result, it suffers from the deficiencies of the Runge-Gross action discussed in Chap. 2. Thus, the following derivation is based on the approach due to van Leeuwen which does not require any stationarity arguments [Lee98]. The starting point in this approach is an expression for the exchange-correlation action functional $A_{xc}[n]$ in terms of the Kohn-Sham orbitals, i.e., $A_{xc}[n] = A_{xc}[\{\varphi_{i\alpha}[n]\}]$. As shown in Chap. 2 the exchange-correlation potential is given by

$$v_{xc\sigma}(\mathbf{r}, t) = \left. \frac{\delta A_{xc}[\{\varphi_{i\alpha}[n]\}]}{\delta n_\sigma(\mathbf{r}, \tau)} \right|_{n_\sigma(\mathbf{r}, t)}. \quad (4.20)$$

In this expression the pseudotime τ parameterizes the Keldysh contour [Kel65, Lee96, Lee98, Lee01, Lee05] and $\delta / \delta n_\sigma(\mathbf{r}, \tau)|_{n_\sigma(\mathbf{r}, t)}$ is the derivative on the Keldysh contour

taken at the physical time-dependent density $n_\sigma(\mathbf{r}, t)$ [Lee98]. Using the functional chain rule and the Kohn-Sham density-response function $\chi_S(\mathbf{r}, \tau; \mathbf{r}', \tau')$ on the Keldysh contour, one can express the exchange-correlation potential on this contour by

$$\int \int_C \chi_{S\sigma,\sigma}(\mathbf{r}, \tau; \mathbf{r}', \tau') v_{xc\sigma}(\mathbf{r}', \tau') dt' d^3r' = \sum_{j=1}^{N_\sigma} \int \int_C \frac{\delta A_{xc}[\{\varphi_{i\tau}\}]}{\delta \varphi_{j\sigma}(\mathbf{r}', \tau')} \frac{\delta \varphi_{j\sigma}(\mathbf{r}', \tau')}{\delta v_{S\sigma}(\mathbf{r}, \tau)} + c.c. dt' d^3r'. \quad (4.21)$$

As in Chap. 2 the expression $\int_C dt'$ denotes $\int_{\tau_i}^{\tau_f} t'(\tau') d\tau'$ with $t'(\tau) = dt(\tau)/d\tau$. τ_i is the initial and τ_f the final pseudotime argument corresponding to the physical time t_0 . In a lengthy calculation (see Appendix A) the Kohn-Sham density-response function $\chi_S(\mathbf{r}, \tau; \mathbf{r}', \tau')$ and $\delta \varphi_{j\sigma}(\mathbf{r}', \tau')/\delta v_{S\sigma}(\mathbf{r}, \tau)$ can be evaluated on the Keldysh contour. Using the resulting expressions in Eq. (4.21) and transforming to physical time one obtains the integral equation

$$\sum_{j=1}^{N_\sigma} \frac{i}{\hbar} \int \int (v_{xc\sigma}(\mathbf{r}', t') - u_{xcj\sigma}(\mathbf{r}', t')) \varphi_{j\sigma}^*(\mathbf{r}', t') \varphi_{j\sigma}(\mathbf{r}, t) \times \sum_{k=1}^{\infty} \varphi_{k\sigma}^*(\mathbf{r}, t) \varphi_{k\sigma}(\mathbf{r}', t') \theta(t - t') dt' d^3r' + c.c. = 0 \quad (4.22)$$

where

$$u_{xcj\sigma}(\mathbf{r}, t) = \frac{1}{\varphi_{j\sigma}^*(\mathbf{r}, t)} \left. \frac{\delta A_{xc}[\{\varphi_{i\tau}\}]}{\delta \varphi_{j\sigma}(\mathbf{r}, \tau)} \right|_{\varphi_{i\tau} = \varphi_{i\tau}(\mathbf{r}, t)}. \quad (4.23)$$

This is the time-dependent optimized effective potential (OEP) equation for the exchange-correlation potential. As one can expect from the Runge-Gross theorem the exchange-correlation potential is fixed only up to a purely time-dependent function. Eq. (4.22) shows that the exchange-correlation potential at time t depends on all prior times t' . Solving this equation is an extremely demanding task due to the time integral and even for one-dimensional problems no such calculations have been performed up to date.

4.2.1 Transformation to coupled differential equations

To derive a practical solution scheme for the time-dependent OEP equation the integral equation for the potential is transformed into a set of coupled differential equations. As in the static case this can be done by defining orbital shifts $\psi_{j\sigma}$ [Ull95, Mu06a]. These shifts are given by

$$\psi_{j\sigma}(\mathbf{r}, t) := -\frac{i}{\hbar} \int \int (v_{xc\sigma}(\mathbf{r}', t') - u_{xcj\sigma}^*(\mathbf{r}', t')) \varphi_{j\sigma}(\mathbf{r}', t') \times \sum_{\substack{k=1 \\ k \neq j}}^{\infty} \varphi_{k\sigma}^*(\mathbf{r}', t') \varphi_{k\sigma}(\mathbf{r}, t) \theta(t - t') dt' d^3r'. \quad (4.24)$$

Again, this definition differs from the function $p_{j\sigma}(\mathbf{r}, t) = -\psi_{j\sigma}^*(\mathbf{r}, t)/\varphi_{j\sigma}^*(\mathbf{r}, t)$ used by Ullrich *et al.* [Ull95]. A straightforward calculation shows that $\psi_{j\sigma}$ satisfies the equation

$$(h_{S\sigma}(\mathbf{r}, t) - i\hbar\partial_t) \psi_{j\sigma}(\mathbf{r}, t) = -(v_{xc\sigma}(\mathbf{r}, t) - u_{xcj\sigma}^*(\mathbf{r}, t) - (\bar{v}_{xcj\sigma}(t) - \bar{u}_{xcj\sigma}^*(t))) \varphi_{j\sigma}(\mathbf{r}, t) \quad (4.25)$$

where

$$\bar{v}_{xcj\sigma}(t) = \int \varphi_{j\sigma}^*(\mathbf{r}, t) v_{xc\sigma}(\mathbf{r}, t) \varphi_{j\sigma}(\mathbf{r}, t) d^3r \quad (4.26)$$

and

$$\bar{u}_{xcj\sigma}(t) = \int \varphi_{j\sigma}^*(\mathbf{r}, t) u_{xcj\sigma}(\mathbf{r}, t) \varphi_{j\sigma}(\mathbf{r}, t) d^3r . \quad (4.27)$$

Due to the orthogonality of the time-dependent Kohn-Sham orbitals the relation

$$\int \psi_{j\sigma}^*(\mathbf{r}, t) \varphi_{j\sigma}(\mathbf{r}, t) d^3r = 0 \quad (4.28)$$

holds. With the definition of the time-dependent orbital shifts the integral equation for the exchange-correlation potential, Eq. (4.22), becomes

$$\sum_{j=1}^{N_\sigma} \psi_{j\sigma}^*(\mathbf{r}, t) \varphi_{j\sigma}(\mathbf{r}, t) + c.c. = g(\mathbf{r}, t) \quad (4.29)$$

where

$$g(\mathbf{r}, t) = \frac{i}{\hbar} \sum_{j=1}^{N_\sigma} |\varphi_{j\sigma}(\mathbf{r}, t)|^2 \int (\bar{u}_{xcj\sigma}(t') - \bar{u}_{xcj\sigma}^*(t')) \theta(t - t') dt' . \quad (4.30)$$

The function g vanishes for a large class of functionals including all functionals which depend on $\{\varphi_{i\alpha}\}$ only through the combination $\varphi_{i\alpha}(\mathbf{r}, t) \varphi_{i\alpha}^*(\mathbf{r}', t)$ [Gro96]. The best-known example for such a functional is the exact-exchange functional, Eq. (2.34). In analogy to the static case the exchange-correlation potential can be expressed in terms of the orbitals and orbital shifts. Multiplying Eq. (4.29) by $v_{xc\sigma}$ and using the time-dependent Kohn-Sham equations in combination with the equation-of-motion for $\psi_{j\sigma}$, one can deduce (see Appendix B)

$$v_{xc\sigma}(\mathbf{r}, t) + f(\mathbf{r}, t) = \frac{1}{2n_\sigma(\mathbf{r}, t)} \sum_{j=1}^{N_\sigma} \left\{ |\varphi_{j\sigma}(\mathbf{r}, t)|^2 (u_{xcj\sigma}(\mathbf{r}, t) + (\bar{v}_{xcj\sigma}(t) - \bar{u}_{xcj\sigma}(t))) - \frac{\hbar^2}{m} \nabla \cdot (\psi_{j\sigma}^*(\mathbf{r}, t) \nabla \varphi_{j\sigma}(\mathbf{r}, t)) \right\} + c.c. \quad (4.31)$$

The difference between the static and the time-dependent equation for $v_{xc\sigma}$ is given by

$$f(\mathbf{r}, t) = \frac{1}{2n_\sigma(\mathbf{r}, t)} \left\{ -\frac{\hbar^2}{2m} \nabla^2 g(\mathbf{r}, t) + i\hbar\partial_t \sum_{j=1}^{N_\sigma} (\psi_{j\sigma}^*(\mathbf{r}, t) \varphi_{j\sigma}(\mathbf{r}, t) - c.c.) \right\} . \quad (4.32)$$

Eq. (4.31) can be solved semi-analytically with the same procedure as in the static case. All orbitals, potentials, and orbital shifts are just replaced by their time-dependent analogon and $\bar{w}_{l\sigma}$ is slightly modified,

$$\bar{w}_{l\sigma}(t) = \bar{w}_{l\sigma}^{\text{stat}}(t) - \int |\varphi_{l\sigma}(\mathbf{r}, t)|^2 f(\mathbf{r}, t) d^3r. \quad (4.33)$$

Here, $\bar{w}_{l\sigma}^{\text{stat}}(t)$ is the static expression of $\bar{w}_{l\sigma}$ (Eq. (4.16)) with the time-dependent orbitals, potentials, and orbital shifts.

The previous equations show that the exact time-dependent OEP can be obtained by solving a set of coupled differential equations. However, the solution of these equations requires initial conditions for the orbitals and orbital shifts. In most real-time simulations the system of interest is in its ground state before the time-dependent external perturbation is turned on [U198b, Pet99, Cal00, Kun03, Rei03, And04, Ca04a, Chu05]. Thus, the ground-state orbitals and orbital shifts are natural candidates for the initial conditions. Since the system must remain stationary without a time-dependent external potential, it is necessary to prove that the time-dependent OEP scheme reduces to the static scheme in this situation. In order to prove that this is indeed the case the orbitals in Eq. (4.22) are replaced by the stationary solution $\varphi_{j\sigma}(\mathbf{r}, t_0) \exp(-i\epsilon_{j\sigma}(t-t_0)/\hbar)$ of the time-dependent Kohn-Sham equations with t_0 being an arbitrary time before the perturbation is turned on. It is reasonable to assume that in this situation the exchange-correlation part of the action reduces to the time integral over the exchange-correlation energy [Gro96]. Thus, the stationary orbital-dependent potential $u_{xcj\sigma}^{\text{stat}}$ becomes

$$u_{xcj\sigma}^{\text{stat}}(\mathbf{r}, t) = \frac{1}{\tilde{\varphi}_{j\sigma}^*(\mathbf{r})} \left. \frac{\delta E_{xc}[\{\tilde{\varphi}_{i\tau}\}]}{\delta \tilde{\varphi}_{j\sigma}(\mathbf{r})} \right|_{\tilde{\varphi}_i(\mathbf{r}) = \varphi_{i\sigma}(\mathbf{r}) \exp(-i\epsilon_{j\sigma}(t-t_0)/\hbar)}. \quad (4.34)$$

This expression does not depend on time if one makes the assumption that $E_{xc}[\{\tilde{\varphi}_{i\tau}\}]$ is invariant under phase transformations $\varphi_j \rightarrow \varphi_j \exp(-i\vartheta_j)$. This is quite reasonable since E_{xc} is a density functional and the density does not change under such transformations. The function g on the right-hand side of Eq. (4.29) also vanishes in this case because at some arbitrary time $u_{xcj\sigma}^{\text{stat}}$ can be chosen real-valued. The time-dependent optimized effective potential equation is then given by

$$\begin{aligned} & \sum_{j=1}^{N_\sigma} \frac{i}{\hbar} \int \int (v_{xc\sigma}^{\text{stat}}(\mathbf{r}') - u_{xcj\sigma}^{\text{stat}}(\mathbf{r}')) \varphi_{j\sigma}^*(\mathbf{r}') \varphi_{j\sigma}(\mathbf{r}') \\ & \times \sum_{\substack{k=1 \\ k \neq j}}^{\infty} \varphi_{k\sigma}^*(\mathbf{r}) \varphi_{k\sigma}(\mathbf{r}') \exp(-i(\epsilon_{j\sigma} - \epsilon_{k\sigma})(t-t')/\hbar) \theta(t-t') dt' d^3r' + c.c. = 0. \end{aligned} \quad (4.35)$$

The integral over t' can be calculated and one obtains the static optimized effective potential equation

$$\lim_{\eta \rightarrow 0^+} \sum_{j=1}^{N_\sigma} \int (v_{xc\sigma}^{\text{stat}}(\mathbf{r}') - u_{xcj\sigma}^{\text{stat}}(\mathbf{r}')) \varphi_{j\sigma}^*(\mathbf{r}') \varphi_{j\sigma}(\mathbf{r}') \sum_{\substack{k=1 \\ k \neq j}}^{\infty} \frac{\varphi_{k\sigma}^*(\mathbf{r}) \varphi_{k\sigma}(\mathbf{r}')}{\epsilon_{j\sigma} - \epsilon_{k\sigma} - i\eta} d^3r' + c.c. = 0.$$

For the last step it is necessary that the lower time boundary is $-\infty$. For a finite lower boundary the exchange-correlation potential has an unphysical time dependence due to memory effects (which are not properly accounted for by a finite time integral [Gro96]).

The same result can be obtained by working with the set of coupled differential equations instead of the integral equation. Since

$$\varphi_{j\sigma}(\mathbf{r}, t) = \varphi_{j\sigma}(\mathbf{r}, t_0) \exp\left(-i\epsilon_{j\sigma}(t - t_0)/\hbar\right) \quad (4.36)$$

holds for a time-independent Hamiltonian, Eq. (4.29) suggests

$$\psi_{j\sigma}(\mathbf{r}, t) = \psi_{j\sigma}(\mathbf{r}, t_0) \exp\left(-i\epsilon_{j\sigma}(t - t_0)/\hbar\right). \quad (4.37)$$

Feeding this ansatz into Eq. (4.25) and using the same arguments for $u_{xcj\sigma}^{\text{stat}}$ as above, one obtains

$$(h_{S\sigma}(\mathbf{r}) - \epsilon_{j\sigma}) \psi_{j\sigma}(\mathbf{r}, t_0) = -(v_{xc\sigma}(\mathbf{r}) - u_{xcj\sigma}^{\text{stat}*}(\mathbf{r}) - (\bar{v}_{xcj\sigma} - \bar{u}_{xcj\sigma}^{\text{stat}*})) \varphi_{j\sigma}(\mathbf{r}, t_0). \quad (4.38)$$

Thus, $\psi_{j\sigma}(\mathbf{r}, t_0)$ must satisfy the equation for the static orbital shifts. Since the difference f between the static and time-dependent equation for $v_{xc\sigma}$ also vanishes (Eq. (4.32)), the time-dependent scheme is reduced exactly to the static one for a system in its ground state.

4.2.2 Approximations to the time-dependent OEP

In addition to the previously mentioned advantages the orbital shifts also provide a good starting point for the construction of approximations to the exact OEP. The best-known approximation derived from Eq. (4.31) is the time-dependent KLI approximation already mentioned in the previous chapter. This approximation has been used successfully to calculate time-dependent processes in the linear, non-linear, and non-perturbative regime, e.g., ionization processes and high-harmonic generation. Applications of it can be found in various fields of physics, e.g., in atomic [Gro96, Ton98, Ton01, Chu05], molecular [Ch01a, Ch01b], and cluster physics [U198a, Ull00, Mar01, Vén01, Ngu04]. It is obtained from Eq. (4.31) by neglecting all terms involving $\psi_{j\sigma}$, i.e., by setting $\psi_{j\sigma}$ to zero. Since the neglected terms vanish when averaged over the density, i.e.,

$$\sum_{j=1}^{N_\sigma} \int \left\{ -\frac{\hbar^2}{m} \nabla \cdot (\psi_{j\sigma}^*(\mathbf{r}, t) \nabla \varphi_{j\sigma}(\mathbf{r}, t)) - i\hbar \partial_t (\psi_{j\sigma}^*(\mathbf{r}, t) \varphi_{j\sigma}(\mathbf{r}, t)) \right\} d^3r + c.c. = 0, \quad (4.39)$$

the time-dependent KLI approximation can be regarded as a mean field approximation to the exact potential [Gra00, Ull95]. The first part in Eq. (4.39) is zero since it can be transformed into a surface integral which gives no contribution for exponentially

decaying orbitals. Due to Eq. (4.28) the second part vanishes after interchanging the time derivative and the space integral. It is worth mentioning that it is possible that even without the space integral the term involving the time derivative vanishes. Since Eq. (4.29) is just an equation for the real part of $\sum_j \psi_{j\sigma}^* \varphi_{j\sigma}$ it is not possible to make any statement about the time derivative of the imaginary part. Evaluating the expression $i\hbar\partial_t \sum_{j=1}^{N_\sigma} (\psi_{j\sigma}^*(\mathbf{r}, t) \varphi_{j\sigma}(\mathbf{r}, t) - c.c.)$ with the equations-of-motion for the orbitals and orbital shifts (Eq. (2.26) and Eq. (4.25)) leads back to the equation for the exchange-correlation potential, Eq. (4.31). Thus, setting the term $i\hbar\partial_t \sum_{j=1}^{N_\sigma} (\psi_{j\sigma}^*(\mathbf{r}, t) \varphi_{j\sigma}(\mathbf{r}, t) - c.c.)$ to zero is in consistency with the equations for the orbitals, orbital shifts, and the exchange-correlation potential.

In order to go one step beyond the time-dependent KLI approximation one can generalize an idea of Krieger *et al.* and approximate the orbital shifts by [Mu06a]

$$\begin{aligned} \psi_{j\sigma}(\mathbf{r}, t) &\approx b_\sigma(t) (v_{xc\sigma}^{\text{KLI}}(\mathbf{r}, t) - u_{xcj\sigma}^*(\mathbf{r}, t) - (\bar{v}_{xcj\sigma}^{\text{KLI}}(t) - \bar{u}_{xcj\sigma}^*(t))) \varphi_{j\sigma}(\mathbf{r}, t) \\ &=: b_\sigma \tilde{\psi}_{j\sigma}(\mathbf{r}, t). \end{aligned} \quad (4.40)$$

This can be viewed as a natural extension of the time-dependent KLI approximation because by construction $\sum_{j=1}^{N_\sigma} \tilde{\psi}_{j\sigma}(\mathbf{r}) \varphi_{j\sigma}(\mathbf{r}, t) + c.c. = 0$, i.e., the approximate shifts formally fulfill an equation in analogy to the OEP equation. Like the exact orbital shifts the approximate orbital shifts are orthogonal to the corresponding Kohn-Sham orbitals. The real-valued $b_\sigma(t)$ is determined from the condition that the approximate orbital shifts $b_\sigma \tilde{\psi}_{j\sigma}(\mathbf{r}, t)$ fulfill Eq. (4.25) ‘on average’, i.e., summed over all j and integrated over space. This condition leads to the equation

$$i\hbar\partial_t b_\sigma(t) = 1 - a_\sigma(t) b_\sigma(t) \quad (4.41)$$

for $b_\sigma(t)$ where

$$a_\sigma(t) = \frac{\sum_{j=1}^{N_\sigma} \int \tilde{\psi}_{j\sigma}^*(\mathbf{r}, t) (i\hbar\partial_t - h_{S\sigma}(\mathbf{r}, t)) \tilde{\psi}_{j\sigma}(\mathbf{r}, t) d^3r}{\sum_{j=1}^{N_\sigma} \int \tilde{\psi}_{j\sigma}^*(\mathbf{r}, t) \tilde{\psi}_{j\sigma}(\mathbf{r}, t) d^3r}. \quad (4.42)$$

For a stationary state the exchange-correlation potential and the orbital-dependent potential in Eq. (4.40) are time-independent and thus, $i\hbar\partial_t \tilde{\psi}_{j\sigma}(\mathbf{r}, t) = \epsilon_{j\sigma} \tilde{\psi}_{j\sigma}(\mathbf{r}, t)$ holds. This observation can be used to avoid the critical evaluation of the time derivative of the orbital shifts in Eq. (4.42) by making the ‘adiabatic’ approximation

$$\sum_j \int \tilde{\psi}_{j\sigma}^*(\mathbf{r}, t) i\hbar\partial_t \tilde{\psi}_{j\sigma}(\mathbf{r}, t) d^3r \approx \sum_j \int \tilde{\psi}_{j\sigma}^*(\mathbf{r}, t) \epsilon_j(t) \tilde{\psi}_{j\sigma}(\mathbf{r}, t) d^3r \quad (4.43)$$

where $\epsilon_{j\sigma}(t) = \langle \varphi_{j\sigma}(t) | h_{S\sigma}(t) | \varphi_{j\sigma}(t) \rangle$. As a consequence of this approximation, the right-hand side of Eq. (4.41) becomes purely real and, since $b_\sigma(t)$ is also real, the time derivative of $b_\sigma(t)$ must vanish leading to $b_\sigma(t) = b_\sigma(0)$. The initial value $b_\sigma(0)$ is obtained from the corresponding ground-state formalism [Kr92b, Mu06a]. It is interesting to note that the same result can be obtained by assuming that $\int \tilde{\psi}_{j\sigma}^*(\mathbf{r}, t) i\hbar\partial_t \tilde{\psi}_{j\sigma}(\mathbf{r}, t) d^3r$ is

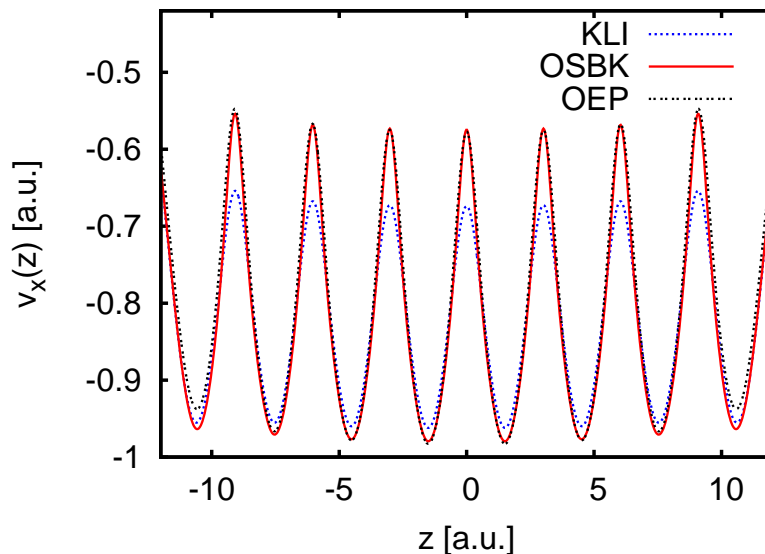


Figure 4.1: The exact-exchange potential of a one-dimensional H_{16} chain with alternating bond lengths of one and two a_0 . The difference between the exact OEP potential and the 'one-step beyond KLI' result hardly can be seen. Nevertheless the static polarizability is considerably different – see Tab. 4.1.

purely real or, in other words, by excluding any exponentially growing or decreasing solutions.

At present not many applications of the previous approximation exist. However, in the case of a one-dimensional Hydrogen chain in combination with the exact-exchange potential the results are quite promising. As discussed in more detail in the next chapter Hydrogen chains provide a severe benchmark for approximations to the exact OEP. As Fig. 4.1 shows, the previous approximation, labeled 'OSBK', is almost identical to the exact-exchange OEP. For comparison, the KLI potential differs clearly from the exact potential. Although the 'OSBK' potential is very similar to the exact OEP, the polariz-

	α^{KLI}	α^{OSBK}	α^{OEP}	Δ
H_8	29.1	28.3	27.0	62
H_{12}	51.6	49.4	46.2	59
H_{16}	75.4	71.5	66.0	59

Table 4.1: Static polarizability of three different H chains in different approximations. The values were obtained from applying a small finite electric field and are given in a.u. $\Delta = (\alpha^{\text{OSBK}} - \alpha^{\text{OEP}})/(\alpha^{\text{KLI}} - \alpha^{\text{OEP}})$ is given in %.

ability can differ considerably as Tab. 4.1 shows. Nevertheless the ‘OSBK’ approximation improves significantly upon the polarizabilities obtained from the standard KLI approximation. Beside this improvement the ‘OSBK’ approximation also offers a possibility to get an idea about the quality of the approximate potentials in situations where the exact OEP is not known. In any case the ‘OSBK’ approximation offers a promising method to go beyond the standard KLI approximation at very low computational cost.

Chapter 5

Numerical study of the OEP

In Chap. 4 the static and the time-dependent optimized effective potential equation have been derived and transformed into a set of coupled differential equations. Since it is in general not possible to solve these equations analytically, a numerical treatment is necessary. In the present chapter numerical methods to solve the set of differential equations are investigated. For the exchange-correlation functional the exact-exchange orbital functional, Eq. (2.34), is used.

5.1 Introductory remarks

The physical systems studied in the following are molecular chains of hydrogen atoms with alternating bond lengths. Since for these systems the KLI approximation fails dramatically [Gis99, Kü04a], such chains provide a severe benchmark for the quality of the full OEP. Although not existing in nature, hydrogen chains are chosen since they mimic the same features as more complicated molecular chains, e.g., high and directional electron mobility and large response coefficients. At the same time they possess a simple electronic structure with one electron per atom. In addition, hydrogen chains are the most difficult to describe due to the importance of the self-interaction error for single Hydrogen atoms.

To reduce the numerical effort the movement of the electrons is restricted to one dimension. This restriction has the additional advantage that one can easily plot and study all quantities, e.g., the Kohn-Sham potential. Especially for developing new methods this is a huge benefit. However, using a one-dimensional grid also has a drawback: the use of the standard Coulomb interaction is not possible. One has to replace it by a ‘soft’ Coulomb potential given by $-1/\sqrt{z^2 + 0.3}$ [Jav88, Lei05] with z being the spatial coordinate. The reason for this is that in one dimension electrons are not able to pass each other due to the singularity in the Coulomb potential. Despite the modified interaction, the one-dimensional approximation leads to qualitatively reasonable results as can be seen in Fig. 5.1. There, the exact-exchange ground-state potential of H_8 in

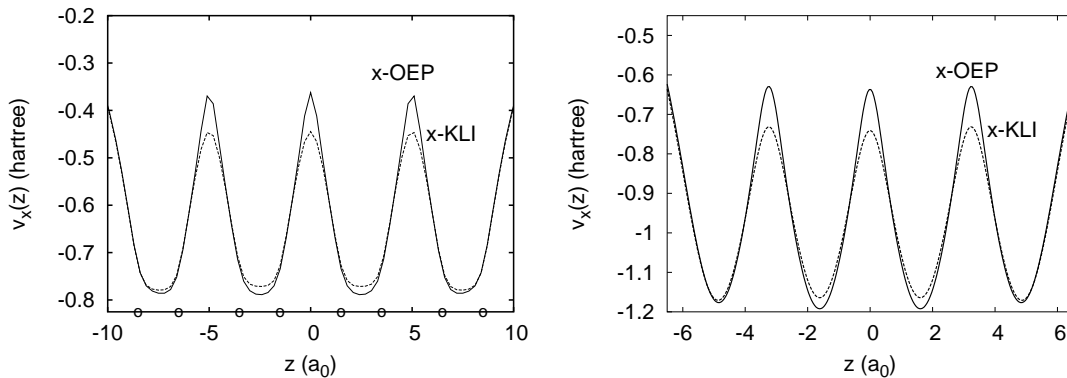


Figure 5.1: Exchange potential v_x of H_8 in the ground state. The exact potential and the KLI potential are plotted. Left: v_x from a calculation in three dimensions taken from [Kü04a]. Right: v_x from a calculation in one dimension with alternating H-H distances of 1.2 and 2.0 a_0 . In both cases the qualitative features are the same.

one dimension and in three dimensions is plotted. Clearly, the shapes of the potential are very similar.

5.2 Static OEP and Kohn-Sham equations

In the following an equidistant real-space grid is used for the description of the system. The grid consists of 800 grid points with a spacing of $\Delta = 0.05 a_0$. Outside the grid the Kohn-Sham orbitals vanish. This real-space approach has several advantages over other methods, e.g., Gaussian basis functions. First, the real-space grid is one of the most unbiased basis sets since the only parameters are the number of grid points and the grid spacing. Second, real-space methods are very intuitive and can be easily parallelized [Kro06]. These aspects are especially important from a practical point of view. Finally, real-space grids are clearly superior to basis functions in situations in which the shape of the density changes dramatically [Cal00, Ma03b]. This fact is especially important if one is interested in a description of strong non-linear processes, e.g., ionization processes, within time-dependent DFT.

To construct the optimized effective potential an iterative procedure based on the Kohn-Sham orbitals and orbital shifts is used [Kü03a, Kü03b, Kü04b]. The main idea in this approach is to solve the Kohn-Sham equations (Eq. (2.21)), the equations for the orbital shifts (Eq. (4.10)) and the equation for the exchange-correlation potential (Eq. (4.14)) self-consistently by an iterative procedure. The starting point for this iteration is a guess for the Kohn-Sham orbitals $\varphi_{j\sigma}$. With these orbitals the KLI potential is constructed as a first approximation. This approximation for the potential can then be used to solve the Kohn-Sham equations for the N_σ lowest eigenvalues and corresponding orbitals. With the new orbitals the potential can be updated and the new lowest eigen-

values and orbitals can be calculated. This procedure is repeated until self-consistency is obtained. From the resulting quantities one can then calculate a first guess for the orbital shifts $\psi_{j\sigma}$ via Eq. (4.10) and the orthogonality condition, Eq. (4.13). With these orbital shifts a better approximation for $v_{xc\sigma}$ can be constructed. Then the Kohn-Sham equations are again solved self-consistently but this time with *fixed* exchange-correlation potential. With the resulting eigenvalues and orbitals one can construct new orbital shifts and a new $v_{xc\sigma}$. This is done until self-consistency with respect to the orbitals, orbital shifts and the Kohn-Sham potential is obtained.

Going through this procedure, one can see that three different problems must be tackled. First, it is necessary to solve the eigenvalue equation for a fixed Hamiltonian. Second, for a given potential and given orbitals Eq. (4.10) must be solved to obtain the orbital shifts. Finally, Eq. (4.14) must be evaluated to obtain the exchange-correlation potential. In the following all three tasks will be discussed separately.

5.2.1 Solving the eigenvalue equation

To solve the eigenvalue problem for a fixed Hamiltonian it is necessary to approximate the kinetic energy on the real-space grid. This is done by a discrete approximation to the Laplacian. Since in one dimension one can afford to work with a small grid spacing, the lowest order approximation is sufficient. In one dimension it is given by [Pre92, Ame92, Tve98]

$$\left. \frac{d^2}{dz^2} f(z) \right|_{z=z_i} \approx \frac{f(z_{i+1}) - 2f(z_i) + f(z_{i-1}))}{\Delta^2} \quad (5.1)$$

Thus, the Kohn-Sham Hamiltonian is represented by a sparse matrix with the elements

$$(h_{S\sigma})_{ij} = \left(\frac{\hbar^2}{m\Delta^2} + v_{S\sigma}(z_i) \right) \delta_{i,j} - \frac{\hbar^2}{2m\Delta^2} (\delta_{i,j-1} + \delta_{i,j+1}) . \quad (5.2)$$

A well suited algorithm for obtaining only the lowest eigenvectors and eigenvalues of such sparse matrices is the damped gradient algorithm [Rei82, Blu92, Kü04b]. This algorithm makes use of the fact that matrix-vector multiplications with sparse matrices can be carried out very fast due to the simple structure of the matrix. The main idea of this algorithm is to project out the eigenvalue of each eigenvector by applying $h_{S\sigma}$ to a first guess and then damping the eigenvectors corresponding to higher eigenvalues stronger than the eigenvector of the lowest eigenvalue. After repeating this procedure often enough just the lowest eigenvalue and eigenvector survives. To obtain the higher eigenvalues the lower eigenvectors are projected out from the iterative solution after each step and thus, the next larger eigenvalue is found. To clarify the exact procedure the different steps with suppressed arguments and spin indices are given in detail in the next paragraph.

First, one makes a guess for φ_j and initializes

$$\varphi_j^{(0)} = \varphi_j^{(\text{init})} \quad , \quad j = 1, \dots, N . \quad (5.3)$$

This guess should not be orthogonal to any of the N exact eigenvectors. Then the iteration is carried out for increasing $j = 1, \dots, N$ according to

$$\begin{aligned}\varphi'_j &= \varphi_j^{(p)} - \frac{\delta}{T + E_{\text{inv}}} (h_S - \langle \varphi_j^{(p)} | h_S | \varphi_j^{(p)} \rangle) \varphi_j^{(p)} \\ \varphi''_j &= \varphi'_j - \sum_{k=1}^{j-1} \varphi_k^{(p)} \langle \varphi_k^{(p)} | \varphi'_j \rangle \\ \varphi_j^{(p+1)} &= [\langle \varphi''_j | \varphi''_j \rangle]^{-1/2} \varphi''_j .\end{aligned}\tag{5.4}$$

In the case of H_4 the step size is $\delta = 1.5$ and $E_{\text{inv}} = 4.5$ a.u. is chosen. In general, $\delta \approx 1$ can be chosen and E_{inv} should be roughly the depth of the Kohn-Sham potential. In the first equation the inverse of the kinetic operator T is needed. However, the full inversion of this operator can be avoided by solving the inhomogeneous linear equation

$$(T + E_{\text{inv}}) \phi = (h_S - \langle \varphi_j^{(p)} | h_S | \varphi_j^{(p)} \rangle) \varphi_j^{(p)}\tag{5.5}$$

in order to obtain

$$\phi = \frac{1}{T + E_{\text{inv}}} (h_S - \langle \varphi_j^{(p)} | h_S | \varphi_j^{(p)} \rangle) \varphi_j^{(p)} .\tag{5.6}$$

To measure the accuracy of an approximate eigenvalue the energy variance is used, i.e.,

$$\Delta\epsilon = \sqrt{\langle \varphi_j | h_S^2 | \varphi_j \rangle - \langle \varphi_j | h_S | \varphi_j \rangle^2} .\tag{5.7}$$

The iteration is carried on until the variance for all φ_j is smaller than a given accuracy. This is chosen to be $5.0 \cdot 10^{-6}$ a.u.

For the self-consistent solution of the Kohn-Sham equations (with constant orbital shifts) the same criterion is used. With the new orbitals the Hamiltonian is updated and Eq. (5.7) is evaluated with the new h_S . Again, if the variance is small enough the iteration of the Kohn-Sham equations is terminated. During the whole procedure it is not necessary to fully converge the eigenvalues for a fixed Hamiltonian since this Hamiltonian changes in the next step. Instead of calculating the ‘exact’ eigenvalues for each fixed Hamiltonian, the Kohn-Sham potential is recalculated each time the φ_j are updated according to Eq. (5.4) until $\Delta\epsilon \leq 5.0 \cdot 10^{-6}$ for all orbitals.

5.2.2 Obtaining the orbital shifts

At first sight the determination of the orbital shifts $\psi_{j\sigma}$ for given Kohn-Sham orbitals and potential seems to be a trivial task. All one has to do is to solve the inhomogeneous linear equation (4.10). However, solving this inhomogeneous linear equation is by no means trivial. The reason for this is, as already mentioned in Chap. 4, that Eq. (4.10) is singular. Only with the additional orthogonality condition it can be uniquely solved. Thus, a special numerical procedure is needed to obtain just the inhomogeneous solution. One such algorithm is the singular value decomposition [Pre92]. But since this algorithm is

too expensive for the present purpose, a different method, namely the conjugate gradient method [Pre92, Gre97], is used [Kü03a]. In this method the solution of a linear equation is constructed iteratively from an initial guess $\psi_{j\sigma}^{\text{init}}$. Writing Eq. (4.10) in the form $A_{j\sigma}\psi_{j\sigma} = rs_{j\sigma}$, the first correction to the initial guess is proportional to $rs_{j\sigma} - A_{j\sigma}\psi_{j\sigma}^{\text{init}}$. This correction is orthogonal to $\varphi_{j\sigma}$ because $A_{j\sigma}\varphi_{j\sigma} = 0$ and $\varphi_{j\sigma} \perp rs_{j\sigma}$. Since the following steps proceed analogously, the final result is also orthogonal to $\varphi_{j\sigma}$ if $\psi_{j\sigma}^{\text{init}}$ is chosen orthogonal to $\varphi_{j\sigma}$. In a practical calculation $\psi_{j\sigma}^{\text{init}} \equiv 0$ is chosen to satisfy this constraint. Numerical inaccuracies in the process can lead to contributions of $\varphi_{j\sigma}$ in $\psi_{j\sigma}$ but these can be easily removed by an orthogonalization procedure. Since the conjugate gradient method is an iterative procedure, it requires a stop criterion. Different possibilities for this exist [Pre92]. For the present calculations the iteration is stopped if $\psi_{j\sigma}$ satisfies

$$\frac{|A_{j\sigma}\psi_{j\sigma} - rs_{j\sigma}|}{|rs_{j\sigma}|} < 5.0 \cdot 10^{-6} . \quad (5.8)$$

with $|\dots|$ being the standard vector norm.

5.2.3 Evaluating the exchange-correlation potential

To obtain the exact optimized effective potential one last step has to be taken: the construction of the potential for given orbitals and orbital shifts according to Eq. (4.14). Two problems must be tackled for this. First, the averaged values $\bar{v}_{xcj\sigma} - \bar{u}_{xcj\sigma}$ must be obtained. This can be done either by the procedure described below Eq. (4.14) or by an iterative process. In the iterative method $v_{xcj\sigma}$ is calculated with an initial guess for $\bar{v}_{xcj\sigma} - \bar{u}_{xcj\sigma}$. With this new $v_{xcj\sigma}$ one can calculate new values for $\bar{v}_{xcj\sigma} - \bar{u}_{xcj\sigma}$. Again, these can be used to obtain a better potential. This is done until convergence is achieved. The convergence is checked by

$$\frac{|v_{xcj\sigma}^{(p+1)} - v_{xcj\sigma}^{(p)}|}{N_{\text{grid}}} < \delta_v \quad (5.9)$$

with N_{grid} the number of grid points, p the iteration index, and $\delta_v = 5.0 \cdot 10^{-6}$. The second problem associated with Eq. (4.14) is the evaluation of the density denominator. Analytically this is not a problem since $\frac{|\varphi_{j\sigma}(\mathbf{r})|^2}{n_\sigma(\mathbf{r})} \leq 1$ and the orbital shifts fall off at least as fast as the corresponding orbitals or even faster [Del01, Kü03b, Kör06]. Nevertheless numerical inaccuracies can strongly magnify during the iteration and spoil the whole procedure. For the ground-state KLI potential the problem is not severe because the inaccuracies in the denominator are canceled by the inaccuracies of $|\varphi_{j\sigma}(\mathbf{r})|^2$ in the numerator. But for the exact potential including the $\nabla \cdot (\dots)$ term the division by the density is critical. A detailed discussion of the encountered problems can be found in the diploma thesis of Körzdörfer [Kör06]. In the present context these problems are circumvented by adding a suitable chosen function to the density, i.e., replacing the

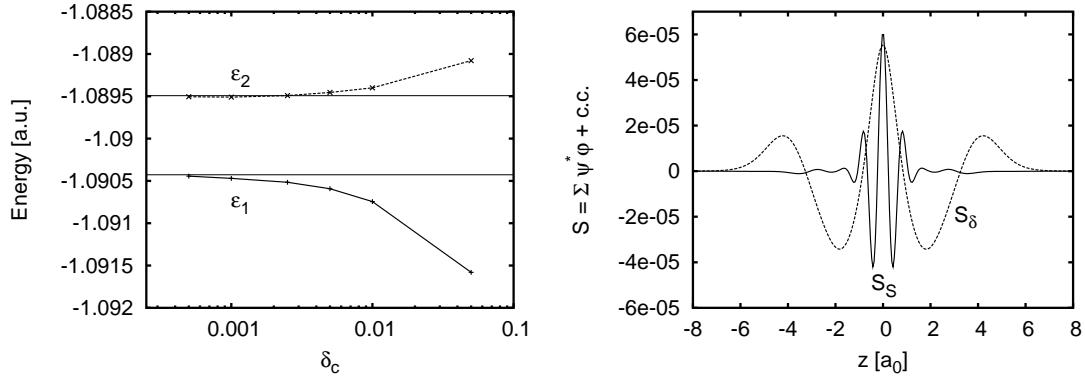


Figure 5.2: Left: Energy of the occupied Kohn-Sham eigenvalues in dependence of the cut-off δ_c for H_4 . The higher eigenvalue ϵ_2 is shifted down by 0.1625 a.u. The horizontal bars indicate the values obtained by the iteration scheme without cut-off parameter. Right: The function S at the end of the iteration. S_δ indicates the result obtained with a cut-off $\delta_c = 0.001$. S_S is the result obtained by updating v_x according to Eq. (5.11).

$1/n_\sigma(\mathbf{r})$ by $1/(n_\sigma(\mathbf{r}) + f_{\text{cut}}(\mathbf{r}))$. The simplest choice for the added function is $f_{\text{cut}} \equiv \delta_c$ with δ_c being a constant. Since it is not guaranteed that this procedure can yield the correct OEP, this workaround should be rather considered as an approximation than a way to construct the exact OEP. In the limit $\delta_c \rightarrow \infty$ the approximation reduces to the KLI approximation.

Despite its approximative character the just described procedure can lead to very accurate results as Tab. 5.1 and Fig. 5.2 shows. In this figure the lowest eigenvalues for an H_4 chain are shown for different δ_c . For comparison the values obtained from a different method (see below) are also indicated by horizontal bars. Since this method does not have any cut-off parameter, it serves as a benchmark for the iteration using δ_c . Fig. 5.2 also shows the function S (defined in Eq. (5.10)) for both schemes. Since this function vanishes for the exact potential, it is a measure for the quality of the obtained solution. Both figures and the values in Tab. 5.1 clearly demonstrate that the method presented above can be used to obtain reliable results, at least for H_4 .

	E_{tot}	E_{kin}	E_{H}	E_{x}	E_{ext}
S -method	-7.8715	0.8374	5.9325	-2.2385	-12.4029
δ_c -method	-7.8715	0.8372	5.9323	-2.2384	-12.4027

Table 5.1: Electronic energies of H_4 in a.u. obtained from different iteration schemes. S -method denotes the iterative procedure of [Kü03a]. The δ_c -method uses the explicit formula with $\delta_c = 0.001$ for v_x . The alternating distance between H atoms is 1 and 2 a_0 . The grid consists of 800 grid points with a distance of 0.05 a_0 .

Before finishing this section, a brief description of a different scheme for obtaining the static exchange-correlation potential must be presented [Kü03a]. Instead of evaluating Eq. (4.14), this method uses the function

$$S_\sigma(\mathbf{r}) = \sum_{j=1}^{N_\sigma} \psi_{j\sigma}^*(\mathbf{r}) \varphi_{j\sigma}(\mathbf{r}) + c.c. \quad (5.10)$$

which, as already pointed out above, is a measure for the error inherent in an approximative solution. For given orbitals and orbital shifts the function S can be calculated and used to construct a new exchange-correlation potential according to

$$v_{xc\sigma}^{(p+1)}(\mathbf{r}) = v_{xc\sigma}^{(p)}(\mathbf{r}) + c S_\sigma(\mathbf{r}) . \quad (5.11)$$

Eq. (4.18) is subsequently enforced by adding the constant $\bar{u}_{xcN_\sigma\sigma} - \bar{v}_{xcN_\sigma\sigma}^{(p+1)}$ to the potential. With the new potential at hand one can calculate new orbitals and orbital shifts which give rise to a new S . The parameter $c > 0$ in Eq. (5.11) has the dimension energy times volume. For H_4 convergence is achieved for a value of approx. 3 in atomic units. The main advantage of this method is that it does not require the evaluation of Eq. (4.14), i.e., it avoids all problems associated with the division by the density.

5.3 Time-dependent OEP and Kohn-Sham equations

The presented algorithm to construct the ground-state exchange-correlation potential suggests a method to obtain the time-dependent potential. Again, the idea is to use the orbital shifts $\psi_{j\sigma}$ to get the potential. In order to do this it is necessary to solve the coupled set of equations consisting of the time-dependent Kohn-Sham equations (Eq. (2.26)), the equations-of-motion for the orbital shifts (Eq. (4.25)), and the equation for $v_{xc\sigma}$ (Eq. (4.31)). For the time-dependent Kohn-Sham equations a formal solution can be given in terms of the propagator (see, e.g., [Sha80])

$$\varphi_{j\sigma}(\mathbf{r}, t) = U(t, t_0) \varphi_{j\sigma}(\mathbf{r}, t_0) = \mathcal{T} \exp \left\{ -\frac{i}{\hbar} \int_{t_0}^t h_{S\sigma}(\mathbf{r}, t') dt' \right\} \varphi_{j\sigma}(\mathbf{r}, t_0) . \quad (5.12)$$

$\mathcal{T} \exp\{\dots\}$ is the time-ordered exponential. In more detail the propagator $U(t, t_0)$ is given by

$$U(t, t_0) = \sum_{k=0}^{\infty} \frac{(-i\hbar)^k}{k!} \int_{t_0}^t \dots \int_{t_0}^t \mathcal{T} \{ h_{S\sigma}(\mathbf{r}, t_1) \dots h_{S\sigma}(\mathbf{r}, t_k) \} dt_1 \dots dt_k . \quad (5.13)$$

Using the property $U(t, t_0) = U(t, t_1)U(t_1, t_0)$, the full propagator can be transformed into the numerically much more convenient form

$$U(t, t_0) = \prod_{k=0}^{N-1} U(t_0 + (k+1)\Delta t, t_0 + k\Delta t) . \quad (5.14)$$

For small time steps Δt many approximations for $U(t + \Delta t, t)$ exist [Ca04b]. One of the most well-known approximative propagation schemes is the Crank-Nicolson method [Pre92, Ame92] which uses (indices suppressed)

$$U(t + \Delta t, t) \approx \frac{1 - i\frac{\Delta t}{2} h_S(\mathbf{r}, t + \Delta t/2)/\hbar}{1 + i\frac{\Delta t}{2} h_S(\mathbf{r}, t + \Delta t/2)/\hbar}. \quad (5.15)$$

Like the true propagator this approximation is unitary and preserves time-reversal symmetry. To avoid the inversion of an operator the orbitals $\varphi(\mathbf{r}, t + \Delta t)$ are obtained from the linear equation

$$\left[1 + i\frac{\Delta t}{2} h_S(\mathbf{r}, t + \Delta t/2)/\hbar\right] \varphi(\mathbf{r}, t + \Delta t) = \left[1 - i\frac{\Delta t}{2} h_S(\mathbf{r}, t + \Delta t/2)/\hbar\right] \varphi(\mathbf{r}, t) \quad (5.16)$$

which can be efficiently solved since h_S is a sparse matrix. This algorithm will be used in the following.

Before looking at the equation-of-motion for the orbital shifts, the self-consistency of the Hamiltonian must be discussed. For a given time-dependent Hamiltonian one can easily propagate the orbitals up to any time t . But for the Kohn-Sham equations the potential, and thus the Hamiltonian, depends on the orbitals via the density, i.e., the time-dependent Hamiltonian is not known at the beginning. Nevertheless Eq. (5.16) can be used to obtain the solution of the Kohn-Sham equations via an iterative procedure. First, one propagates the orbitals with $h_S(\mathbf{r}, t)$ to obtain a first guess for $\varphi(\mathbf{r}, t + \Delta t)$. With the new orbitals an approximate $h_S(\mathbf{r}, t + \Delta t)$ can be calculated. Using the interpolation $h_S(\mathbf{r}, t + \Delta t/2) \approx (h_S(\mathbf{r}, t) + h_S(\mathbf{r}, t + \Delta t))/2$, a better approximation for $\varphi(\mathbf{r}, t + \Delta t)$ is obtained. After this the same procedure is repeated until convergence is achieved. For small time steps it is very often sufficient to use just one iteration. For a time-dependent KLI calculation or a calculation using an explicit density functional all required procedures are known at this point. However, for the full time-dependent optimized effective potential the orbital shifts must be also taken into account. Since this has not been done before, the next subsection is devoted to the question if it is possible to construct the exact time-dependent potential from the propagated orbitals and orbital shifts.

5.3.1 Study of the coupled equations for the orbitals and orbital shifts

In order to construct the exact time-dependent OEP via the orbital shifts it is necessary to find an algorithm to propagate them in time, i.e., to solve Eq. (4.25). The simplest differencing scheme for this equation is obtained by a simple time centering (again indices are suppressed)

$$i\hbar \frac{\psi(\mathbf{r}, t + \Delta t) - \psi(\mathbf{r}, t)}{\Delta t} = h_S(\mathbf{r}, t + \Delta t/2) \frac{1}{2} (\psi(\mathbf{r}, t + \Delta t) + \psi(\mathbf{r}, t)) + \frac{1}{2} (rs(\mathbf{r}, t + \Delta t) + rs(\mathbf{r}, t)) \quad (5.17)$$

where $rs(\mathbf{r}, t)$ is the inhomogeneity

$$rs(\mathbf{r}, t) = (v_{xc}(\mathbf{r}, t) - u_{xc}^*(\mathbf{r}, t) - (\bar{v}_{xc}(t) - \bar{u}_{xc}^*(t))) \varphi(\mathbf{r}, t) . \quad (5.18)$$

The complete propagation scheme consists of the following steps (with space coordinates neglected):

1. Given the Hamiltonian $h_S(t)$ a first guess for $\varphi(t + \Delta t)$ and thus for $u_{xc}^*(t + \Delta t)$ and $\bar{u}_{xc}^*(t + \Delta t)$ is calculated via Eq. (5.16).
2. With the quantities from the previous step the orbital shifts $\psi(t)$ are propagated with Eq. (5.17) to obtain a first guess for $\psi(t + \Delta t)$. In this step the unknown quantities $h_S(t + \Delta t/2)$ and $v_{xc}(t + \Delta t/2)$ are approximated by the corresponding quantities at time t , i.e., $h_S(t)$ and $v_{xc}(t)$.
3. $h_S(t + \Delta t)$ and $v_{xc}(t + \Delta t)$ (via Eq. (4.31)) are obtained. In addition, $h_S(t + \Delta t/2) \approx (h_S(t) + h_S(t + \Delta t))/2$ is calculated.
4. Given $h_S(t + \Delta t/2)$ an improved approximation for $\varphi(t + \Delta t)$ is constructed. This procedure is repeated until self-consistency is obtained.

As a first test the most simple situation is considered, namely the propagation of the ground state. For this special case the exact solution is known: both orbitals and orbital shifts should just obtain a phase factor $\exp(-i\epsilon_{j\sigma}(t - t_0)/\hbar)$ and the exchange-correlation potential as well as all observables should stay unchanged. As a typical result Fig. 5.3 shows the resulting dipole moment $e \int z n(z, t) dz$. One can clearly see that it does not stay zero like it should, but starts to oscillate with increasing amplitude. The same observation is made for the total energy and other observables. Different values for the time step and the grid spacing do not change the results qualitatively, and neither does using other external potentials, e.g., harmonic ones.

To clarify the nature of this instability several tests have been carried out. First, different splitting schemes (cf. Ref. [Ame92], and Appendix C) for the orbital shifts have been tested, namely an implicit scheme, an explicit one and a predictor-corrector method. Additionally, a split-operator scheme [Pre92] using a Crank-Nicolson step for the homogenous part of the orbital shift propagation and different methods for the inhomogeneous part have been tested. Generally, none of these methods solves the encountered problems.

As a second test one can carry out a procedure to circumvent problems stemming from the required self-consistency of the coupled equations. In this procedure one first does a KLI calculation and saves the resulting exchange potential for all times. Then one propagates the orbital shifts with the saved KLI potential. Thus one obtains a first approximation for the time-dependent orbital shifts. From these shifts one can calculate a new approximation for the exchange potential at all times and propagate the

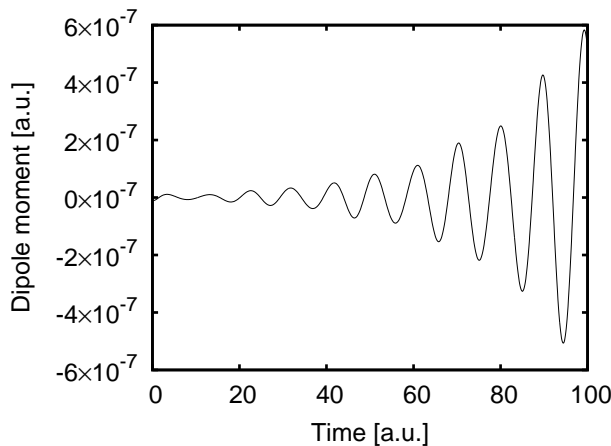


Figure 5.3: The time evolution of the dipole moment from the coupled propagation of the KS orbitals and orbital shifts. The initial state is the ground state and no external time-dependent potential is applied. Thus, the correct solution would be a straight line at zero. Other observables, e.g., the total energy, show the same oscillations with increasing amplitude.

orbitals in this *fixed* potential (the Hartree part is still calculated dynamically). After this one propagates the orbital shifts again with the new orbitals and obtains a new approximation for the exchange potential. This procedure is repeated until convergence is achieved. Again, the solution shows the same instabilities.

Finally, one can do a simple ‘linearization’ by fixing the exchange-correlation potential and propagating orbitals and orbital shifts without other restrictions. This leads to a stable solution. In a next step, which goes beyond this most simple linearization, one can use the exact time-dependence for the orbitals, i.e., the $\varphi_j(\mathbf{r}, t)$ are calculated not from a numerical propagation but from the numerically obtained ground-state orbitals multiplied with the analytically known phase factor $\exp(-i\epsilon_{j\sigma}(t - t_0)/\hbar)$ (see Chap. 4). The orbital shifts are numerically propagated and v_{xc} is evaluated numerically according to Eq.(4.31). In this way the non-linearities in Eq. (4.25) are fully taken into account, but not the coupling between Eq. (4.25) and Eq. (2.26). The result is that the calculation is stable and the exchange-correlation potential and the orbital shifts show the behavior expected from the exact solution. Reversing the role of orbitals and orbital shifts, i.e., propagating the shifts analytically and the orbitals numerically, leads to the same result, i.e., a stable and correct solution.

From this observation one concludes that the coupling between the orbitals and the orbital shifts seems to be the crucial problem and not the separate differential equations. This is supported by the observation that the cut-off of the $1/n$ term influences the instability. For a large value of δ the influence of the term containing the orbitals and orbital shifts is reduced and one can observe a slower increasing amplitude of the

oscillations. As previously mentioned in the limit $\delta \rightarrow \infty$ the KLI approximation is obtained which is found to be perfectly stable.

In general, since the whole scheme is based on non-linear, coupled partial differential equations, any exact statement about existence and stability of a solution is highly non-trivial from a rigorous point of view. As a consequence, one can just give some suggestions what may cause the problems. First of all, it cannot be ruled out that the underlying set of coupled equations is unstable. In this case any inaccuracy unavoidably introduced by the numerical treatment inevitably blows up. For sure, this would be the worst case. A different possibility is that the problem is related in a complicated way to the numerical division by the density. This can be the case if the whole scheme is critically sensitive on the asymptotic behavior of the term containing the orbital shifts. Since in a time-dependent calculation no way to obtain the correct asymptotic behavior is known, this would also be a severe problem. Lastly, the most comfortable reason would be that the splitting schemes used above violate some unknown exact constraints on the orbital shifts, e.g., norm conservation. This violation in combination with the coupling could then lead to instabilities. In this case a propagation scheme that respects this property could solve the problem. Unfortunately, up to date little is known about the orbital shifts beside their orthogonality on the corresponding orbitals. Definitely, a deeper knowledge about the properties of the orbital shifts would be of great value for either setting up a stable propagation scheme or for developing further approximate solutions like the ‘OSBK’ approximation proposed in Chap. 4.

Chapter 6

Exact properties of the xc potential

The great importance of accurate approximations to the exchange-correlation potential has already been mentioned several times in the previous chapters. In this context it has also been pointed out that it is important to include as many exact properties as possible in approximate exchange-correlation potentials. Especially the fundamental conservation laws of energy, particle number, and momentum should be respected. Beside these conservation laws two theorems exist which are satisfied by the exact time-dependent exchange-correlation potential. One is the ‘Harmonic-Potential theorem’ [Dob94] and the other one is the ‘Zero-Force theorem’ [Vig95, Gro96]. As shown below the ‘Zero-Force theorem’ corresponds to Newton’s third law and thus guarantees momentum conservation.

In connection with the two theorems the question arises which existing approximations satisfy them. As discussed below the time-dependent LDA and the time-dependent exact-exchange OEP satisfy both theorems. In contrast, the exact-exchange KLI approximation only satisfies the ‘Harmonic-Potential theorem’, but violates the ‘Zero-Force theorem’.

6.1 ‘Harmonic-Potential theorem’

The ‘Harmonic-Potential theorem’ is a general statement about an interacting system in a harmonic external potential with a perturbation $\mathbf{F}(t) \cdot \sum_j \mathbf{r}_j$ where $\mathbf{F}(t)$ is an arbitrary time-dependent function, i.e., the Hamiltonian of the system of interest is given by

$$H(\mathbf{r}_1, \dots, \mathbf{r}_N, t) = H_0(\mathbf{r}_1, \dots, \mathbf{r}_N) - \mathbf{F}(t) \cdot \sum_{j=1}^N \mathbf{r}_j \quad (6.1)$$

where

$$H_0(\mathbf{r}_1, \dots, \mathbf{r}_N) = \sum_{j=1}^N \left(-\frac{\hbar^2}{2m} \nabla_j^2 + \frac{1}{2} \mathbf{r}_j \cdot \mathbf{K} \cdot \mathbf{r}_j \right) + W(|\mathbf{r}_k - \mathbf{r}_l|) \quad (6.2)$$

is the time-independent part of the Hamiltonian. In Eq. (6.2) the term $W(|\mathbf{r}_k - \mathbf{r}_l|)$ denotes the particle-particle interaction between all particles. The spring-constant matrix \mathbf{K} can be assumed to be symmetric without loss of generality. The statement of the ‘Harmonic-Potential theorem’ is that any state of the form

$$\psi(\mathbf{r}_1, \dots, \mathbf{r}_N, t) = \exp \left(-i(E_k t + \hbar N S(t) - Nm \dot{\mathbf{x}}(t) \cdot \mathbf{R}) / \hbar \right) \psi_k(\bar{\mathbf{r}}_1, \dots, \bar{\mathbf{r}}_N) \quad (6.3)$$

is a solution of the time-dependent Schrödinger equation if the following conditions are fulfilled ($\dot{\mathbf{x}} = d\mathbf{x}/dt$):

- the state $\psi_k(\mathbf{r}_1, \dots, \mathbf{r}_N)$ is an eigenstate with eigenvalue E_k of the interacting Hamiltonian $H_0(\mathbf{r}_1, \dots, \mathbf{r}_N)$,
- the phase angle $S(t)$ is given by

$$S(t) = \frac{1}{\hbar} \int_{t_0}^t \frac{m}{2} \dot{\mathbf{x}}(t')^2 - \frac{1}{2} \mathbf{x}(t') \cdot \mathbf{K} \cdot \mathbf{x}(t') dt' \quad (6.4)$$

and $\mathbf{x}(t)$ is a solution of the differential equation

$$m \ddot{\mathbf{x}} = -\mathbf{K} \cdot \mathbf{x} + \mathbf{F}(t), \quad (6.5)$$

- $\bar{\mathbf{r}}_j = \mathbf{r}_j - \mathbf{x}(t)$ and $\mathbf{R} = \frac{1}{N} \sum_j \mathbf{r}_j$ holds.

As a consequence, all densities evolving from a stationary initial state by applying a time-dependent potential $\mathbf{F}(t) \cdot \sum_j \mathbf{r}_j$ are given by $n(\mathbf{r}, t) = n_k(\mathbf{r} - \mathbf{x}(t))$. Here, $n_k(\mathbf{r})$ is the density of the initial state ψ_k and $\mathbf{x}(t)$ is the solution of $m \ddot{\mathbf{x}} = -\mathbf{K} \cdot \mathbf{x} + \mathbf{F}(t)$.

Focusing on DFT, the question arises which constraints the exchange-correlation potential must satisfy to reproduce the previously discussed results. In order to find this out an ansatz similar to Eq. (6.3) is made for the Kohn-Sham orbitals. Inserting this ansatz into the time-dependent Kohn-Sham equations reveals that the Hartree and the exchange-correlation potential must rigidly follow a rigidly shifted density [Dob94]. In more detail,

$$v_H[n(\mathbf{r} - \mathbf{x}(t))](\mathbf{r}, t) = v_H[n(\mathbf{r})](\mathbf{r} - \mathbf{x}(t)) \quad (6.6)$$

$$v_{xc}[n(\mathbf{r} - \mathbf{x}(t))](\mathbf{r}, t) = v_{xc}[n(\mathbf{r})](\mathbf{r} - \mathbf{x}(t)) \quad (6.7)$$

must hold. For the Hartree potential this condition is always satisfied due to the translation invariance of the term $1/|\mathbf{r} - \mathbf{r}'|$.

In the time-dependent LDA the exchange-correlation potential has the form $v_{xc}(\mathbf{r}, t) = f(n(\mathbf{r}, t))$ where $f(x)$ is a smooth function of x . In other words the LDA exchange-correlation potential only depends on \mathbf{r} and t via the dependence of the density on these

variables. As a consequence, the time-dependent LDA exchange-correlation potential satisfies Eq. (6.7) and therefore the ‘Harmonic-Potential theorem’.

For the exact time-dependent OEP and also for the time-dependent KLI potential Eq. (6.7) is satisfied if the orbital-dependent potentials $u_{xcj}(\mathbf{r}, t)$ have the property

$$u_{xcj}[\{\varphi_l(\mathbf{r} - \mathbf{x}(t))\}](\mathbf{r}, t) = u_{xcj}[\{\varphi_l(\mathbf{r})\}](\mathbf{r} - \mathbf{x}(t)). \quad (6.8)$$

Before proving this statement, it should be mentioned that the orbital-dependent potentials from the exact-exchange functional satisfy this property and thus, the ‘Harmonic-Potential theorem’. As in the case of the Hartree potential the deeper reason for this is the translation invariance of the term $1/|\mathbf{r} - \mathbf{r}'|$. To prove the statement given above one makes the ansatz

$$\varphi_j(\mathbf{r}, t) = \exp(-i(\epsilon_j t + \hbar S(t) - m \dot{\mathbf{x}}(t) \cdot \mathbf{r}) / \hbar) \varphi_j^0(\mathbf{r} - \mathbf{x}(t)) \quad (6.9)$$

for the time-dependent Kohn-Sham orbitals. In this expression the function $S(t)$ is defined as in Eq. (6.4), $\mathbf{x}(t)$ satisfies Eq. (6.5), and φ_j^0 is the initial eigenstate with eigenvalue ϵ_j . The total density and the orbital densities are in this case $n^0(\mathbf{r} - \mathbf{x}(t))$ and, respectively, $n_j^0(\mathbf{r} - \mathbf{x}(t))$. Thus, for orbital-dependent potentials $u_{xcj}(\mathbf{r}, t)$ which satisfy Eq. (6.8) the time-dependent KLI potential

$$v_{xc}^{\text{KLI}}(\mathbf{r}, t) = \frac{1}{2n(\mathbf{r}, t)} \sum_{j=1}^N |n_j(\mathbf{r}, t)|^2 (u_{xcj}(\mathbf{r}, t) + (\bar{v}_{xcj}(t) - \bar{u}_{xcj}(t))) + c.c. \quad (6.10)$$

satisfies Eq. (6.7) and, as a consequence, justifies the previous ansatz ($\bar{v}_{xcj}(t)$ and $\bar{u}_{xcj}(t)$ are the averaged potentials, see Chap. 3 and 4). For the exact time-dependent OEP one has to take into account the orbital shifts, too. For this purpose the derivation of the static OEP equation from the time-dependent OEP equation in Chap. 4 suggests the same ansatz 6.9 for the orbital shifts. Evaluating the additional $\nabla \cdot (\dots)$ term with the expressions for the orbitals and orbital shifts leads to

$$\begin{aligned} \nabla \cdot (\psi_j^*(\mathbf{r}, t) \nabla \varphi_j(\mathbf{r}, t)) &= \nabla \cdot (\psi_j^{0*}(\mathbf{r} - \mathbf{x}(t)) \nabla \varphi_j^0(\mathbf{r} - \mathbf{x}(t))) \\ &+ \nabla \cdot \left(i \frac{m}{\hbar} \dot{\mathbf{x}}(t) \psi_j^{0*}(\mathbf{r} - \mathbf{x}(t)) \varphi_j^0(\mathbf{r} - \mathbf{x}(t)) \right). \end{aligned} \quad (6.11)$$

Since the initial orbitals and orbital shifts are chosen real-valued, the second term is purely imaginary and does not contribute to the potential. The function $f(\mathbf{r}, t)$ in Eq. (4.31) also vanishes in this situation. Thus, the exact time-dependent OEP satisfies Eq. (6.7). A lengthy but straightforward calculation finally shows that the ansatz for the orbital shifts is consistent with the resulting equation-of-motion for the time-dependent orbital shifts.

As shown by Vignale [Vig95] the constraint (6.7) can also be derived by describing an interacting many-particle system in an accelerated reference frame¹. As a result one

¹For the accelerated reference frame a Cartesian coordinate system with axes parallel to the original coordinate system is used. In addition, it is assumed that at $t = 0$ the two coordinate systems coincide and the relative velocity vanishes.

obtains that the exchange-correlation functional for the action must satisfy

$$A_{\text{xc}}[n'] = A_{\text{xc}}[n] \quad (6.12)$$

where $n'(\mathbf{r}, t) = n(\mathbf{r} + \mathbf{x}(t), t)$ is the density in the accelerated coordinate system. The vector $\mathbf{x}(t)$ is the origin of the accelerated reference frame relative to the original coordinate system. Due to the definition of the exchange-correlation potential as a functional derivative of A_{xc} with respect to the density the relation

$$A_{\text{xc}}[n + \delta n] - A_{\text{xc}}[n] = \int_C \int v_{\text{xc}}[n](\mathbf{r}', \tau) \delta n(\mathbf{r}', \tau) d^3r dt \quad (6.13)$$

holds. Using the same relation for the transformed density n' and combining the two relations with Eq. (6.12) leads to the desired result (after transformation to physical time)

$$v_{\text{xc}}[n'](\mathbf{r}, t) = v_{\text{xc}}[n](\mathbf{r} + \mathbf{x}(t)) . \quad (6.14)$$

Thus, Eq. (6.12) offers a convenient method to check if an approximate exchange-correlation potential satisfies the ‘Harmonic-Potential theorem’. However, it is important to keep in mind that this method only works if the exchange-correlation potential is given by the functional derivative of some known exchange-correlation action functional. This constraint plays an important role in the context of the ‘Zero-Force theorem’ which is the subject of the next section.

6.2 ‘Zero-Force theorem’

In order to derive the ‘Zero-Force theorem’ it is necessary to calculate the second time derivative of the dipole moment of an interacting system [Gro96]. Using the Ehrenfest theorem and $\frac{d}{dt}[\hat{H}(t), \hat{\mathbf{r}}] \equiv 0$, one obtains the equation

$$\frac{d^2}{dt^2} \int \mathbf{r} n(\mathbf{r}, t) d^3r = -\frac{1}{\hbar^2} \langle \psi(t) | [\hat{H}(t), [\hat{H}(t), \hat{\mathbf{r}}]] | \psi(t) \rangle \quad (6.15)$$

where the operator $\hat{\mathbf{r}}$ is given by

$$\hat{\mathbf{r}} = \int \mathbf{r} \hat{n}(\mathbf{r}, t) d^3r \quad (6.16)$$

and $\hat{H}(t) = \hat{T} + \hat{W} + \hat{V}_{\text{ext}}(t)$ is the Hamiltonian of the interacting system. Calculating the double commutator in Eq. (6.15) leads to the result

$$m \frac{d^2}{dt^2} \int \mathbf{r} n(\mathbf{r}, t) d^3r = - \int n(\mathbf{r}, t) \nabla v_{\text{ext}}(\mathbf{r}, t) d^3r . \quad (6.17)$$

The physical meaning of this equation is revealed by using the continuity equation for the density to obtain

$$\frac{d}{dt} \mathbf{P}(t) := \frac{d}{dt} \int m \mathbf{j}(\mathbf{r}, t) d^3r = - \int n(\mathbf{r}, t) \nabla v_{\text{ext}}(\mathbf{r}, t) d^3r \quad (6.18)$$

where $\mathbf{j}(\mathbf{r}, t)$ is the current of the system. Eq. (6.18) states that the change of the system’s total momentum is equal to the net force exerted from the external potential on the system, i.e., Newton’s third law.

Carrying out the same calculation for a non-interacting Kohn-Sham system with Kohn-Sham potential $v_S(\mathbf{r}, t)$, one finds

$$\frac{d}{dt}\mathbf{P}_S(t) := \frac{d}{dt} \int m \mathbf{j}_S(\mathbf{r}, t) d^3r = - \int n(\mathbf{r}, t) \nabla v_S(\mathbf{r}, t) d^3r \quad (6.19)$$

where $\mathbf{j}_S(\mathbf{r}, t)$ is the Kohn-Sham current

$$\mathbf{j}_S(\mathbf{r}, t) = \frac{\hbar^2}{2mi} \sum_{k=1}^N (\varphi_k^*(\mathbf{r}, t) \nabla \varphi_k(\mathbf{r}, t) - c.c.) . \quad (6.20)$$

Since by definition $n_S(\mathbf{r}, t) = n(\mathbf{r}, t)$ holds, it follows from Eq. (6.17) and Eq. (6.18) that $\mathbf{P}_S(t) = \mathbf{P}(t)$ must hold. Thus, equating Eq. (6.18) and Eq. (6.19) leads to

$$- \int n(\mathbf{r}, t) \nabla v_{\text{ext}}(\mathbf{r}, t) d^3r = - \int n(\mathbf{r}, t) \nabla v_S(\mathbf{r}, t) d^3r . \quad (6.21)$$

Inserting $v_S(\mathbf{r}, t) = v_H(\mathbf{r}, t) + v_{\text{xc}}(\mathbf{r}, t) + v_{\text{ext}}(\mathbf{r}, t)$, one obtains

$$0 = - \int n(\mathbf{r}, t) (\nabla v_H(\mathbf{r}, t) + \nabla v_{\text{xc}}(\mathbf{r}, t)) d^3r . \quad (6.22)$$

Since the integral over the Hartree potential vanishes, the final result is given by

$$\int n(\mathbf{r}, t) \nabla v_{\text{xc}}(\mathbf{r}, t) d^3r = 0 . \quad (6.23)$$

This statement is called the ‘Zero-Force theorem’. Beside the derivation given here it can also be derived from the transformation property (6.12) of the action [Vig95]. However, the presented derivation has the advantage that it is independent of any action principle arguments.

Since the time-dependent LDA obeys Eq. (6.12), the ‘Zero-Force theorem’ and the ‘Harmonic-Potential theorem’ are both satisfied by this approximation. As shown by von Barth the exact-exchange OEP also satisfies the ‘Zero-Force theorem’ *if* the full time-dependent OEP equation is solved [Ba05a]. However, since this is a crucial requirement for the proof, this observation cannot be used to make a statement about the time-dependent KLI potential. In fact, it is possible to find situations in which the ‘Zero-Force theorem’ is violated by the exact-exchange time-dependent KLI potential [Mu07a]. One such situation is discussed in the following.

In order to demonstrate that the time-dependent exact-exchange KLI approximation violates the ‘Zero-Force theorem’ one can calculate the response of a Na₅ cluster to a small dipole excitation². This cluster has a planar geometry (oriented in the $(x - y)$ -plane in the following) and provides a critical test case due to its rather ‘soft’ electron

²For the calculation a modified version of the PARSEC program [Kro06] is used. Further numerical details can be found in Chap. 8 and in Ref. [Mu07a].

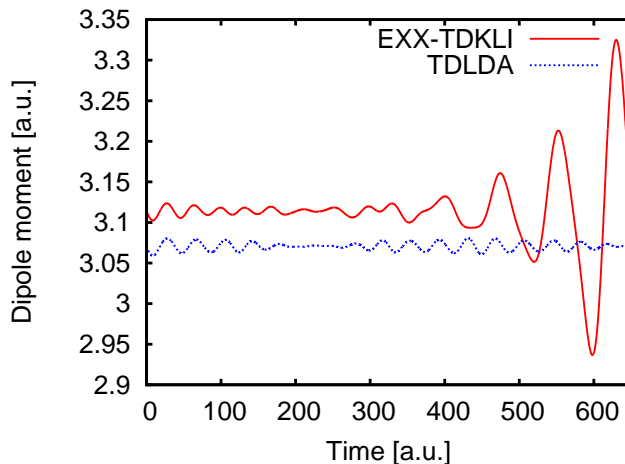


Figure 6.1: y -component of the dipole moment of Na_5 after an initial boost of $|\mathbf{p}_{\text{boost}}| = 3.834 \times 10^{-4} \hbar a_0^{-1}$. In contrast to the time-dependent LDA result, the time-dependent exact-exchange KLI curve shows an increasing amplitude of the oscillation. The time-dependent exact-exchange KLI curve is slightly shifted for better comparison. Rydberg atomic units are used throughout.

cloud. After the ground-state calculation the system is excited by a momentum boost $\exp(i \mathbf{r} \cdot \mathbf{p}_{\text{boost}}/\hbar)$ with $|\mathbf{p}_{\text{boost}}| = 3.834 \times 10^{-4} \hbar a_0^{-1}$, corresponding to a total excitation energy of the system of 1.0×10^{-5} eV, applied to all Kohn-Sham orbitals. The boost has equal strength in x -, y -, and z -direction. After the boost the resulting excited state is propagated in real time with fixed ions.

Fig. 6.1 shows the resulting y -component of the dipole moment $d_y(t) = e \int y n(\mathbf{r}, t) d^3r$ (with e being the electron’s charge). For a while the amplitude shows reasonable oscillations in agreement with the initial boost. But after about 400 a.u., it increases rapidly and steadily. For comparison the same quantity is plotted for a time-dependent LDA calculation. There, no increasing amplitude is observed.

To demonstrate that the increasing amplitude is connected to a violation of the ‘Zero-Force theorem’ one can monitor the expected time derivative of the total momentum, i.e., one calculates the right-hand side of Eq. (6.18) with the external potential coming from the ions. In addition, one can evaluate the left-hand side of Eq. (6.23), which should be zero. Fig. 6.2 shows the result obtained from Eq. (6.18) and the sum of Eq. (6.23) and Eq. (6.18). One observes that the total force from the external potential on the electron density, Eq. (6.18), differs significantly from the total force obtained from the sum of both equations. This clearly demonstrates that v_x violates the ‘Zero-Force theorem’ and contributes to the total force. Since the time-dependent dipole moment is connected to the total force $\mathbf{F}(t)$ via (see Eq. (6.17) and (6.18))

$$m \partial_t^2 \mathbf{d}(t) = e \partial_t \mathbf{P}(t) = e \mathbf{F}(t), \quad (6.24)$$

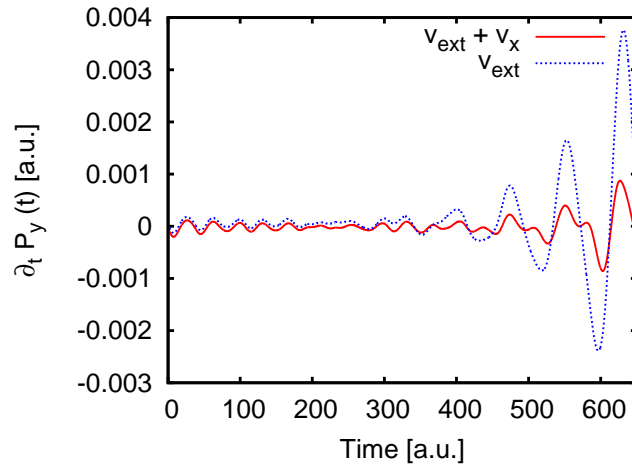


Figure 6.2: Time derivative of the y -component of the total momentum of the electron density. ‘ $v_{\text{ext}} + v_x$ ’ and ‘ v_{ext} ’ label the results calculated via Eq. (6.18) with the external potential or, respectively, the external and the exchange potential. The violation of the ‘Zero-Force theorem’ is visible in the difference between ‘ $v_{\text{ext}} + v_x$ ’ and ‘ v_{ext} ’.

it follows that the violation of the ‘Zero-Force theorem’ leads to a wrong time-dependent dipole moment and to a self-excitation of the system. Finally, one can check that Eq. (6.24) holds for the Kohn-Sham system. To do this one calculates the force from the total Kohn-Sham potential, i.e.,

$$\mathbf{F}(t) := - \int n(\mathbf{r}, t) \nabla v_S(\mathbf{r}, t) d^3r, \quad (6.25)$$

and compares it to the time derivative of the Kohn-Sham current, Eq. (6.20), from the calculation. The current is connected to the total momentum via $\mathbf{P}(t) = m \int \mathbf{j}_S(\mathbf{r}, t) d^3r$. By explicitly calculating the second time derivative of the monitored dipole signal, one can confirm that Eq. (6.24) holds in the calculation as it should be.

To study the influence of the ‘Zero-Force theorem’ violation in more detail one can carry out the same calculation for a Na_9^+ cluster. In contrast to Na_5 , this cluster can be considered as one of the most ‘forgiving’ systems because of its spherical shape and the positive charge leading to a stable ‘plasmon’-like oscillation when excited. Fig. 6.3 shows the resulting violation of Eq. (6.23). A close look reveals that the ‘Zero-Force theorem’ is slightly violated again. But, in contrast to Na_5 , the violation does not increase in time. Checking the time-dependent dipole moment shows that it is also stable. Beside the stronger binding forces a possible explanation for this observation could be that the higher inversion symmetry of the almost spherical Na_9^+ leads to an error cancellation in the course of one density oscillation and thus to a strongly reduced increase of the violation. In any case, the result clearly corroborates the intuitive expectation that the system properties have a strong influence on the degree of the violation of the ‘Zero-Force theorem’.

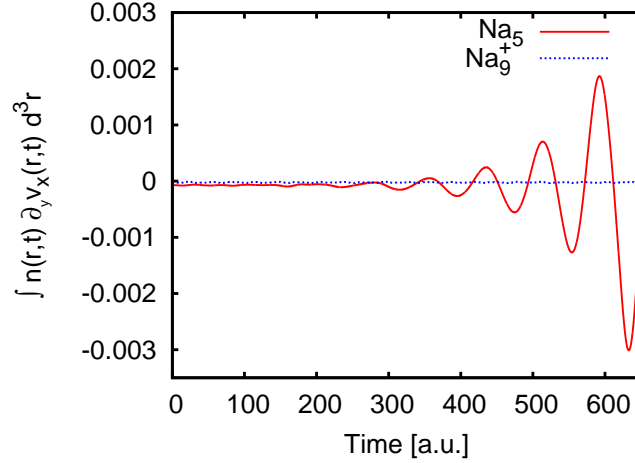


Figure 6.3: Violation of the ‘Zero-Force theorem’ for Na_9^+ and Na_5 . Again, the y -component is plotted. Both systems are excited by a momentum boost corresponding to an excitation of the system by 1.0×10^{-5} eV. In contrast to Na_5 , the resulting curve for Na_9^+ does not increase in time. The resulting dipole moment of Na_9^+ is also observed to be stable.

In addition to the system properties one can also expect an influence of the excitation energy on the ‘Zero-Force’ violation. And indeed, this can be found. Fig. 6.4 shows the results for Na_5 excited with three different boost strengths of $3.834 \times 10^{-4} \hbar a_0^{-1}$ (1.0×10^{-5} eV), $6.062 \times 10^{-4} \hbar a_0^{-1}$ (2.5×10^{-5} eV), and $8.573 \times 10^{-4} \hbar a_0^{-1}$ (5.0×10^{-5} eV). Obviously, the deviation from zero varies with the boost strength. The importance of the excitation energy can also be demonstrated by considering the extreme situation of no excitation at all. In this case the time-dependent Kohn-Sham orbitals are given by the ground-state orbitals multiplied by a time-dependent phase factor $\exp(-i\epsilon_k t/\hbar)$ containing the Kohn-Sham eigenvalue ϵ_k . But since this phase factor does not influence the potential, the whole system remains in a stationary state and the violation of the ‘Zero-Force theorem’ remains constant. This constant violation does not lead to a non-stationary state since $\int n(\mathbf{r},t) \nabla v_S(\mathbf{r},t) d^3r$ vanishes due to the ground-state iteration. In other words, for the ground-state density the total force from the external and the exchange-correlation potential are in equilibrium leading to a stationary state.

Beside the just discussed aspects there are three other conditions under which a violation of the ‘Zero-Force theorem’ in a time-dependent KLI calculation may not be observed. First, for short time scales the accumulation of the violation can be too small to show up significantly. Certainly, this time scale depends on the two aspects discussed above: the excitation strength and the system properties. The second situation occurs when a strong, ionizing external field is applied to the system as in Chap. 3. This can hide the error in the exchange-correlation potential completely. Finally, for spin-saturated two-particle systems the time-dependent KLI and the time-dependent OEP

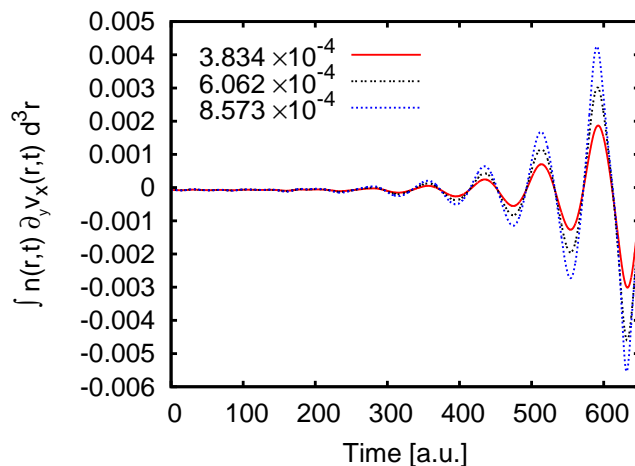


Figure 6.4: Violation of the ‘Zero-Force theorem’ for Na_5 excited with different boosts of 3.834×10^{-4} , 6.062×10^{-4} , and $8.573 \times 10^{-4} \hbar a_0^{-1}$. Only the y -component is plotted.

potential coincide and, as a consequence, the ‘Zero-Force theorem’ is rigorously satisfied if the time-dependent KLI potential comes from a ‘conserving approximation’ [Ba05a].

From the numerical results presented in the previous paragraphs the question may arise whether it is possible to analytically prove the violation of ‘Zero-Force theorem’. As discussed above any potential obtained from an exchange-correlation action which obeys Eq. (6.12) satisfies the ‘Zero-Force theorem’ and the ‘Harmonic-Potential theorem’. Actually, the same arguments show that if $v_{xc}(\mathbf{r},t)$ satisfies Eq. (6.7) *and* is the functional derivative of some exchange-correlation action functional, it must also satisfy the ‘Zero-Force theorem’. Since the exact-exchange KLI potential satisfies the ‘Harmonic-Potential theorem’, one concludes from the numerical results that the potential in general cannot be obtained as the functional derivative of some exchange-correlation action. This result is in line with earlier results for the static Slater potential [OuY90]. In any case the missing knowledge of an action expression which yields the exact-exchange KLI potential makes any analytical statements extremely difficult. A hand-waving argument, however, is provided by the expression for the exact-exchange time-dependent OEP involving the orbitals and orbital shifts. Since the full expression satisfies the ‘Zero-Force theorem’, it is not surprising that the time-dependent KLI approximation, which neglects the terms containing the orbital shifts, violates the ‘Zero-Force theorem’.

Finally, a comment about the generalization of the previous results to KLI potentials from other exchange-correlation functionals is in place. Clearly, the possibility that other expressions lead to a KLI potential which satisfies the ‘Zero-Force theorem’ cannot be ruled out from the example given above. However, since the exact-exchange functional in combination with the OEP is a ‘conserving approximation’ [Ba05a] and this property is destroyed by using the KLI potential, it is highly plausible that this also happens if other orbital functionals are used.

6.3 Energy conservation and other constraints

In ground-state DFT the energy of a system is of crucial importance since it is used to find the ground-state density. As pointed out earlier the decisive role of the energy is lost in time-dependent situations. However, the time-dependent energy is still very useful for several reasons. For example, it allows to analyze the energy absorbed by a system in the course of a laser pulse. Furthermore, analyzing the different energy contributions offers a possibility to study the energy transfer from, e.g., the electronic to the ionic degrees of freedom. In addition, the conservation of the total energy can be used as a sensitive measure for the numerical accuracy. In any case having an approximation for the time-dependent energy is highly desirable.

According to the Ehrenfest theorem the time-evolution of the exact time-dependent energy $E(t) = \langle \psi(t) | \hat{T} + \hat{W} + \hat{V}(t) | \psi(t) \rangle$ is given by

$$\frac{dE(t)}{dt} = \langle \psi(t) | \partial_t \hat{V}(t) | \psi(t) \rangle . \quad (6.26)$$

As expected the total energy is conserved for time-independent external potentials. It is clear that this property should also be satisfied by any DFT approximation for the time-dependent energy. However, due to the time-dependence of the Hartree and the exchange-correlation potential it is by no means obvious that a time-independent external potential yields a constant energy in a DFT calculation. In order to derive a condition which guarantees energy conservation in such situations the time-dependent energy is written in the form

$$E(t) = T_S[n(\mathbf{r}, t)] + E_H[n(\mathbf{r}, t)] + E_{\text{ext}}[n(\mathbf{r}, t)] + \tilde{E}_{\text{xc}}[n](t) . \quad (6.27)$$

Similar to the static case Eq. (6.27) actually *defines* the energy contribution $\tilde{E}_{\text{xc}}[n](t)$. The expression (6.27) is a natural candidate for the time-dependent energy because it reduces to the ground-state energy if the time-dependent exchange-correlation energy $\tilde{E}_{\text{xc}}[n](t)$ has the property $\tilde{E}_{\text{xc}}[n_0(\mathbf{r})](t) = E_{\text{xc}}[n(\mathbf{r})]$ with $n_0(\mathbf{r})$ being the ground-state density and $E_{\text{xc}}[n(\mathbf{r})]$ the ground-state exchange-correlation energy. Calculating the time derivative of Eq. (6.27), one obtains

$$\begin{aligned} \frac{dE(t)}{dt} &= \frac{d\tilde{E}_{\text{xc}}[n](t)}{dt} - \frac{i}{\hbar} \sum_{j=1}^N \langle \varphi_j(t) | [\hat{t} + \hat{v}_H(t) + \hat{v}(t), \hat{h}_S(t)] | \varphi_j(t) \rangle \\ &\quad + \sum_{j=1}^N \langle \varphi_j(t) | \partial_t \hat{v}(t) | \varphi_j(t) \rangle \\ &= \frac{d\tilde{E}_{\text{xc}}[n](t)}{dt} + \frac{i}{\hbar} \sum_{j=1}^N [\langle \varphi_j(t) | [\hat{v}_{\text{xc}}(t), \hat{h}_S(t)] | \varphi_j(t) \rangle - i\hbar \langle \varphi_j(t) | \partial_t \hat{v}(t) | \varphi_j(t) \rangle] \\ &= \frac{d\tilde{E}_{\text{xc}}[n](t)}{dt} + \frac{i}{\hbar} \sum_{j=1}^N [\langle \varphi_j(t) | [\hat{v}_{\text{xc}}(t), \hat{t}] | \varphi_j(t) \rangle - i\hbar \langle \varphi_j(t) | \partial_t \hat{v}(t) | \varphi_j(t) \rangle] . \end{aligned} \quad (6.28)$$

In this equation $\hat{h}_S(t) = \hat{t} + \hat{v}_H(t) + \hat{v}(t) + \hat{v}_{xc}(t)$ is the Kohn-Sham Hamiltonian with $\hat{t} = \frac{\hat{p}^2}{2m}$. For time-independent external potentials the total energy must be constant and Eq. (6.28) leads to the condition

$$\frac{d\tilde{E}_{xc}[n](t)}{dt} = -\frac{i}{\hbar} \sum_{j=1}^N \langle \varphi_j(t) | [\hat{v}_{xc}(t), \hat{t}] | \varphi_j(t) \rangle . \quad (6.29)$$

Since the time-dependent exact-exchange KLI potential violates the ‘Zero-Force theorem’, it is hardly surprising that the total energy evaluated with the Fock exchange integral is also not conserved in the calculations presented above. In contrast, the time-dependent LDA satisfies Eq. (6.29) as one can readily verify by calculating

$$\begin{aligned} \frac{dE_{xc}^{\text{LDA}}[n(\mathbf{r}, t)]}{dt} &= \int \int \frac{\delta E_{xc}^{\text{LDA}}[n(\mathbf{r}, t)]}{\delta n(\mathbf{r}', t')} \partial_{t'} n(\mathbf{r}', t') dt' d^3 r' \\ &= \int \int v_{xc}(\mathbf{r}', t') \delta(t - t') \partial_{t'} n(\mathbf{r}', t') dt' d^3 r' \\ &= -\frac{i}{\hbar} \sum_{j=1}^N \langle \varphi_j(t) | [\hat{v}_{xc}(t), \hat{t}] | \varphi_j(t) \rangle . \end{aligned} \quad (6.30)$$

Before closing this chapter a remark about other constraints is in place. One important conservation law which has not yet been mentioned is particle-number conservation. This conservation law can be easily satisfied in a Kohn-Sham calculation by using real-valued exchange-correlation potentials. For such potentials the Kohn-Sham system obeys the continuity equation for the density and, as a consequence, the particle number is conserved.

In connection with the continuity equation it is worth mentioning that the continuity equation does not answer the question whether the interacting and the Kohn-Sham current are identical. Despite several attempts to answer this prominent question a rigorous answer is still missing [Ma02b]. The only possible statement from the continuity equation is that

$$\partial_t (n(\mathbf{r}, t) - n_S(\mathbf{r}, t)) + \nabla \cdot (\mathbf{j}(\mathbf{r}, t) - \mathbf{j}_S(\mathbf{r}, t)) = \nabla \cdot \mathbf{j}_{xc}(\mathbf{r}, t) = 0 \quad (6.31)$$

must hold because the densities $n(\mathbf{r}, t)$ and $n_S(\mathbf{r}, t)$ are equal. In this equation $\mathbf{j}_{xc}(\mathbf{r}, t)$ is defined as the difference between the current $\mathbf{j}(\mathbf{r}, t)$ of the interacting system and the Kohn-Sham current $\mathbf{j}_S(\mathbf{r}, t)$. From the equation

$$\int \mathbf{j}(\mathbf{r}, t) d^3 r = \int \mathbf{r} \partial_t n(\mathbf{r}, t) d^3 r = \int \mathbf{j}_S(\mathbf{r}, t) d^3 r \quad (6.32)$$

follows the identity

$$\int (\mathbf{j}(\mathbf{r}, t) - \mathbf{j}_S(\mathbf{r}, t)) d^3 r = \int \mathbf{j}_{xc}(\mathbf{r}, t) d^3 r = 0 . \quad (6.33)$$

A connection between $\mathbf{j}_{\text{xc}}(\mathbf{r}, t)$ and the exchange-correlation potential can be obtained from angular momentum considerations. The angular momentum of the interacting system is defined by

$$\mathbf{L}(t) = \int m \mathbf{r} \times \mathbf{j}(\mathbf{r}, t) d^3r \quad (6.34)$$

and the time derivative is given by [Lee01]

$$\frac{d}{dt} \mathbf{L}(t) = \int m \mathbf{r} \times \partial_t \mathbf{j}(\mathbf{r}, t) d^3r = - \int n(\mathbf{r}, t) \mathbf{r} \times \nabla v(\mathbf{r}, t) d^3r . \quad (6.35)$$

Subtracting the angular momentum of the Kohn-Sham system, one obtains

$$\frac{d}{dt} (\mathbf{L}(t) - \mathbf{L}_S(t)) = \int m \mathbf{r} \times \partial_t \mathbf{j}_{\text{xc}}(\mathbf{r}, t) d^3r = \int n(\mathbf{r}, t) \mathbf{r} \times \nabla (v_S(\mathbf{r}, t) - v(\mathbf{r}, t)) d^3r .$$

Since the integral involving the Hartree potential vanishes [Lee01], the final result is

$$\int m \mathbf{r} \times \partial_t \mathbf{j}_{\text{xc}}(\mathbf{r}, t) d^3r = \int n(\mathbf{r}, t) \mathbf{r} \times \nabla v_{\text{xc}}(\mathbf{r}, t) d^3r . \quad (6.36)$$

Due to the fact that $\mathbf{j}_{\text{xc}}(\mathbf{r}, t)$ is generally not known this relation cannot be used to make any statements about approximative exchange-correlation potentials in time-dependent situations. However, in static situations Eq. (6.36) reduces to

$$\int n(\mathbf{r}) \mathbf{r} \times \nabla v_{\text{xc}}(\mathbf{r}) d^3r = 0 . \quad (6.37)$$

This equation states that the torque due to the exchange-correlation potential vanishes in the ground state. As all other theorems mentioned above the LDA respects Eq. (6.37). To prove this statement the invariance of $E_{\text{xc}}^{\text{LDA}}$ under rotations is used, i.e.,

$$E_{\text{xc}}^{\text{LDA}}[n'] = E_{\text{xc}}^{\text{LDA}}[n] \quad (6.38)$$

where $n'(\mathbf{r}) = n(\mathbf{r} + \alpha \hat{\mathbf{u}} \times \mathbf{r})$ holds. The unit vector $\hat{\mathbf{u}}$ is the rotation axis and α the angle of rotation. For infinitesimal angles α one can write

$$n(\mathbf{r} + \alpha \hat{\mathbf{u}} \times \mathbf{r}) = n(\mathbf{r}) + \alpha (\hat{\mathbf{u}} \times \mathbf{r}) \cdot \nabla n(\mathbf{r}) . \quad (6.39)$$

Combining this result with

$$E_{\text{xc}}[n + \delta n] = E_{\text{xc}}[n] + \underbrace{\int \frac{\delta E_{\text{xc}}[n]}{\delta n(\mathbf{r})} \delta n(\mathbf{r}) d^3r}_{v_{\text{xc}}(\mathbf{r})} \quad (6.40)$$

and using the property (6.38) one obtains

$$\alpha \int v_{\text{xc}}(\mathbf{r}) (\hat{\mathbf{u}} \times \mathbf{r}) \cdot \nabla n(\mathbf{r}) d^3r = -\alpha \hat{\mathbf{u}} \cdot \int v_{\text{xc}}(\mathbf{r}) (\mathbf{r} \times \nabla n(\mathbf{r})) d^3r = 0 . \quad (6.41)$$

Since the rotation axis and rotation angle is arbitrary,

$$\int v_{\text{xc}}(\mathbf{r}) (\mathbf{r} \times \nabla n(\mathbf{r})) d^3r = - \int n(\mathbf{r}) (\mathbf{r} \times \nabla v_{\text{xc}}(\mathbf{r})) d^3r = 0 \quad (6.42)$$

holds. Thus, the LDA satisfies Eq. (6.37).

Chapter 7

Photoelectron spectra from Kohn-Sham DFT

Up to this point mainly fundamental aspects of DFT have been discussed in the present work. This changes in the next two chapters. There, two different approaches to calculate photoelectron spectra in the framework of DFT are investigated. The systems for which the two approaches are tested and compared are small anionic sodium clusters.

7.1 Photoelectron spectroscopy in cluster physics

Although being used in all areas of physics, photoelectron spectroscopy is especially important in the context of nanoscale materials. For these materials photoelectron spectroscopy is one of the most important experimental tools since it is almost the only method that provides access to the electronic and ionic structures of these materials. The direct observation of the electronic shell structure in sodium clusters [Wri02] is just one example for the power of the method. As indicated above another application is the determination of the ionic structure. Since the electronic structure, and thus the photoelectron spectrum, depends on the ionic configuration, comparing the measured photoelectron spectrum with the results from first-principle calculations allows the identification of the ionic structure. This interplay between theory and experiment has already been used successfully in many cases [Kie96, Ako00, Kha01, Kro02, Mos03, Ber04, Man04, Håk04, Kos07].

Clearly, the just mentioned method can only work if reliable calculations for the system of interest can be performed. Since most of the measured systems consist of many electrons, DFT is an especially well-suited tool due to its low numerical costs. Unfortunately, evaluating the photoelectron spectrum from a Kohn-Sham DFT calculation is not an easy task since only the highest occupied Kohn-Sham eigenvalue has a rigorous connection to the photoelectron spectrum: it is equal to the ionization potential [Lev84, Alm85, Per97]. Thus, it yields the position of the first peak in the photoelectron

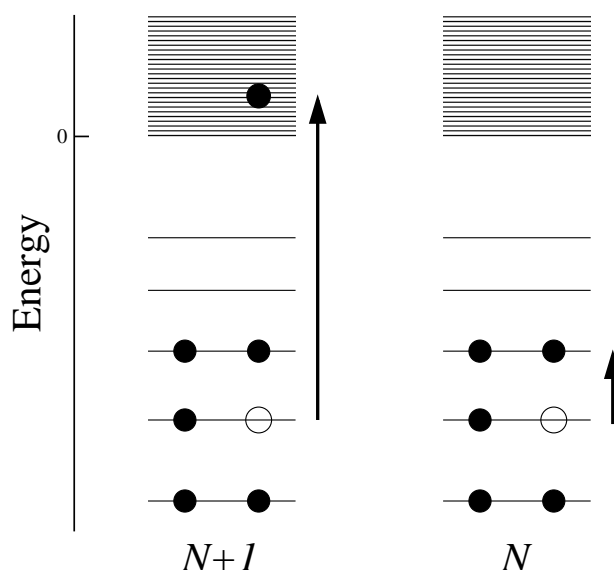


Figure 7.1: Schematic view of two different approaches to calculate the photoelectron spectrum of a system consisting of $(N + 1)$ electrons. Left: The process is described as a strong excitation of the $(N + 1)$ -electron system. Right: The photoelectron has already been detected and the remaining N -electron system is left in an excited state. The link between the kinetic energy of the photoelectron and the energy of the excited state of the N -electron system is provided by energy conservation.

spectrum. It is the aim of this chapter to present and discuss methods how the other peaks can be obtained from a static DFT calculation. In the next chapter the same subject is treated in the framework of time-dependent DFT.

7.2 Theoretical background

Before discussing any results, the theoretical background of the following calculations is presented in more detail. Fig. 7.1 schematically shows two approaches how the peak positions in the photoelectron spectrum of a system consisting of $(N + 1)$ electrons can be calculated. On the left hand side the process is described as an excitation process from the ground state to an energetically high-lying state with continuum contributions. Since Kohn-Sham eigenvalue differences are zeroth-order approximations to excitation energies [Gör96, Fil97], the Kohn-Sham density of states of the $(N + 1)$ -electron system can be used to obtain an approximate photoelectron spectrum. This procedure is used in the present chapter and in many others, e.g., the previously cited publications [Ako00, Kha01, Kro02, Mos03, Ber04, Man04, Håk04, Kos07]. In addition to the just given argument this approach is supported by the work of Chong *et al.* [Cho02]. In this work well founded arguments are given that Kohn-Sham eigenvalues can be interpreted as approximations to relaxed vertical ionization potentials. As shown in the

cited publication this is especially true if the eigenvalues are calculated from quasi-exact Kohn-Sham potentials obtained from highly accurate *ab initio* densities.

On the right-hand side of Fig. 7.1 the situation after the photoelectron has been detected is considered. In this case the remaining system is left in an energetically low-lying excited state of the N -electron system. To connect the excitation energies of this system to the photoelectron spectrum energy conservation is used. Before the photon is absorbed the total energy is given by $E_0^{(N+1)} + \hbar\omega$ where $E_0^{(N+1)}$ is the ground-state energy of the ‘mother’ system containing $N + 1$ electrons and $\hbar\omega$ is the photon energy. After the detection of the photoelectron the total energy is given by the kinetic energy of the photoelectron E_{kin} and the energy of the remaining ‘daughter’ system with N electrons. Since the total energy is conserved, it follows that

$$E_{\text{bind},j} = E_{\text{kin}} - \hbar\omega = E_0^{(N+1)} - E_0^{(N)} - \Delta E_j^{(N)} \quad (7.1)$$

must hold. Here, $E_0^{(N)}$ is the ground-state energy of the ‘daughter’ system and $\Delta E_j^{(N)}$ are its excitation energies. This approach is used in the next chapter and in the publications [Bon89, Ehr03]. It is important to note that ionic relaxation processes are neglected in Eq. (7.1), i.e., it is assumed that the ions do not move during the time interval between the photon absorption and the photoelectron detection. As a consequence, the excitation energies of the ‘daughter’ system must be calculated in the ionic configuration of the ‘mother’ system. For the first peak in the photoelectron spectrum the kinetic energy of the photoelectron is maximal. In this case the ‘daughter’ system is in its ground state, i.e., $\Delta E_j^{(N)}$ is zero and the peak position is at $E_0^{(N+1)} - E_0^{(N)}$.

Looking at a measured photoelectron spectrum as, e.g., shown in Fig. 7.2, it is obvious that a photoelectron spectrum does not only consist of peak positions, but also peak heights. In first-order perturbation theory the probability for a transition from the ground state $|\psi_0\rangle$ with energy E_0 to a final state $|\psi_f\rangle$ with energy E_f is proportional to

$$\underbrace{|\langle\psi_f|\hat{D}|\psi_0\rangle|^2}_{\rightarrow \text{peak height}} \underbrace{\delta(E_0 + \hbar\omega - E_f)}_{\rightarrow \text{peak position}} \quad (7.2)$$

where ω is the laser frequency and \hat{D} is the dipole operator describing the perturbing laser field in dipole approximation. Since the matrix elements depend on the full interacting many-particle wavefunctions calculating these exactly is close to being impossible. Fortunately, the experimental spectra considered in the following indicate that the matrix elements do not play a crucial role in the more weakly bound part of the spectrum one is mostly interested in. In other words, even without access to the matrix elements a reasonable comparison between the experimental and the theoretical spectra can be made, at least in the weakly bound regions.

7.3 Results for anionic sodium clusters

To understand the following work it is necessary to give a brief summary of earlier results by Moseler *et al.* [Mos03]. In the cited publication the authors have measured and calculated the photoelectron spectra of sodium cluster anions with 4 to 19 atoms. The calculated photoelectron spectra have been based on LDA and GGA Kohn-Sham eigenvalues, i.e., the occupied ground-state Kohn-Sham eigenvalues have been interpreted as binding energies. The comparison between the theoretical and experimental photoelectron spectra has revealed the following facts: i) For many clusters the ground-state eigenvalue spectrum and the measured photoelectron spectrum match quite reasonably. ii) In some cases the measured spectra cannot be explained based solely on the ground-state configuration of the ions. The reason for this is the finite temperature in the experiment (approx. 300 K). On the energy scale of the electrons such a temperature (corresponding to approx. 0.03 eV) plays no significant role, however, on the ionic level it results in an ensemble of different ionic structures. If different isomers are taken into account theoretically, e.g., through Langevin molecular dynamics [Mos03], then the observed spectra can be reproduced. iii) Although the theoretical and experimental spectra in this sense match qualitatively for all clusters studied in the work, there is a systematic discrepancy between theory and experiment: the width of the experimental spectrum, i.e., the energetic difference between the highest peak observed in the photoelectron spectrum and the lowest, is about 0.2 – 0.4 eV smaller than the width of the theoretical spectrum. This effect is seen for all cluster sizes and is a puzzling observation since sodium clusters (due to the free-electron-like behavior of the valence electron) are usually considered to be among the most benevolent systems for (semi-)local functionals like the LDA or GGA.

7.3.1 Photoelectron spectra from the exact-exchange OEP

Due to the discussed advantages of the exact-exchange OEP it is natural to check whether the differences in the widths of the spectra may be cured by using this potential. As documented in the work by Moseler *et al.* [Mos03] the width of the spectrum for all clusters beyond Na_9^- is overestimated by LDA and GGA calculations in a similar way. Thus, it is sufficient to consider only small clusters. Fig. 7.2 shows the experimentally measured photoelectron spectrum of Na_5^- and the results from the LDA and the exact-exchange OEP calculation (numerical details can be found in Ref. [Mu06b]). For both cases the Kohn-Sham eigenvalues are convoluted with Gaussians of 0.08 eV width to make visual comparison easier. For the same reason the LDA and the exact-exchange OEP spectrum are rigidly shifted in such a way that their first peak is aligned with the first experimental peak, i.e., the highest occupied eigenvalue is lined up with the experimental vertical detachment energy. The unshifted results are reported in Tab. 7.1.

As one can infer from Tab. 7.1 the corresponding shift is smaller for the exact-

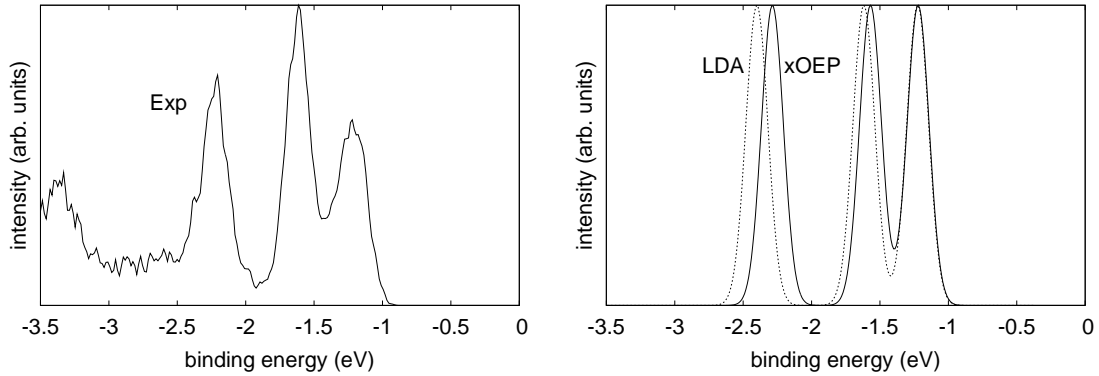


Figure 7.2: Left: The experimental photoelectron spectrum of Na_5^- from Ref. [Mos03]. Right: Spectrum obtained from Kohn-Sham eigenvalues with Gaussian broadening, $\sigma = 0.08$ eV. Full line: exact-exchange OEP. Dashed line: LDA. The exact-exchange OEP leads to a smaller separation between highest and lowest peak and thus is closer to the experimental results.

exchange OEP than for the LDA. This confirms that the bare eigenvalues of the exact-exchange OEP are a much better approximation to electron removal energies than the LDA eigenvalues. Considering the correct $-1/r$ -behavior of the exact-exchange OEP and the canceled Hartree self-interaction, this observation is hardly surprising.

Figure 7.2 immediately reveals that qualitatively the spectra obtained from LDA and exact-exchange OEP are very similar, but quantitatively, there are differences. The width of the exact-exchange OEP spectrum is smaller by somewhat more than 0.1 eV and the exact-exchange OEP spectrum is thus in better agreement with the experimental result. In order to check whether the same is true for other clusters the spectra for Na_7^- , Na_9^- , and Na_{19}^- have been calculated. The results are shown in Tab. 7.1 and confirm that the exact-exchange OEP consistently reduces the width.

However, Tab. 7.1 also shows that a discrepancy remains between theory and experiment. One might argue that these differences are at the limits of what can be expected from DFT and the experiments anyway. However, there are several reasons that suggest that the observed differences should be taken seriously. First, as said previously, sodium clusters are the paradigm systems where the LDA/GGA functional can be expected to be accurate. Second, for many materials with an electronic structure that one expects to be more complicated than the one of sodium [Ako00, Kro02, Håk04], the Kohn-Sham eigenvalues match the experimental spectra remarkably well and much better than for the ‘simple’ sodium. Third, the fact that the experimental width is observed to be smaller than the theoretical one for all cluster sizes excludes statistical experimental errors as an explanation for the differences. And finally, as mentioned above, the results of Chong *et al.* [Cho02] show that Kohn-Sham eigenvalues from accurate Kohn-Sham potentials can be very accurate approximations to electron removal energies. Therefore,

	Na ₅ ⁻	Na ₇ ⁻	Na ₉ ⁻	Na ₁₉ ⁻
$\varepsilon_{\text{H}}^{\text{LDA}}$	0.072	-0.103	-0.215	-0.645
$\varepsilon_{\text{H}}^{\text{xOEP}}$	-0.861	-1.121	-1.153	-1.294
$\varepsilon_{\text{L}}^{\text{LDA}}$	-1.111	-1.554	-1.963	-3.185
$\varepsilon_{\text{L}}^{\text{xOEP}}$	-1.926	-2.477	-2.773	-3.748
W_{LDA}	1.183	1.451	1.748	1.615
W_{xOEP}	1.065	1.356	1.620	1.516
W_{Exp}	0.99	1.11	1.33	1.17

Table 7.1: The highest (ε_{H}) and lowest (ε_{L}) occupied Kohn-Sham eigenvalues, and the corresponding width of the spectrum $W = \varepsilon_{\text{H}} - \varepsilon_{\text{L}}$ for four sodium clusters as obtained in LDA and exact-exchange OEP calculations, compared to the experimentally measured width W_{Exp} . All values in eV. For Na₁₉⁻ only the experimentally resolved part of the spectrum is taken into account (i.e., the deepest level is excluded).

in the next subsection other influences that might contribute to the discrepancy between theory and experiment are investigated.

7.3.2 Comparison between different theoretical approaches

A possible reason for the differences between the experimental and the theoretical results is the usage of pseudopotentials [Phi59, Tro91, Kü00c]. The main idea behind these potentials is to absorb the influence of the nucleus and the more strongly bound electrons in an effective potential. This potential can be constructed either in an empirical or in a non-empirical way [Kü00c]. Generally, pseudopotentials must be non-local in order to give results in agreement with all-electron calculations [Phi59, Bac82, Tro91]. The main advantages of pseudopotentials are the reduced number of explicitly treated electrons and the reduced size of the employed basis sets. In the case of a real-space grid for instance, extremely small grid spacings are required to accurately describe the strong oscillations due to the high kinetic energy of the more deeply bound orbitals. By using pseudopotentials this can be avoided. It is clear that the use of pseudopotentials is only justified as long as the strongly bound electrons are not affected by the surroundings.

In the calculations discussed above only the sodium's 3s valence electron has been treated explicitly. For the LDA and GGA calculations first-principles pseudopotentials constructed according to the scheme of Troullier and Martins [Tro91] have been used. Since this scheme cannot be applied straightforwardly for the exact-exchange functional [Byl95, Eng01], an empirical pseudopotential has been employed for the exact-exchange OEP calculation. Due to the particularly simple electronic structure of sodium with one

	ε_H	ε_L	W
LDA nc. rel.	0.072	-1.111	1.183
LDA cc. urel.	0.068	-1.115	1.183
LDA cc. rel.	0.104	-1.146	1.250
GGA cc. rel.	0.148	-1.040	1.188

Table 7.2: Highest and lowest Kohn-Sham eigenvalue of Na_5^- and their difference W in eV as obtained with LDA pseudopotentials with and without non-linear core correction and with the GGA of Ref. [Per96] with core correction. nc.: without non-linear core correction; cc.: with non-linear core correction; rel.: geometry relaxed to lowest energy; urel.: geometry kept fixed at ‘LDA without core correction’-values.

valence electron above otherwise completely filled shells, a purely local pseudopotential can be constructed [Küm98, Kü00a]. For the construction of this empirical pseudopotential the atomic eigenvalues have been used as a criterion in the fitting of the pseudopotential parameters. It is important to point out that it is not just the pseudopotential that makes the difference in the width of the LDA and exact-exchange OEP spectra: even if the same pseudopotential is employed for both functionals, the exact-exchange OEP leads to a width that is about 0.1 eV smaller [Kü03b].

There is, however, another source of errors related to the use of a pseudopotential. In the standard Troullier-Martins construction one obtains the pseudopotential by unscreening the total Kohn-Sham potential with the valence electrons’ contribution to the Hartree and the exchange-correlation potential. The non-linear dependence of the exchange-correlation potential on the density is usually neglected in this step, i.e., the unscreening is linearized. The error introduced in this way can be minimized by using a non-linear partial core correction [Lou82]. Studies show that this correction indeed can be necessary to accurately describe Na clusters within the Troullier-Martins scheme [Kro00]. One can imagine that the core correction might also affect the width of the eigenvalue spectrum, e.g., by having a larger influence on the lower eigenvalues than on the higher ones. Therefore, the LDA calculations for the test case Na_5^- have been repeated with a core-corrected pseudopotential. This has been done once with the ionic positions fixed to the values obtained in the calculation without core correction (termed unrelaxed core correction in Tab. 7.2) and once with a relaxed cluster structure found from an additional total energy minimization with the core-corrected pseudopotential. For the sake of completeness the eigenvalues obtained from the GGA of Ref. [Per96] in combination with the corresponding core-corrected GGA pseudopotential and the relaxed geometry are also shown in Tab. 7.2.

Comparing the first and the second line of Tab. 7.2, one notes that the LDA eigenval-

ues obtained with the non-linear core-corrected pseudopotential for fixed ionic geometry are just uniformly shifted by a tiny amount, and the width of the spectrum is identical to the one obtained without core correction. Only when the ionic geometry is relaxed do the effects of the core correction on the width become noticeable, as seen in the third line of Tab. 7.2. That the core-correction affects results indirectly, via the bond-length, is in agreement with earlier findings on the influence of core-corrections [Kro00] and in line with studies that have shown the importance of bond-length effects in Na clusters [Kü00a, Kü00b]. However, whereas the core correction in previous studies has improved the agreement with experiment, the opposite is true in the present case: the change goes in the wrong direction since the highest eigenvalue goes up in energy and the lowest eigenvalue goes down, i.e., the total width of the spectrum increases. However, the fourth line which shows the GGA results reveals that this is not to be overinterpreted: employing the GGA with the corresponding core-corrected pseudopotential and fully relaxing the ionic geometry brings the width back to the value that it had in the LDA calculation without core correction. Therefore, these results in summary seem to indicate that the way in which the core-valence interaction is treated in the pseudopotential approach may lead to uncertainties of about 0.1 eV in the width of the spectrum, but it is not at the heart of the discrepancy between the theoretical and experimental photoelectron spectra.

In order to test the effect of relaxation one can calculate the Kohn-Sham eigenvalues with the transition state concept [Per81], i.e., one occupies one spin-orbital with only a half electron. Again, the effect is moderate and furthermore it goes in the wrong direction. E.g., for Na_5^- one obtains the eigenvalues (in eV) $\varepsilon_{1,\uparrow}(occ = 0.5) = -2.502$, $\varepsilon_{2,\uparrow}(occ = 0.5) = -1.658$, $\varepsilon_{3,\uparrow}(occ = 0.5) = -1.198$, i.e., the ‘bandwidth’ is too large by about 0.3 eV. Since Kohn-Sham eigenvalues from accurate potentials are approximations to *relaxed* electron removal energies, one does not expect that the transition state concept, which is an approximation itself, needs to be taken into account in further considerations.

The above considerations show that the observed discrepancies are not due to deficiencies in the ‘technical’ treatment of the clusters. Therefore, the question arises whether a different way of relating the Kohn-Sham eigenvalues to the measured photoelectron spectra leads to different conclusions and clears up the situation. Specifically, a scheme which is believed [Jel03] to convert Kohn-Sham eigenvalues into electron binding energies is tested by applying it to the LDA eigenvalues of Na_5^- and Na_7^- . The calculations are based on what in Ref. [Jel03] is called the ‘integer valued grid’ since this is supposed to be accurate for atomic clusters [Jel03]. Tab. 7.3 shows the corrections that have to be added to the negative of each eigenvalue in order to obtain the corresponding electron binding energy. Since the density is not spin polarized in the cases studied here, the same correction applies to the first and second eigenvalue, third and fourth eigenvalue, etc. The last column shows the width of the spectrum that results from the ‘corrected’ eigenvalues.

Cluster	Δ_2	Δ_4	Δ_6	Δ_8	W
Na_5^-	1.361	1.309	1.279	–	1.265
Na_7^-	1.438	1.350	1.321	1.313	1.576

Table 7.3: ‘Corrections’ Δ_i that have to be added to the negative of the i -th LDA Kohn-Sham eigenvalue to obtain the corresponding electron binding energy according to the scheme of Ref. [Jel03]. All values are in eV and have been calculated according to the ‘integer-grid scheme’[Jel03]. W is the width of the spectrum that results from the ‘corrected’ eigenvalues. Note that the ‘corrections’ make the width larger, i.e., worsen the agreement with experiment (compare Tab. 7.1).

The first fact that becomes evident from Tab. 7.3 is that the ‘corrections’ are very similar for all eigenvalues of a given cluster. Thus, the scheme in the present cases does hardly more than shifting the whole spectrum by a constant. The second conclusion from Tab. 7.3 is that the small differences in the corrections to the individual eigenvalues which make the scheme a little different from a rigid shift actually influence the width of the spectrum in the wrong way: instead of making the energetic difference between the most strongly bound and the most loosely bound electron smaller, the corrections make the difference larger. Thus, the width of the spectrum increases and agreement with experiment becomes worse. This is not considered to be a serious issue since the effect is rather small. But these findings are in line with the fact that the scheme of Ref. [Jel03] is not a rigorous density functional for obtaining electron binding energies, but rather a procedure which makes use of information from total energy differences in a not unpalatable but nevertheless *ad hoc* way.

To summarize, the calculations presented above confirm that better approximations for the Kohn-Sham potential, as provided, e.g., by the exact-exchange OEP, lead to Kohn-Sham eigenvalues that are better approximations to electron removal energies than LDA eigenvalues. In particular, the width of the occupied eigenvalue spectrum is reduced and thus in better agreement with experiments. However, the theoretically predicted width of the photoelectron spectra is still overestimated by the exact-exchange OEP Kohn-Sham eigenvalues. Thus, the question arises whether the approach based on the excitation energies of the ‘daughter’ system can remove the discrepancy between the theoretical and experimental results. This question is the subject of the next chapter.

Chapter 8

Photoelectron spectra from TDDFT

As described in Chap. 7 theoretical photoelectron spectra can be obtained by calculating the excitation energies of the ‘daughter’ system. In the framework of time-dependent DFT one can use the full linear density-response function to obtain the excitation energies of a system. This function provides access to the excitation energies since it has poles at these energies. The crucial observation for DFT is that the interacting linear density-response function can be expressed in terms of the Kohn-Sham response function and the exchange-correlation kernel $f_{xc}(\mathbf{r}, t, \mathbf{r}', t') = \left. \frac{\delta v_{xc}(\mathbf{r}, t)}{\delta n(\mathbf{r}', t')} \right|_{n_0}$ (n_0 being the ground-state density) [Pet96, Cas96, Gro96]. Nowadays, most applications use the matrix equation of Casida [Cas96] to obtain the excitation energies.

Alternatively, the excitation energies can be extracted from a spectral analysis of the time-dependent density coming from a real-time propagation [Yab96, Cal00, Mar01]. In this approach the exchange-correlation kernel is not needed, but instead, the time-dependent Kohn-Sham equations are solved without explicit linearization. To illustrate this approach imagine one has created a time-dependent density $n(\mathbf{r}, t)$ of an interacting system by, e.g., a laser excitation. Assuming that the system is confined by the same time-independent potential before and after the laser pulse, one can write the excited density in terms of the eigenstates $|\psi_j\rangle$ of the interacting system in the time-independent potential. It reads

$$n(\mathbf{r}, t) = \langle \psi(t) | \hat{n} | \psi(t) \rangle = \sum_{j,k} c_j^* c_k \langle \psi_j | \hat{n} | \psi_k \rangle \exp(-i(E_k - E_j)t/\hbar) \quad (8.1)$$

where E_j is the eigenvalue corresponding to $|\psi_j\rangle$ and \hat{n} is the density operator. Assuming that the time-dependent state $|\psi(t)\rangle$ is dominated by the ground state, i.e., $c_0 \gg c_j$, one can write

$$n(\mathbf{r}, t) \approx |c_0|^2 n_0(\mathbf{r}) + \sum_j c_0^* c_j \langle \psi_0 | \hat{n} | \psi_j \rangle \exp(-i(E_j - E_0)t/\hbar) + c.c. \quad (8.2)$$

Here, $n_0(\mathbf{r})$ is the ground-state density of the system. If one now calculates the Fourier transform of $n(\mathbf{r}, t)$ one gets peaks at the exact excitation energies of the system. Since time-dependent DFT in principle provides one with the exact time-dependent density, this is an easy method to obtain the excitation energies of the interacting system from a time-dependent DFT calculation.

In a practical calculation two problems must be solved to get the excitation energies from this scheme. First, one has to create a time-dependent density which is dominated by the ground-state density and, in addition, contains the excited states of interest. The second problem is how to extract the excitation energies from the time-dependent density in practice. Since the density in every space point at all times cannot be stored, a full Fourier transform of Eq. (8.2) giving $n(\mathbf{r}, \omega)$ is not possible. To overcome this problem several possibilities exist. One is to evaluate $n(\mathbf{r}, \omega)$ only for some points in space [Küm01], e.g., in the center of the cluster. A different method is to Fourier transform certain moments of the density distribution, e.g., the dipole moment

$$\mathbf{d}(t) = e \int \mathbf{r} n(\mathbf{r}, t) d^3r . \quad (8.3)$$

Obviously, some excitations are filtered out by this procedure because the Fourier spectrum of the dipole moment only shows excitation energies of states which can be coupled to the ground state via the dipole operator. In order to get non-dipole active excitations one has to record also higher moments, e.g., quadrupole moments. In the following the time-dependent dipole and quadrupole moments are used to extract the excitation energies of the systems of interest.

8.1 Numerical details

In order to obtain the results presented in this chapter and in Chap. 6 a numerical scheme for solving the time-dependent Kohn-Sham equations in three dimensions has been implemented into a modified version of the PARSEC program package [Kro06]. The main features of this implementation are presented in this subsection. Originally, the PARSEC program package solves the static Kohn-Sham equations in combination with pseudopotentials on a real-space grid with a high-order approximation to the Laplacian (up to twelfth-order). This can be done either on a single processor or on several processors due to the implemented parallelization. Using PARSEC as a starting point, several numerical routines which solve the time-dependent Kohn-Sham equations in real-time have been added to the original package. The general philosophy is to use the PARSEC routines to solve the static Kohn-Sham equations and then use the resulting ground-state quantities as initial conditions for the time-dependent equations.

In contrast to the one-dimensional implementation presented in Chap. 5 a different approximation for the propagator is used in three dimensions. Instead of the Crank-Nicolson method a fourth-order Taylor approximation is used, i.e., the propagator is

approximated by [Yab96, Ca04b]

$$\hat{U}(t + \Delta t, t) \approx \sum_{n=0}^4 \left(-i \frac{\Delta t}{\hbar} \hat{h}_S(t + \Delta t/2) \right)^n. \quad (8.4)$$

The advantage of this method is that one does not have to solve any linear equations to obtain the Kohn-Sham orbitals at later times. One only has to apply the Hamiltonian several times to the initial Kohn-Sham orbitals. Thus, for a real-space grid only matrix-vector multiplications are needed. Since the Hamiltonian is sparse, these multiplications can be performed very efficiently. For the Hamiltonian in Eq. (8.4) the approximation

$$\hat{h}_S(t + \Delta t/2) \approx \frac{\hat{h}_S(t) + \hat{h}_S(t + \Delta t)}{2} \quad (8.5)$$

is used. The Hamiltonian $\hat{h}_S(t + \Delta t)$ is calculated from approximated Kohn-Sham orbitals obtained from a time step with $\hat{h}_S(t + \Delta t/2) \approx \hat{h}_S(t)$. The main other aspects of the implementation are listed in the following.

- For the time-dependent exchange-correlation potential either the time-dependent LDA, the time-dependent exact-exchange KLI potential, or the time-dependent Perdew-Zunger self-interaction correction KLI potential can be used [Per81, Kör06].
- For the excitation of the system a momentum boost is implemented. This boost is realized by multiplying all ground-state orbitals with a phase factor $\exp(i \mathbf{r} \cdot \mathbf{p}_{\text{boost}}/\hbar)$. In addition, a time-dependent laser field in dipole approximation can be applied to the system. Implemented are the common pulse shapes, i.e., a \sin^2 envelope, a Gaussian envelope and a linear up and down ramping with a constant amplitude in between. Additionally, the same shape without an oscillating field can be used. All different potentials and the required parameters are plotted in Fig. 8.1.
- The atomic cores consisting of the nuclei and the core electrons can be propagated according to classical equations-of-motion with Hellmann-Feynman forces [Jin94]. The equations-of-motion are solved with a second-order symplectic leapfrog algorithm (named si2.a in Ref. [Gra94]). The implemented scheme allows a non-adiabatic treatment of couplings between the electronic and ionic degrees of freedom [Saa96, Cal00, Ca04a, Hey05].
- For strong ionizing excitations absorbing boundary conditions can be activated to prevent that the ionized density is reflected back into the system by the boundary of the numerical box [Rei06]. The absorbing boundary is realized by multiplying the Kohn-Sham orbitals in a boundary layer after every time step by a mask function, i.e.,

$$\varphi_j(\mathbf{r}, t) = \varphi_j(\mathbf{r}, t) \sin^p \left(\frac{\pi d}{2B_{\text{Bl}}} \right), \quad \text{for } d \leq B_{\text{Bl}} \quad (8.6)$$

where d is the distance from the point \mathbf{r} to the surface of the numerical box and B_{BI} is the thickness of the absorbing boundary layer provided by the user. The damping exponent p has a default value of 0.02 [Rei06] and can be also changed by the user. The \sin^p is chosen because it goes smoothly from zero to one. Since all absorbing potentials also lead to a reflection in a quantum mechanical treatment, the boundary layer should not be chosen too small to guarantee minimal backscattering.

- As in the static part of the code the routines connected to the propagation are parallelized.

All in all the additional routines contribute around 4000 new lines of code and comments to PARSEC.

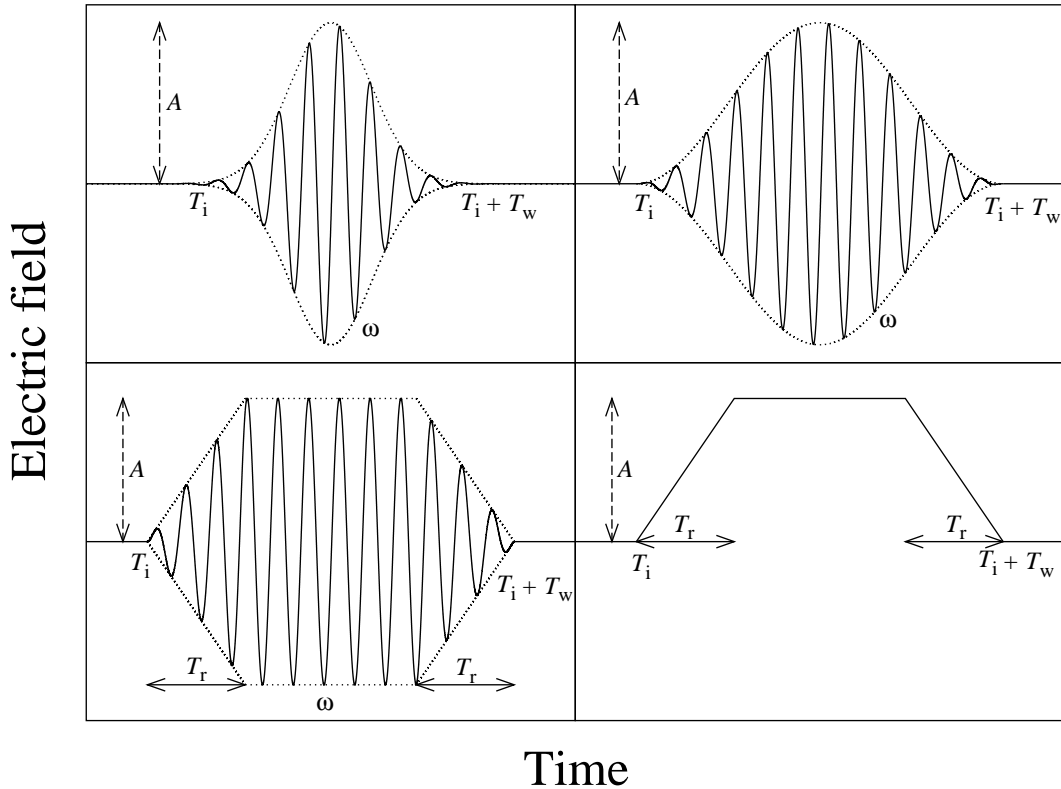


Figure 8.1: Schematic view of different pulse shapes implemented in the modified version of the PARSEC code. Upper left corner: Gaussian envelope, upper right corner: \sin^2 envelope, lower left corner: linear envelope, and lower right corner: linearly ramped field. The pulses are characterized by an amplitude A , a laser frequency ω , a starting time T_i , and a pulse duration T_w . The linearly shaped pulses are additionally characterized by a ‘ramping’ time T_r and the Gaussian pulses by the full width at half maximum T_{FWHM} (not plotted).

8.2 Anionic sodium clusters

8.2.1 Technical aspects

For the ionic ground-state configurations of the ‘mother’ systems optimized structures obtained with the PARSEC program package are used. The generalized-gradient approximation of Perdew *et al.* (PBE) [Per96] has been employed for the geometry optimization. The ionic cores are treated consistently with norm conserving non-local pseudopotentials [Tro91]. A time step of 0.003 fs is used and the total propagation time is 75 fs. In the propagation the ionic cores are also described by norm conserving non-local pseudopotentials. Furthermore, the ionic structures are fixed during the propagation. The grid spacing is $0.7 a_0$ and the grid radius varies between 20 and $23 a_0$ depending on the system. The time-dependent density is created by applying a boost $\exp(i \mathbf{r} \cdot \mathbf{p}_{\text{boost}}/\hbar)$ to the ground-state Kohn-Sham orbitals. The total excitation energy of the system is $E_{\text{excit}} = 1.0 \times 10^{-5}$ eV, i.e., a boost strength $|p_{\text{boost}}| = \sqrt{2m_e E_{\text{excit}}/N}$ is applied to each Kohn-Sham orbital (with m_e being the electron mass and N the number of electrons). In addition, the calculations are repeated with a boost strength reduced by a factor of 1.0×10^{-2} . Using these two small boost strengths allows one to check whether the created time-dependent density is dominated by the ground-state density (see below).

Instead of applying the same boost vector $\mathbf{p}_{\text{boost}}$ to all Kohn-Sham orbitals, and thus creating a coherent velocity field, the boost directions for different Kohn-Sham orbitals are varied. This is necessary since applying the same boost direction to all Kohn-Sham orbitals corresponds to first order in $\mathbf{p}_{\text{boost}}$ to a dipole excitation of the system, i.e., from the resulting time-dependent density it is only possible to retrieve the excitation energies of ‘dipole-active’ states. By applying different boost directions to different Kohn-Sham orbitals one models a general excitation mechanism creating a time-dependent density containing excited states with different symmetry properties. In detail, one randomly chooses a boost direction (no symmetry axis of the considered cluster) for the first orbital and then chooses a coordinate system such that this direction is the first diagonal (for the remaining rotational degree of freedom a random angle is chosen). After this one boosts the second orbital in the opposite direction of the first boost. The third orbital is then boosted in the direction of the second diagonal of the chosen coordinate system, the fourth again in the opposite direction and so on. For Na_9 , the ninth orbital is boosted again in the same direction as the first orbital. Since the only purpose of this procedure is to create a time-dependent density without any particular symmetries, the relative orientation of the cluster with respect to the boost directions is not considered to be of special importance.

Finally, the time-dependent local-density approximation for the exchange-correlation potential is used for the propagation. Since the linear response of the homogeneous electron gas is the same in this approximation and in the PBE functional, the differences in the resulting excitation energies can be expected to be small in the low-energy regime.

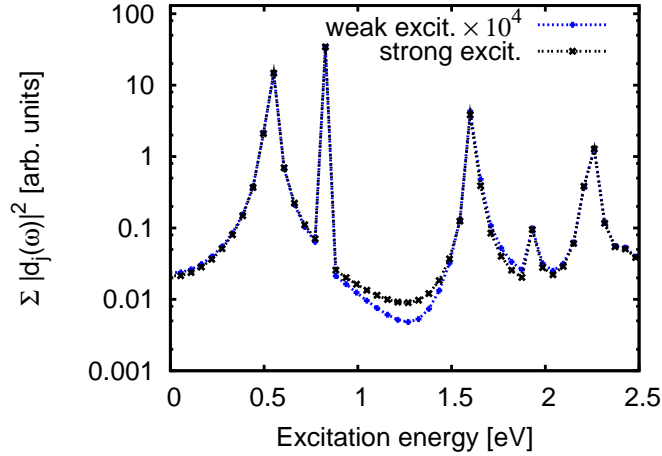


Figure 8.2: Dipole power spectrum of Na_3 resulting from an incoherent boost excitation. The result obtained from a total excitation of 1×10^{-5} eV is labeled ‘strong excit.’ whereas the label ‘weak excit.’ corresponds to a boost reduced by a factor of 1×10^{-2} . Clearly, the dipole power spectrum scales quadratically with the boost strength indicating that the peak positions correspond to excitation energies between the ground state and excited states.

8.2.2 Results for Na_3^-

Fig. 8.2 shows the dipole power spectra of Na_3 resulting from two boost strengths differing by a factor of 10^2 . The dipole power spectrum is given by

$$D(\omega) := \sum_{j=1}^3 |d_j(\omega)|^2 \quad (8.7)$$

where $d_j(\omega)$ is the Fourier transform of the j -th component of the dipole moment, Eq. (8.3). For small momentum boosts first-order perturbation theory predicts a linear dependence of the expansion coefficients c_j in Eq. (8.1) on the boost strength. As a consequence, reducing the boost strength by a factor of c suppresses peaks corresponding to energy differences between two excited eigenstates by a factor of c^4 in the power spectrum. Since peaks corresponding to transitions between the ground state and an excited eigenstate are only suppressed by a factor of c^2 , changing the boost strength allows one to distinguish between these two kinds of excitations. As one can see in Fig. 8.2, the results for the two boost strengths are almost identical except for the predicted factor of 10^4 . Thus, one concludes that all the peak positions in the dipole power spectrum of Fig. 8.2 correspond to energy differences between the ground state energy and the energy eigenvalues of the excited eigenstates.

The situation is different for the power spectrum resulting from the quadrupole moments. In Fig. 8.3 the quantity

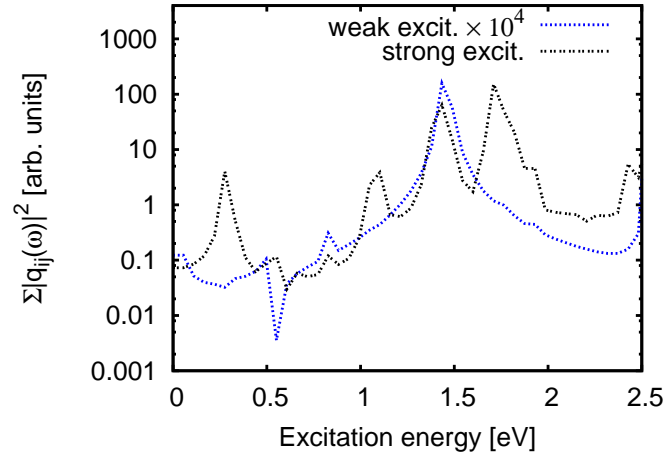


Figure 8.3: Sum of the absolute square of the Fourier-transformed components of the quadrupole tensor resulting from the same excitations as in Fig. 8.2. In contrast to the dipole power spectrum some peaks vanish with reduced boost strength indicating that they correspond to energy differences between excited states.

$$Q(\omega) := \sum_{\substack{i=1 \\ j \geq i}}^3 |q_{ij}(\omega)|^2 \quad (8.8)$$

is plotted for the same two excitation boosts. In this equation, $q_{ij}(\omega)$ is the Fourier transform of the quadrupole moment

$$q_{ij}(t) = \int n(\mathbf{r}, t) (3x_i x_j - r^2 \delta_{ij}) d^3 r, \quad (8.9)$$

$$r^2 = \sum_{i=1}^3 x_i^2,$$

and the sum only runs over the independent components of the quadrupole tensor. Clearly, the quadrupole spectra for the different excitation strengths differ considerably. For instance, the three large peaks at around 0.3, 1.1, and 1.7 eV vanish almost completely. Thus, one concludes that they belong to transition energies between different excited states. Indeed, one can see that these energies are exactly equal to the energy differences between the first excited state and the other excited states from the dipole spectrum.

The reason why there are no peaks at these energies in the dipole spectrum can easily be understood if one takes the geometry of Na_3 into account. Since Na_3 has a linear ionic configuration, the ground state has even parity. Thus, the dipole spectrum only shows excited states with odd parity. Since two states with odd parity cannot be coupled by the dipole operator, transitions between these states do not show up in the dipole spectrum.

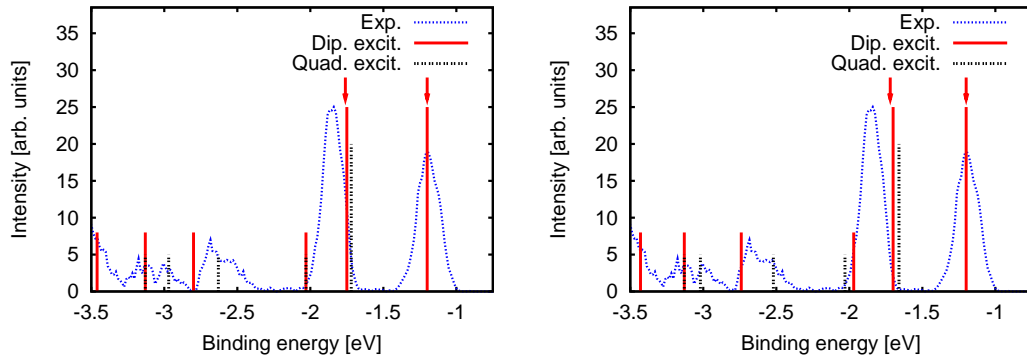


Figure 8.4: Measured photoelectron spectrum of Na_3^- ('Exp.>') and theoretical photoelectron spectrum obtained from the excitation energies of Na_3 . Excitation energies from the dipole spectrum are labeled 'Dip. excit.' whereas 'Quad. excit.' labels excitation energies deduced from the quadrupole moments. Arrows indicate the result obtained from the Kohn-Sham DOS. Left part: results obtained from the ionic ground-state configuration at zero temperature. Right part: results obtained from an ionic configuration with a larger bond length to simulate a higher temperature. For most peaks the agreement with the experimental photoelectron spectrum is clearly improved.

After the identification of the true excitation energies one can now compare the results with the measured photoelectron spectrum. In Fig. 8.4 the excitation energies of Na_3 , the Kohn-Sham density of states (DOS) of Na_3^- and the measured photoelectron spectrum (of Na_3^-) are plotted. The positions of the occupied Kohn-Sham eigenvalues are indicated by arrows, long bars indicate excitation energies from the dipole spectrum and shorter bars excitation energies from the quadrupole moments. In addition, excitation energies leading to peaks below the strongest bound experimental peak are reduced in their overall height. For better comparison the Kohn-Sham DOS and the excitation spectrum are both rigidly shifted in such a way that the most weakly bound peak coincides with the experimental one.

As the left part of Fig. 8.4 shows the peak positions that one obtains from the Kohn-Sham DOS are close to the experimental peak positions. Unlike to the case of larger Na clusters the width is slightly smaller than the energy difference between the two large experimental peaks but it is still reasonable. However, since there are only two occupied Kohn-Sham orbitals in Na_3^- the Kohn-Sham DOS picture fails completely to describe the higher lying peaks in the measured spectrum.

As one expects from Eq. (7.1) the photoelectron spectrum obtained from the excitation energies shows a much richer structure than the Kohn-Sham DOS. One striking feature for instance is the second excitation around -2.0 eV. It seems that the energy difference between this peak and the one at -1.7 eV is too large in the calculation and that they are merged to one peak in the experimental photoelectron spectrum. However,

in general, the dynamically calculated excitation energies and the energies obtained from the experimental photoelectron spectrum are close to each other even for the stronger bound peaks. To see if the remaining discrepancy can be further reduced by taking temperature effects into account one can repeat the calculations with a larger bond length. Due to the net negative charge of the cluster one can expect that other geometry changes, e.g., bending, only play a minor role in the case of Na_3^- . The new bond length is approximately 6.8 instead of 6.5 a_0 . This new value for the bond length l of the cluster is obtained from an estimate for the thermal expansion at $T = 300$ K. It is based on the formula $\beta = \frac{1}{l} \frac{\partial l}{\partial T}$ for the linear thermal expansion coefficient β which one can roughly estimate by $\beta \approx 2\beta_{\text{bulk}}$ [Kü00b], where β_{bulk} is the bulk value for crystalline sodium at room temperature.

The result can be seen in the right part of Fig. 8.4. For most peaks one can observe a small shift towards lower absolute binding energies. Except for the peak at -1.7 eV the agreement between the experimental and theoretical spectrum is slightly improved by the increased bond length. Especially the broader peak at around -2.6 eV is nicely reproduced in this case. All in all, both calculations show that for Na_3^- the main advantage of the ‘excitation picture’ is the reproduction of the deeper bound structures in the photoelectron spectrum.

8.2.3 Results for Na_5^- , Na_7^- , and Na_9^-

Fig. 8.5 shows the experimental photoelectron spectrum of Na_5^- , the Kohn-Sham DOS, and the photoelectron spectrum obtained from the excitation energies of Na_5 . The labeling is the same as in the corresponding previous figures. As for Na_3^- the Kohn-Sham DOS is in acceptable agreement with the first large peaks although the strongest bound large peak has a too negative binding energy in the Kohn-Sham DOS. As one can see these peaks are also well described by the excitation energies of the ‘daughter’ system with the additional advantage that the last peak at -2.2 eV is better reproduced. In this approach it consists of four close-lying excitations.

Beyond the peak at -2.2 eV the comparison with the experimental measurement is difficult since no clear peak structures can be observed. Perhaps the accumulation of excited states around -3.3 eV can be associated with the measured peak in this region, but for the reasons given below, one has to be very cautious in making comparisons in this part of the spectrum.

As one can see from the results for Na_7^- and Na_9^- discussed below the problem of comparing the deeper lying part of the measured photoelectron spectrum with calculated excitation energies is not specific to Na_5^- . In general, the density of excited states grows with the excitation energy, i.e., more and more states appear in the theoretical calculation. On the other hand, as mentioned previously, the photoelectron spectrum depends not only on the positions of the excited states but also on the matrix element of the perturbing operator \hat{D} between the initial and the final state. Taking the ground

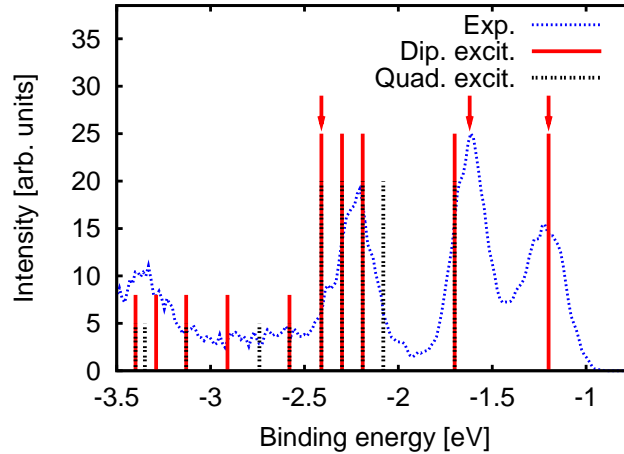


Figure 8.5: Same as in Fig. 8.4 but for Na_5^- . Although both, the Kohn-Sham DOS and the photoelectron spectrum from the excitation energies, describe the measured photoelectron spectrum acceptable the large peak at -2.2 eV is much better reproduced by the excitation energies from the ‘daughter’ system.

state of the ‘mother’ system for the initial state and a product state consisting of one photoelectron with momentum \mathbf{k} for the final state one obtains matrix elements of the form $\langle \mathbf{k}, \psi_j^{(N)} | \hat{D} | \psi_0^{(N+1)} \rangle$. It is intuitively clear that these matrix elements are much larger for low-lying states than for energetically high-lying ones which in an independent-particle picture would correspond to removing one particle and exciting a second one above the Fermi level. Especially, in the case of truly independent particles this process cannot happen if the perturbing operator is a one-particle operator like the dipole operator. Thus, many energetically high-lying eigenstates of the ‘daughter’ system are hardly or even not at all excited in the experiment. Since the mentioned matrix elements depend on the interacting many-particle wavefunctions, calculating these exactly is close to being impossible. Especially, retrieving these matrix elements from a time-dependent DFT propagation of the ‘daughter’ system is not trivial because the propagation only provides information about matrix elements between excited states and the N -particle ground state and not the $(N + 1)$ -particle ground state.

However, as the presented calculations show, the matrix elements do not play a very important role in the part of the spectrum that one is mainly interested in. Nevertheless the calculations also clearly indicate that one has to consider them if the deeper lying parts of the spectrum are of interest. A possible method how this can be done in a time-dependent DFT calculation can be found at the end of this chapter.

The results for Na_7^- are shown in Fig. 8.6. As said previously in the region below -2.5 eV it is difficult to compare theory and experiment due to the great number of close lying transitions. As in Na_5^- the Kohn-Sham DOS describes the strongest bound

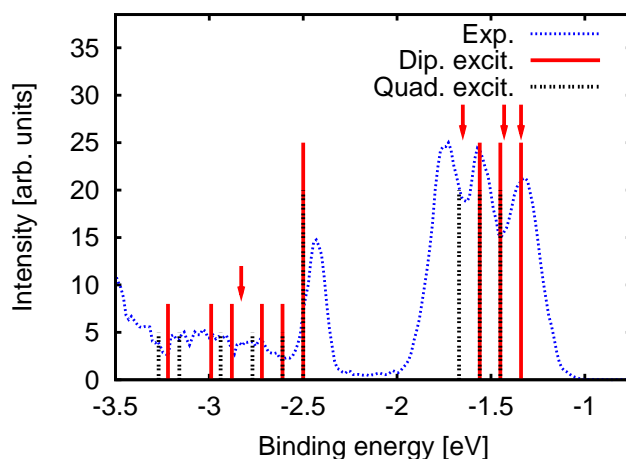


Figure 8.6: Same as in Fig. 8.4 but for Na_7^- . Especially, the peak at -2.4 eV is much more accurately described by the excitation energies than by the Kohn-Sham DOS. In the weakly bound region thermal effects play an significant role in the case of Na_7^- . This explains the rather poor agreement between the theoretical values calculated at zero temperature and the measured curve between -1.3 and -1.7 eV.

large peak worst. In this case it is already off by 0.4 eV. In contrast, the peak position obtained from the time-dependent LDA excitation energies is considerably closer to the experimental peak. It is only off by 0.1 eV. Thus, the overestimation of the spectrum's width by the Kohn-Sham DOS discussed in the previous chapter is not observed in the result obtained from the time-dependent LDA calculation. The remaining difference of 0.1 eV between the width of the theoretical and the experimental spectrum can be easily caused by technical aspects like the employed pseudopotential and exchange-correlation potential. In addition, thermal effects like bond elongation and structural isomerization can shift the obtained width by 0.1 eV [Kü00b, Mos01, Mos03]. Considering that the experimental photoelectron spectra are obtained from clusters with a temperature of around 250-300 K, the difference between the theoretical result at zero temperature and the experimental result is hardly surprising. At these temperatures the larger anionic sodium clusters behave liquidlike [Mos03]. Consequently, many different ionic configurations are present in the experiment and show up in the measured spectra.

This aspect must also be kept in mind if the theoretical and experimental results are compared in the region between -1.3 and -1.7 eV. In this region both the zero temperature Kohn-Sham DOS result and the zero temperature result from the excitation energies do not describe the measured photoelectron spectrum very accurately. Especially, the excitation peak at -1.45 eV does not fit very well. However, from Ref. [Mos03] it is known that the agreement between the experimental and the Kohn-Sham DOS result in this energy region is significantly improved if different ionic structures are taken

into account via Born-Oppenheimer Langevin molecular-dynamics [Bar93]. Therefore, one can expect that the agreement between the experimental and the time-dependent LDA result is also improved if different ionic structures are taken into account. Due to the more complicated structures and the growing number of isomers the inclusion of the temperature influence on the ionic structures of larger clusters is much more involved than in the case of Na_3^- . Additionally, combining Born-Oppenheimer Langevin molecular-dynamics with the calculation of excitation energies is substantially more expensive than combining such a molecular dynamics scheme with a Kohn-Sham DOS calculation. Thus, including thermal effects in the present study is beyond the scope of the present work.

Finally, the theoretical results for Na_9^- are compared in Fig. 8.7 with the measured photoelectron spectrum. This cluster is the first one which has a clear peak in the range between the highest and lowest occupied Kohn-Sham eigenvalue which is completely absent in the Kohn-Sham DOS, i.e., the experimental photoelectron spectrum shows six clear peaks whereas the Kohn-Sham DOS consists of only five peaks: the peak around -2.4 eV is completely missing in the Kohn-Sham DOS. In addition, the strongest bound peak in the Kohn-Sham DOS is off by 0.5 eV. In other words, the Kohn-Sham DOS result is inaccurate to the extent of being useless below -2.2 eV. As for Na_7^- the splitting of the large peak around -1.8 eV is reproduced if different ionic structures are used [Mos03].

In contrast to the Kohn-Sham DOS result the photoelectron spectrum obtained from the excitation energies is close to the measured curve over the whole range. Below the lowest lying peak at -2.7 eV the comparison is again difficult without knowing the matrix elements mentioned above. For the two peaks at -2.7 and -2.4 eV the theoretical values are off by 0.1 eV. Especially since Na_9^- , in contrast to Na_7^- , is not a closed-shell cluster, one can expect that such energy differences can be easily caused by ionic structure modifications induced by finite temperatures. As expected from Ref. [Mos03] the splitting of the peak at -1.8 eV is also not reproduced by the zero temperature time-dependent LDA calculation. All in all, the experimental result in the weaker bound part of the spectrum is described equally well by the Kohn-Sham DOS and the excitation energies of the ‘daughter’ system. However, in the stronger bound part the time-dependent calculation yields a much more realistic description of the photoelectron spectrum than the Kohn-Sham DOS. Since this emerges as a general observation for all systems studied, it is discussed on general grounds in the following section.

8.2.4 Conclusion

In general, the photoelectron spectra for all clusters studied in this work can be divided into three parts. The first part consists of large, ‘weakly’ bound peaks, the second of large, ‘strongly’ bound peaks, and finally a ‘less structured’ region below the strongest-bound large experimental peak. Except for Na_3^- no comparisons between the theoretical and the experimental results can be made in the third region. As previously discussed

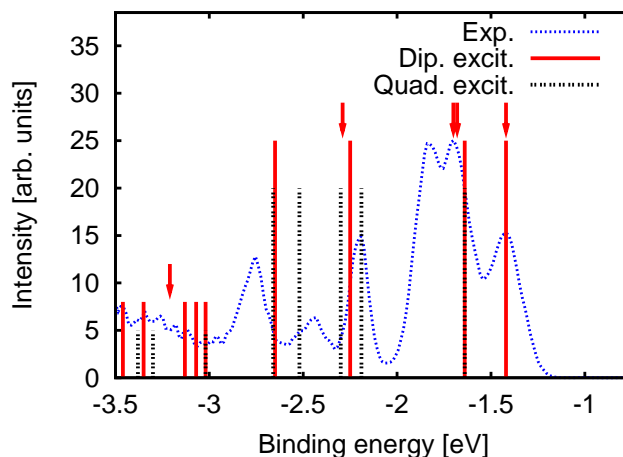


Figure 8.7: Same as in Fig. 8.4 but for Na_9^- . As in Na_7^- especially the stronger bound part of the spectrum is described more accurately by the calculated excitation energies than by the Kohn-Sham DOS.

the main reason for this is the missing access to the transition matrix elements between the ground and the excited states. Since the number of excited states can grow very rapidly, one can expect that the omission of the transition matrix elements can cause severe problems if more complex systems are examined. A possible way to overcome this problem is by including the information of the matrix elements in the initial density, i.e., by creating an initial density that only includes the states which are really excited in the ionization process.

In the middle part of the spectrum the results obtained from the excitation energies are clearly superior to the results from the Kohn-Sham DOS. Especially, the position of the strongest bound large peak is much better reproduced by the time-dependent approach than by the Kohn-Sham DOS. Thus, using the ‘excitation-energy’ picture cures the main problem that plagues theoretical results obtained from the Kohn-Sham DOS for sodium clusters, namely the prediction of a significantly too large width of the spectrum. In addition, the photoelectron spectrum from the time-dependent LDA excitations can describe an experimental peak in the photoelectron spectrum of Na_9^- which is completely missing in the Kohn-Sham DOS. The remaining differences between the experimental and the theoretical results are all small enough to be explainable by technical details or the finite temperature (250-300 K) of the ionic structures in the experiment. In particular the finite temperature can be expected to be responsible for the difference since the considered clusters behave liquidlike at this temperature and thus, the measured photoelectron spectra result from many different ionic structures / isomers which differ from the theoretical zero temperature ground-state structures used for the calculations.

Finally, in the most weakly bound part of the spectrum one finds that the time-dependent results and the ones from the Kohn-Sham DOS are very similar. Since the Kohn-Sham DOS at finite temperature is in very good agreement with the experimental result [Mos03], it is extremely likely that also the excitation energies calculated from higher temperature ionic structures will describe the experimental photoelectron spectra very well in this region.

Generally, these findings are in line with earlier results [Pe82b, Cho02] which report a worse agreement between the Kohn-Sham DOS results and the experimental values for stronger bound levels. In addition, the results clearly show that the agreement between the theoretical and the experimental spectrum is considerably improved for small sodium clusters if the photoelectron spectrum is extracted from the true excitation energies of the ‘daughter’ system and not the Kohn-Sham DOS. This shows the importance of taking effects beyond the independent-particle picture into account in the interpretation of photoelectron spectra.

Chapter 9

Summary and Conclusion

Offering the possibility to describe an interacting many-particle system solely in terms of its density, density-functional theory has been the subject of a tremendous number of scientific publications covering fundamental aspects and applications. Despite the enormous efforts made in the field many aspects are still not sufficiently understood and need to be investigated. Of paramount interest in this context are the properties of the unknown exchange-correlation potential. As has been described in Chap. 2 this local potential allows one to replace an interacting system by a non-interacting system which has the same electronic density. The advantage of this replacement is that for a given exchange-correlation potential one can obtain the electronic density of an interacting system by just solving one-particle Schrödinger equations. In contrast to the full interacting many-particle problem these equations can be solved extremely efficient. As stated by the Hohenberg-Kohn and Runge-Gross theorem the knowledge of the density in principle allows one to calculate any observable of interest. Thus, the full interacting many-particle problem can in principle be solved by calculating the solution of one-particle Schrödinger equations *if* the exact exchange-correlation potential is known. However, as stated above the exact exchange-correlation potential is not known and must be approximated in any practical calculation. In Chap. 2 the idea behind the most common approximation for this potential, namely the local-density approximation, has been presented together with one of its most prominent failures: the self-interaction error. As discussed at the end of Chap. 2 approximations based directly on the density cannot solve this problem completely. However, potentials constructed from the Kohn-Sham orbitals, i.e., from those orbitals which solve the Kohn-Sham equations, can solve this problem. Since the Kohn-Sham orbitals are implicit functionals of the density, any expression constructed from these orbitals is a legitimate density functional. This is the basis of orbital functionals.

As has been shown in Chap. 3 orbital functionals are also a promising concept because they can show a discontinuous behavior when the particle number is changed. Such a discontinuous behavior of the exchange-correlation potential under particle-

number changes is required in the fractional particle-number formalism of static and time-dependent density-functional theory. The discussion given in Chap. 3 furthermore shows that even in situations in which the particle number is an integer the exchange-correlation potential can have a behavior similar to the discontinuous behavior in the fractional particle-number formalism. This feature can be expected to play a crucial role in any time-dependent process involving a particle transfer between two separated sub-systems, e.g., charge-transfer excitations in molecules and molecular dissociation.

Due to the presented reasons using orbital functionals is highly desirable. Unfortunately, this is not trivial since the exchange-correlation potential must be obtained from the complicated optimized effective potential integral equation. In ground-state density-functional theory this equation can be solved by transforming the integral equation into a set of coupled differential equations. As has been demonstrated in Chap. 4 the time-dependent optimized effective potential equation can also be transformed into a set of coupled differential equations. In contrast to the static case, however, Chap. 5 shows that no converging method to solve the time-dependent coupled differential equations exists at present. Thus, one of the most pressing problems of time-dependent density-functional theory, namely the construction of the time-dependent optimized effective potential, is an unsolved problem. Hopefully future work will cure this problem. At present, the ‘OSBK’ approximation which has been put forward in Chap. 4 can be used to go beyond the commonly used Krieger-Li-Iafrate approximation.

The missing access to the time-dependent optimized effective potential turns out to be particularly severe since the popular Krieger-Li-Iafrate approximation to the time-dependent optimized effective potential violates the ‘Zero-Force theorem’, i.e., Newton’s third law. This has been demonstrated in Chap. 6. In this chapter it has also been shown that the violation of the ‘Zero-Force theorem’ can lead to a completely wrong time evolution of the density. Considering this, the observation that the time-dependent Krieger-Li-Iafrate potential satisfies the ‘Harmonic-Potential theorem’ is only a cold comfort. In the case of strong external potentials one can hope that the dynamics is dominated by the external fields and the violation of the ‘Zero-Force theorem’ plays only a minor role. However, if one is interested in extracting the excitation energies from a real-time propagation as done in Chap. 8 the violation of the ‘Zero-Force theorem’ can be an insurmountable obstacle. The fact that the time-dependent local-density approximation satisfies all the constraints discussed in Chap. 6 demonstrates how resourceful this approximation is despite all its drawbacks.

In contrast to the chapters 2 - 6 which have mainly dealt with fundamental aspects of density-functional theory the last two chapters have been dedicated to an application of density-functional theory in the field of cluster physics. Quite generally, clusters are an aggregation of atoms or molecules. The number of constituents in one cluster can vary between a few units and several thousand units, i.e., clusters are scalable objects and provide a bridge between atomic / molecular physics and solid state physics. Due to

the resulting large differences in particle numbers density-functional theory is a perfect tool for this area of physics.

Of particular interest in cluster physics are the electronic and ionic structures of clusters. Due to the small size of many clusters photoelectron spectroscopy is very often the only method that provides access to these structures. Whereas the electronic structure can directly be accessed by photoelectron spectroscopy this is not possible for the ionic structure. However, comparing the measured photoelectron spectrum with theoretical results obtained from first-principle calculations for different ionic structures allows one to identify the ionic structure of the measured cluster. Clearly, using this elegant interplay between experiment and theory can only work if reliable methods exist to calculate the photoelectron spectrum. In Chap. 7 and Chap. 8 different theoretical approaches to obtain the photoelectron spectrum from density-functional calculations have been investigated and compared to experimental results for small anionic sodium clusters. Since sodium clusters are among the most studied clusters, both experimentally and theoretically, they provide a well-suited test ground for such comparisons of different methods. In addition, due to their electronic structure with one ‘quasi free’ valence electron per atom these clusters are the paradigm representative for metal-like clusters. As a consequence, the local-density approximation can be expected to work well in this case.

The most common method to obtain the photoelectron spectrum from a density-functional calculation has been studied in Chap. 7. In this method the Kohn-Sham eigenvalues obtained from a ground-state calculation are interpreted as binding energies. This procedure turns out to work quite well for the outer valence states, i.e., for the weakly bound peaks in the photoelectron spectrum. However, the more strongly bound peaks of the experimental spectrum are not accurately reproduced by this approach. As shown in Chap. 7 this observation holds for different approximate exchange-correlation potentials and can also not be explained by technical aspects of the calculations. This indicates that the observed discrepancy between the theoretical and experimental results is rather due to the interpretation of the Kohn-Sham eigenvalues as binding energies than due to the approximate exchange-correlation potentials employed. However, to ultimately prove this statement it would be highly desirable to calculate the exact Kohn-Sham eigenvalues, i.e., the eigenvalues resulting from the exact exchange-correlation potential. Unfortunately, this requires the knowledge of the exact density and calculating this density from quantum-chemical ab-initio methods requires a huge effort for larger systems.

In Chap. 8 it has been explained that the second approach to obtain the photoelectron spectrum is based on the interpretation of the photoelectron spectrum as a measurement of the excited states of the remaining system, i.e., the system without the photoelectron. Since excitation energies can be calculated by time-dependent density-functional theory, at least the peak positions can be obtained from time-dependent density-functional

theory. As shown in Chap. 8 this approach considerably improves the agreement between the theoretical and the experimental results. Especially, the more strongly bound parts of the spectrum are much better reproduced in this approach than in the previous approach based on the Kohn-Sham eigenvalues. However, this second approach also clearly demonstrates the major drawback of both methods, namely the missing access to the peak heights. Developing methods for extracting these heights from a density-functional calculation is one of the main future tasks in the density-functional treatment of photoelectron spectroscopy.

Appendix A

The density-response function on the Keldysh contour

In this appendix $\delta\varphi_{j\sigma}(\mathbf{r}', \tau')/\delta v_{S\sigma}(\mathbf{r}, \tau)$ and the Kohn-Sham density-response function $\chi_{S\sigma}(\mathbf{r}, \tau; \mathbf{r}', \tau')$ on the Keldysh contour are calculated. This calculation demonstrates how the Keldysh formalism leads to a response function which is symmetric under the transformation $\mathbf{r}', \tau' \longleftrightarrow \mathbf{r}, \tau$ on the Keldysh contour, but becomes causal when transformed to physical time. Thus, the following derivation also gives an idea how the Keldysh formalism solves the ‘symmetry-causality paradox’ which plagues the Runge-Gross action [Gro95, Gro96, Lee98].

To calculate $\delta\varphi_{j\sigma}(\mathbf{r}', \tau')/\delta v_{S\sigma}(\mathbf{r}, \tau)$ one adds a small perturbation $\delta v_{S\sigma}(\mathbf{r}, \tau)$ with $\tau_i < \tau < \tau_f$ to the Kohn-Sham Hamiltonian and solves the Schrödinger equation on the Keldysh contour for this perturbed problem, i.e., one determines the solution of

$$(i\hbar t'(\tau)^{-1}\partial_\tau - h_{S\sigma}(\mathbf{r}, \tau) + \delta v_{S\sigma}(\mathbf{r}, \tau)) \varphi'_{j\sigma}(\mathbf{r}, \tau) = 0 . \quad (\text{A.1})$$

Since the solution $\varphi_{k\sigma}$ of the unperturbed equation provides a complete orthonormal basis set, one can write the perturbed orbitals in the form

$$\varphi'_{j\sigma}(\mathbf{r}, \tau) = \sum_{k=1}^{\infty} c_{jk\sigma}(\tau) \varphi_{k\sigma}(\mathbf{r}, \tau) . \quad (\text{A.2})$$

Inserting this ansatz into Eq. (A.1), one obtains

$$i\hbar t'(\tau)^{-1} \sum_{k=1}^{\infty} \dot{c}_{jk\sigma}(\tau) \varphi_{k\sigma}(\mathbf{r}, \tau) = \sum_{k=1}^{\infty} c_{jk\sigma}(\tau) \delta v_{S\sigma}(\mathbf{r}, \tau) \varphi_{k\sigma}(\mathbf{r}, \tau) . \quad (\text{A.3})$$

The orthogonality of $\varphi_{l\sigma}^*$ can be used to reduce the sum on the left side to just one constant. The result is

$$\dot{c}_{jl\sigma}(\tau) = \frac{t'(\tau)}{i\hbar} \sum_{k=1}^{\infty} c_{jk\sigma}(\tau) \int \varphi_{l\sigma}^*(\mathbf{r}, \tau) \delta v_{S\sigma}(\mathbf{r}, \tau) \varphi_{k\sigma}(\mathbf{r}, \tau) d^3r . \quad (\text{A.4})$$

The usual ansatz $c_{jk\sigma}(\tau) = c_{jk\sigma}^{(0)}(\tau) + c_{jk\sigma}^{(1)}(\tau) + \dots$ for a perturbation expansion in combination with a proper collection of corresponding orders on each side of Eq. (A.4) yields the following set of coupled differential equations

$$\begin{aligned} \dot{c}_{jl\sigma}^{(0)}(\tau) &= 0 \\ \dot{c}_{jl\sigma}^{(1)}(\tau) &= \frac{t'(\tau)}{i\hbar} \sum_{k=1}^{\infty} c_{jk\sigma}^{(0)}(\tau) \int \varphi_{l\sigma}^*(\mathbf{r}, \tau) \delta v_{S\sigma}(\mathbf{r}, \tau) \varphi_{k\sigma}(\mathbf{r}, \tau) d^3r \\ &\vdots \end{aligned} \quad (\text{A.5})$$

Before integrating these differential equations, it is necessary to specify the boundary conditions. Since $\varphi'_{j\sigma}$ evolves from τ_i forward in pseudotime and $\delta v_{S\sigma}(\mathbf{r}, \tau_i)$ is zero, $\delta\varphi_{j\sigma}(\mathbf{r}, \tau_i) = \varphi'_{j\sigma}(\mathbf{r}, \tau_i) - \varphi_{j\sigma}(\mathbf{r}, \tau_i)$ must vanish. This implies $c_{jk\sigma}^{(0)}(\tau_i) = \delta_{j,k}$ and $c_{jk\sigma}^{(1)}(\tau_i) = 0$. Given the first condition the differential equation for $c_{jk\sigma}^{(0)}(\tau)$ can be immediately integrated yielding $c_{jk\sigma}^{(0)}(\tau) = \delta_{j,k}$. Feeding this result into the equation for $c_{jl\sigma}^{(1)}(\tau)$ and using the second condition one obtains

$$c_{jl\sigma}^{(1)}(\tau) = \frac{1}{i\hbar} \int \int_{\tau_i}^{\tau} \varphi_{l\sigma}^*(\mathbf{r}, \tau') \delta v_{S\sigma}(\mathbf{r}, \tau') \varphi_{j\sigma}(\mathbf{r}, \tau') t'(\tau') d\tau' d^3r. \quad (\text{A.6})$$

Thus, the first-order correction is

$$\begin{aligned} \delta\varphi_{j\sigma}(\mathbf{r}, \tau) &= \sum_{k=1}^{\infty} c_{jk\sigma}^{(1)}(\tau) \varphi_{k\sigma}(\mathbf{r}, \tau) \\ &= \sum_{k=1}^{\infty} \frac{1}{i\hbar} \int \int_{\tau_i}^{\tau} t'(\tau') \varphi_{k\sigma}^*(\mathbf{r}', \tau') \delta v_{S\sigma}(\mathbf{r}', \tau') \varphi_{j\sigma}(\mathbf{r}', \tau') t'(\tau') d\tau' d^3r' \varphi_{k\sigma}(\mathbf{r}, \tau). \end{aligned} \quad (\text{A.7})$$

To calculate the functional derivative of $\delta\varphi_{j\sigma}$ with respect to $\delta v_{S\sigma}$ one has to take care of the integration measure. Since

$$\int \int f(\mathbf{r}', \tau') \frac{\delta v_{S\sigma}(\mathbf{r}, \tau)}{\delta v_{S\sigma}(\mathbf{r}', \tau')} t'(\tau') d\tau' d^3r' = f(\mathbf{r}, \tau) \quad (\text{A.8})$$

must hold for any test function f , the functional derivative is given by

$$\frac{\delta v_{S\sigma}(\mathbf{r}, \tau)}{\delta v_{S\sigma}(\mathbf{r}', \tau')} = t'(\tau)^{-1} \delta(\tau - \tau') \delta(\mathbf{r} - \mathbf{r}'). \quad (\text{A.9})$$

With this in mind $\delta\varphi_{j\sigma}/\delta v_{S\sigma}$ is finally obtained as

$$\frac{\delta\varphi_{j\sigma}(\mathbf{r}, \tau)}{\delta v_{S\sigma}(\mathbf{r}', \tau')} = -\frac{i}{\hbar} \theta(\tau - \tau') \varphi_{j\sigma}(\mathbf{r}', \tau') \sum_{k=1}^{\infty} \varphi_{k\sigma}^*(\mathbf{r}', \tau') \varphi_{k\sigma}(\mathbf{r}, \tau). \quad (\text{A.10})$$

When calculating the same functional derivative for the complex conjugate $\varphi_{j\sigma}^*$, one has to be careful with the boundary condition [Lee98]. Since $\varphi_{j\sigma}^*$ evolves from τ_f backwards in time (see, e.g., Eq. (2.28)), $\delta\varphi_{j\sigma}^*$ has to satisfy the condition $\delta\varphi_{j\sigma}^*(\mathbf{r}, \tau_f) = 0$. Carrying out a similar calculation as above leads to

$$\frac{\delta\varphi_{j\sigma}^*(\mathbf{r}, \tau)}{\delta v_{S\sigma}(\mathbf{r}', \tau')} = -\frac{i}{\hbar} \theta(\tau' - \tau) \varphi_{j\sigma}^*(\mathbf{r}', \tau') \sum_{k=1}^{\infty} \varphi_{k\sigma}(\mathbf{r}', \tau') \varphi_{k\sigma}^*(\mathbf{r}, \tau). \quad (\text{A.11})$$

In analogy to the static case the density-response function on the Keldysh time contour $\chi_{S\sigma,\sigma}(\mathbf{r}, \tau; \mathbf{r}', \tau')$ can be calculated and one obtains

$$\begin{aligned} \chi_{S\sigma,\sigma}(\mathbf{r}, \tau; \mathbf{r}', \tau') &= -\frac{i}{\hbar} \sum_{j=1}^{\infty} \sum_{k=1}^{\infty} f_j \theta(\tau - \tau') \varphi_{j\sigma}^*(\mathbf{r}, \tau) \varphi_{j\sigma}(\mathbf{r}', \tau') \varphi_{k\sigma}(\mathbf{r}, \tau) \varphi_{k\sigma}^*(\mathbf{r}', \tau') \\ &\quad + f_j \theta(\tau' - \tau) \varphi_{j\sigma}^*(\mathbf{r}', \tau') \varphi_{j\sigma}(\mathbf{r}, \tau) \varphi_{k\sigma}(\mathbf{r}', \tau') \varphi_{k\sigma}^*(\mathbf{r}, \tau) \end{aligned} \quad (\text{A.12})$$

with f_j being the occupation number of the j -th orbital. As expected this expression is symmetric on the Keldysh time contour. Nevertheless it becomes causal when transformed to physical time. In order to demonstrate this the density response in physical time due to a physical potential variation $\delta v_{S\sigma}(\mathbf{r}, t)$ is calculated. One obtains

$$\begin{aligned} \delta n_{\sigma}(\mathbf{r}, t) &= \int \int_C \chi_{S\sigma,\sigma}(\mathbf{r}, \tau; \mathbf{r}', \tau') \delta v_{S\sigma}(\mathbf{r}', \tau') dt' d^3r' \quad (\text{A.13}) \\ &= -\frac{i}{\hbar} \sum_{j=1}^{\infty} \sum_{k=1}^{\infty} \int \int_{\tau_{\text{F}}}^{\tau} f_j \varphi_{j\sigma}^*(\mathbf{r}, \tau) \varphi_{j\sigma}(\mathbf{r}', \tau') \varphi_{k\sigma}(\mathbf{r}, \tau) \varphi_{k\sigma}^*(\mathbf{r}', \tau') \delta v_{S\sigma}(\mathbf{r}', \tau') t'(\tau') d\tau' \\ &\quad + \int_{\tau}^{\tau_{\text{F}}} f_j \varphi_{j\sigma}^*(\mathbf{r}', \tau') \varphi_{j\sigma}(\mathbf{r}, \tau) \varphi_{k\sigma}(\mathbf{r}', \tau') \varphi_{k\sigma}^*(\mathbf{r}, \tau) \delta v_{S\sigma}(\mathbf{r}', \tau') t'(\tau') d\tau' d^3r' \\ &= -\frac{i}{\hbar} \sum_{j=1}^{\infty} \sum_{k=1}^{\infty} \int \int_{t_0}^t f_j \varphi_{j\sigma}^*(\mathbf{r}, t) \varphi_{j\sigma}(\mathbf{r}', t') \varphi_{k\sigma}(\mathbf{r}, t) \varphi_{k\sigma}^*(\mathbf{r}', t') \delta v_{S\sigma}(\mathbf{r}', t') dt' \\ &\quad - \int_{\tau_{\text{F}}}^{\tau} f_j \varphi_{j\sigma}^*(\mathbf{r}', \tau') \varphi_{j\sigma}(\mathbf{r}, \tau) \varphi_{k\sigma}(\mathbf{r}', \tau') \varphi_{k\sigma}^*(\mathbf{r}, \tau) \delta v_{S\sigma}(\mathbf{r}', \tau') t'(\tau') d\tau' d^3r'. \end{aligned}$$

Since the physical potential $\delta v_{S\sigma}(\mathbf{r}, t)$ is equal on the forward and backward time branch, the second integral reduces to

$$\begin{aligned} \int \int_{\tau_{\text{F}}}^{\tau} f_j \varphi_{j\sigma}^*(\mathbf{r}', \tau') \varphi_{j\sigma}(\mathbf{r}, \tau) \varphi_{k\sigma}(\mathbf{r}', \tau') \varphi_{k\sigma}^*(\mathbf{r}, \tau) \delta v_{S\sigma}(\mathbf{r}', \tau') t'(\tau') d\tau' d^3r' &= \\ \int \int_{t_0}^t f_j \varphi_{j\sigma}^*(\mathbf{r}', t') \varphi_{j\sigma}(\mathbf{r}, t) \varphi_{k\sigma}(\mathbf{r}', t') \varphi_{k\sigma}^*(\mathbf{r}, t) \delta v_{S\sigma}(\mathbf{r}', t') dt' d^3r'. \end{aligned} \quad (\text{A.14})$$

For exchange-correlation functionals which depend on occupied and unoccupied orbitals¹ Eq. (4.21) is replaced by

$$\begin{aligned} \int \int_C \chi_{S\sigma,\sigma}(\mathbf{r}, \tau; \mathbf{r}', \tau') v_{\text{xc}\sigma}(\mathbf{r}', \tau') dt' d^3r' &= \\ \sum_{j=1}^{\infty} \int \int_C \frac{\delta A_{\text{xc}}[\{\varphi_{i\tau}\}]}{\delta \varphi_{j\sigma}(\mathbf{r}', \tau')} \frac{\delta \varphi_{j\sigma}(\mathbf{r}', \tau')}{\delta v_{S\sigma}(\mathbf{r}, \tau)} + c.c. dt' d^3r'. \end{aligned} \quad (\text{A.15})$$

¹Such functionals are typically obtained from higher orders in the perturbation expansion of v_{xc} or A_{xc} , see, e.g., Ref. [Gör97]

Inserting Eq. (A.12) and Eq. (A.10) into Eq. (A.15), one obtains after a transformation to physical time

$$\begin{aligned} & \sum_{j=1}^{\infty} \frac{i}{\hbar} \int \int (f_j v_{xc\sigma}(\mathbf{r}', t') - u_{xcj\sigma}(\mathbf{r}', t')) \varphi_{j\sigma}^*(\mathbf{r}', t') \varphi_{j\sigma}(\mathbf{r}, t) \\ & \times \sum_{k=1}^{\infty} \varphi_{k\sigma}^*(\mathbf{r}, t) \varphi_{k\sigma}(\mathbf{r}', t') \theta(t - t') dt' d^3r' + c.c. = 0 \quad (\text{A.16}) \end{aligned}$$

with

$$u_{xcj\sigma}(\mathbf{r}, t) = \frac{1}{\varphi_{j\sigma}^*(\mathbf{r}, t)} \left. \frac{\delta A_{xc}[\{\varphi_{i\tau}\}]}{\delta \varphi_{j\sigma}(\mathbf{r}, \tau)} \right|_{\varphi_{i\tau} = \varphi_{i\tau}(\mathbf{r}, t)}. \quad (\text{A.17})$$

This is the time-dependent optimized effective potential (OEP) equation for the exchange-correlation potential. For exchange-correlation action functionals which depend only on occupied orbitals, e.g., the exact-exchange functional, Eq. (A.16) reduces to the well-known expression (4.22).

Appendix B

The xc potential in terms of the orbitals and orbital shifts

In this appendix the expression for the exchange-correlation potential in terms of the orbitals and orbital shifts, Eq. (4.31), is derived. Starting point are the time-dependent Kohn-Sham equations

$$i\hbar\partial_t \varphi_{j\sigma}(\mathbf{r}, t) = h_{S\sigma}(\mathbf{r}, t) \varphi_{j\sigma}(\mathbf{r}, t) , \quad (\text{B.1})$$

the equation-of-motion for the orbital shifts

$$(i\hbar\partial_t - h_{S\sigma}(\mathbf{r}, t)) \psi_{j\sigma}(\mathbf{r}, t) = (v_{xc\sigma}(\mathbf{r}, t) - u_{xcj\sigma}^*(\mathbf{r}, t) - (\bar{v}_{xcj\sigma}(t) - \bar{u}_{xcj\sigma}^*(t))) \varphi_{j\sigma}(\mathbf{r}, t) , \quad (\text{B.2})$$

and the OEP equation in terms of the orbitals and orbital shifts

$$\sum_{j=1}^{N_\sigma} \psi_{j\sigma}^*(\mathbf{r}, t) \varphi_{j\sigma}(\mathbf{r}, t) + c.c. = g(\mathbf{r}, t) . \quad (\text{B.3})$$

Multiplying Eq. (B.3) by $v_{xc\sigma}$ and using the time-dependent Kohn-Sham equations to replace $v_{xc\sigma}\varphi_{j\sigma}$, one obtains

$$\sum_{j=1}^{N_\sigma} \psi_{j\sigma}^*(\mathbf{r}, t) (i\hbar\partial_t + \frac{\hbar^2}{2m}\nabla^2 - v_H(\mathbf{r}, t) - v(\mathbf{r}, t)) \varphi_{j\sigma}(\mathbf{r}, t) + c.c. = v_{xc\sigma}(\mathbf{r}, t) g(\mathbf{r}, t) . \quad (\text{B.4})$$

Using the identity

$$\sum_{j=1}^{N_\sigma} \psi_{j\sigma}^*(\mathbf{r}, t) i\hbar\partial_t \varphi_{j\sigma}(\mathbf{r}, t) = \sum_{j=1}^{N_\sigma} i\hbar\partial_t (\psi_{j\sigma}^*(\mathbf{r}, t) \varphi_{j\sigma}(\mathbf{r}, t)) - \varphi_{j\sigma}(\mathbf{r}, t) i\hbar\partial_t \psi_{j\sigma}^*(\mathbf{r}, t) ,$$

one can transform Eq. (B.4) into

$$v_{xc\sigma}(\mathbf{r}, t) g(\mathbf{r}, t) - I(\mathbf{r}, t) = \sum_{j=1}^{N_\sigma} \psi_{j\sigma}^*(\mathbf{r}, t) \left(\frac{\hbar^2}{2m}\nabla^2 - v_H(\mathbf{r}, t) - v(\mathbf{r}, t) \right) \varphi_{j\sigma}(\mathbf{r}, t) - \varphi_{j\sigma}(\mathbf{r}, t) i\hbar\partial_t \psi_{j\sigma}^*(\mathbf{r}, t) + c.c. \quad (\text{B.5})$$

where

$$I(\mathbf{r}, t) := i\hbar\partial_t \sum_{j=1}^{N_\sigma} (\psi_{j\sigma}^*(\mathbf{r}, t) \varphi_{j\sigma}(\mathbf{r}, t) - c.c.) \quad (\text{B.6})$$

is used. Replacing $-i\hbar\partial_t \psi_{j\sigma}^*(\mathbf{r}, t)$ with the help of Eq. (B.2) leads to

$$\begin{aligned} v_{\text{xc}\sigma}(\mathbf{r}, t) g(\mathbf{r}, t) - I(\mathbf{r}, t) &= \sum_{j=1}^{N_\sigma} \psi_{j\sigma}^*(\mathbf{r}, t) \frac{\hbar^2}{2m} \nabla^2 \varphi_{j\sigma}(\mathbf{r}, t) \\ &\quad + \varphi_{j\sigma}(\mathbf{r}, t) \left(-\frac{\hbar^2}{2m} \nabla^2 + v_{\text{xc}\sigma}(\mathbf{r}, t) \right) \psi_{j\sigma}^*(\mathbf{r}, t) \\ &\quad + |\varphi_{j\sigma}(\mathbf{r}, t)|^2 (v_{\text{xc}\sigma}(\mathbf{r}, t) - u_{\text{xc}j\sigma}(\mathbf{r}, t) \\ &\quad \quad - (\bar{v}_{\text{xc}j\sigma}(t) - \bar{u}_{\text{xc}j\sigma}(t))) + c.c. \end{aligned} \quad (\text{B.7})$$

From Eq. (B.3) follows that

$$\sum_{j=1}^{N_\sigma} \varphi_{j\sigma}(\mathbf{r}, t) v_{\text{xc}\sigma}(\mathbf{r}, t) \psi_{j\sigma}^*(\mathbf{r}, t) + c.c. = v_{\text{xc}\sigma}(\mathbf{r}, t) g(\mathbf{r}, t) \quad (\text{B.8})$$

holds. Thus, Eq. (B.7) reduces to

$$\begin{aligned} -I(\mathbf{r}, t) &= \sum_{j=1}^{N_\sigma} \psi_{j\sigma}^*(\mathbf{r}, t) \frac{\hbar^2}{2m} \nabla^2 \varphi_{j\sigma}(\mathbf{r}, t) - \varphi_{j\sigma}(\mathbf{r}, t) \frac{\hbar^2}{2m} \nabla^2 \psi_{j\sigma}^*(\mathbf{r}, t) \\ &\quad + |\varphi_{j\sigma}(\mathbf{r}, t)|^2 (v_{\text{xc}\sigma}(\mathbf{r}, t) - u_{\text{xc}j\sigma}(\mathbf{r}, t) \\ &\quad \quad - (\bar{v}_{\text{xc}j\sigma}(t) - \bar{u}_{\text{xc}j\sigma}(t))) + c.c. \end{aligned} \quad (\text{B.9})$$

Using

$$\begin{aligned} \varphi_{j\sigma}(\mathbf{r}, t) \nabla^2 \psi_{j\sigma}^*(\mathbf{r}, t) &= \nabla^2 (\psi_{j\sigma}^*(\mathbf{r}, t) \varphi_{j\sigma}(\mathbf{r}, t)) - \psi_{j\sigma}^*(\mathbf{r}, t) \nabla^2 \varphi_{j\sigma}(\mathbf{r}, t) \\ &\quad - 2 (\nabla \psi_{j\sigma}^*(\mathbf{r}, t)) (\nabla \varphi_{j\sigma}(\mathbf{r}, t)) \end{aligned} \quad (\text{B.10})$$

and

$$\sum_{j=1}^{N_\sigma} \nabla^2 (\psi_{j\sigma}^*(\mathbf{r}, t) \varphi_{j\sigma}(\mathbf{r}, t) + c.c.) = \nabla^2 g(\mathbf{r}, t) \quad (\text{B.11})$$

in Eq. (B.9) leads to

$$\begin{aligned} \frac{\hbar^2}{2m} \nabla^2 g(\mathbf{r}, t) - I(\mathbf{r}, t) &= \sum_{j=1}^{N_\sigma} \psi_{j\sigma}^*(\mathbf{r}, t) \frac{\hbar^2}{m} \nabla^2 \varphi_{j\sigma}(\mathbf{r}, t) + \frac{\hbar^2}{m} (\nabla \psi_{j\sigma}^*(\mathbf{r}, t)) (\nabla \varphi_{j\sigma}(\mathbf{r}, t)) \\ &\quad + |\varphi_{j\sigma}(\mathbf{r}, t)|^2 (v_{\text{xc}\sigma}(\mathbf{r}, t) - u_{\text{xc}j\sigma}(\mathbf{r}, t) \\ &\quad \quad - (\bar{v}_{\text{xc}j\sigma}(t) - \bar{u}_{\text{xc}j\sigma}(t))) + c.c. \end{aligned} \quad (\text{B.12})$$

This equation can be solved for $v_{\text{xc}\sigma}(\mathbf{r}, t)$ and one obtains the desired result, Eq. (4.31).

Appendix C

Finite differencing scheme for the orbital shift's equation-of-motion

In this small appendix another finite differencing scheme is presented. It is based on the formal solution

$$\psi(\mathbf{r}, t) = U(t, t_0) \psi(\mathbf{r}, t_0) - \frac{i}{\hbar} \int_{t_0}^t U(t, t') r s(\mathbf{r}, t') dt' \quad (\text{C.1})$$

for the inhomogeneous Schrödinger equation

$$i\hbar\partial_t \psi(\mathbf{r}, t) = h_S(\mathbf{r}, t) \psi(\mathbf{r}, t) + r s(\mathbf{r}, t) \quad (\text{C.2})$$

In Eq. (C.1) the propagator $U(t, t_0)$ is given by

$$U(t, t_0) = \sum_{k=0}^{\infty} \frac{(-i\hbar)^k}{k!} \int_{t_0}^t \dots \int_{t_0}^t \mathcal{T}\{h_S(\mathbf{r}, t_1) \dots h_S(\mathbf{r}, t_k)\} dt_1 \dots dt_k . \quad (\text{C.3})$$

Approximating the integral in Eq. (C.1) by

$$\int_{t_0}^t U(t, t') r s(\mathbf{r}, t') dt' \approx \Delta t U(t, t_0) r s(\mathbf{r}, t_0) \quad (\text{C.4})$$

leads to

$$\psi(\mathbf{r}, t) \approx U(t, t_0) \left(\psi(\mathbf{r}, t_0) - \frac{i}{\hbar} \Delta t r s(\mathbf{r}, t_0) \right) \quad (\text{C.5})$$

Using the Crank-Nicolson approximation for $U(t, t_0)$ one obtains the equation

$$\left[1 + i \frac{\Delta t}{2} h_S(\mathbf{r}, t + \Delta t/2)/\hbar \right] \psi(\mathbf{r}, t + \Delta t) = \left[1 - i \frac{\Delta t}{2} h_S(\mathbf{r}, t + \Delta t/2)/\hbar \right] \tilde{r}s(\mathbf{r}, t) \quad (\text{C.6})$$

where $\tilde{r}s(\mathbf{r}, t)$ is given by

$$\tilde{r}s(\mathbf{r}, t) = \psi(\mathbf{r}, t) - \frac{i}{\hbar} \Delta t r s(\mathbf{r}, t) . \quad (\text{C.7})$$

For the Hamiltonian $h_S(\mathbf{r}, t + \Delta t/2)$ the same approximation is used as in the orbital propagation, i.e.,

$$h(\mathbf{r}, t + \Delta t/2) \approx \frac{1}{2}(h(\mathbf{r}, t + \Delta t) + h(\mathbf{r}, t)) . \quad (\text{C.8})$$

As a consequence, this algorithm guarantees that the orbital shifts are exactly orthogonal to the corresponding orbitals for any time step Δt .

Unfortunately, this algorithm also leads to instabilities. This observation in combination with the fact that the presented algorithm has already been used successfully to solve the inhomogeneous Schrödinger equation [Ser05] is a further indication the instabilities are not caused by the propagation algorithm used for the orbital shifts.

Bibliography

- [Ako00] J. Akola, M. Manninen, H. Häkkinen, U. Landman, X. Li, and L.-S. Wang, Phys. Rev. B **62**, 13216 (2000).
- [Alm85] C.-O. Almbladh and U. von Barth, Phys. Rev. B **31**, 3231 (1985).
- [Ame92] W. F. Ames, *Numerical Methods for Partial Differential Equations*, (Academic Press, San Diego, 1992).
- [And77] T. Ando, Z. Phys. B **26**, 263 (1977).
- [And04] K. Andrae, P.-G. Reinhard, and E. Suraud, Phys. Rev. Lett. **92**, 173402 (2004).
- [Aye00] P. W. Ayers, Proc. Natl. Acad. Sci. U.S.A. **97**, 1959 (2000).
- [Bac82] G. B. Bachelet, D. R. Hamann, and M. Schlüter, Phys. Rev. B **26**, 4199 (1982).
- [Bar72] U. von Barth and L. Hedin, J. Phys. C **5**, 1629 (1972).
- [Bar93] R. Barnett and U. Landman, Phys. Rev. B **48**, 2081 (1993).
- [Ba05a] U. von Barth, N. E. Dahlen, R. van Leeuwen, and G. Stefanucci, Phys. Rev. B **72**, 235109 (2005).
- [Ba05b] R. J. Bartlett, I. Grabowski, S. Hirata, and S. Ivanov, J. Chem. Phys. **122**, 034104 (2005).
- [Bec88] A. D. Becke, Phys. Rev. A **38**, 3098 (1988).
- [Bec92] A. D. Becke, J. Chem. Phys. **98**, 1372 (1992).
- [Bec97] A. D. Becke, J. Chem. Phys. **107**, 8554 (1997).
- [Ber04] N. Bertram, Y. D. Kim, G. Ganteför, Q. Sun, P. Jena, J. Tamuliene, and G. Seifert, Chem. Phys. Lett. **396**, 341 (2004).
- [Byl95] D. M. Bylander and L. Kleinman, 1995, Phys. Rev. B **52**, 14566 (1995).
- [Blu92] V. Blum, G. Lauritsch, J. A. Maruhn, and P.-G. Reinhard, J. Comput. Phys. **100**, 364 (1992).

- [Bon89] V. Bonačić-Koutecký, P. Fantucci, and J. Koutecký, *J. Chem. Phys.* **91**, 3794 (1989).
- [Bon01] A. Facco Bonetti, E. Engel, R. N. Schmid, and R. M. Dreizler, *Phys. Rev. Lett.* **86**, 2241 (2001).
- [Cal00] F. Calvayrac, P.-G. Reinhard, E. Suraud, and C. A. Ullrich, *Phys. Rep.* **337**, 493 (2000).
- [Cas96] M. E. Casida, in *Recent Developments and Applications in Modern Density-Functional Theory*, edited by J. M. Seminario, (Elsevier, Amsterdam, 1996).
- [Ca04a] A. Castro, M. A. L. Marques, J. A. Alonso, G. F. Bertsch, and A. Rubio, *Eur. Phys. J. D* **28**, 211 (2004).
- [Ca04b] A. Castro, M. A. L. Marques, and A. Rubio, *J. Chem. Phys.* **121**, 3425 (2004).
- [Cep80] D. M. Ceperly and B. J. Alder, *Phys. Rev. Lett.* **45**, 566 (1980).
- [Cha98] B. Champagne, E. A. Perpète, S. J. A. van Gisbergen, E.-J. Baerends, J. G. Snijders, C. Soubra-Ghaoui, K. A. Robins, and B. Kirtman, *J. Chem. Phys.* **109**, 10489 (1998).
- [Ch01a] X. Chu and Shih-I Chu, *Phys. Rev. A* **63**, 023411 (2001).
- [Ch01b] X. Chu and Shih-I Chu, *Phys. Rev. A* **64**, 063404 (2001).
- [Cho02] D. P. Chong, O. V. Gritsenko, and E. J. Baerends, *J. Chem. Phys.* **116**, 1760 (2002).
- [Chu05] Shih-I Chu, *J. Chem. Phys.* **123**, 062207 (2005).
- [Coh99] C. Cohen-Tannoudji, B. Diu, and F. Laloë, *Quantenmechanik*, (Walter de Gruyter, Berlin, 1999).
- [Dan84] P. Danielewicz, *Ann. Phys. (N.Y.)* **152**, 239 (1984).
- [Del01] F. Della Sala and A. Görling, *J. Chem. Phys.* **115**, 5718 (2001).
- [Del02] F. Della Sala and A. Görling, *Phys. Rev. Lett.* **89**, 033003 (2002).
- [Dob94] J. F. Dobson, *Phys. Rev. Lett.* **73**, 2244 (1994).
- [Dre90] R. M. Dreizler and E. K. U. Gross, *Density Functional Theory*, (Springer, Berlin, 1990).
- [Ehr03] O. T. Ehrler, J. M. Weber, F. Furche, and M. M. Kappes, *Phys. Rev. Lett.* **91**, 113006 (2003).

- [Eng93] E. Engel and S. H. Vosko, *Phys. Rev. A* **47**, 2800 (1993).
- [Eng94] E. Engel and S. H. Vosko, *Phys. Rev. B* **50**, 10498 (1994).
- [Eng01] E. Engel, A. Hoock, R. N. Schmid, R. M. Dreizler, and N. Chetty, *Phys. Rev. B* **64**, 125111 (2001).
- [Fil97] C. Filippi, C. J. Umrigar, and X. Gonze, *J. Chem. Phys.* **107**, 9994 (1997).
- [Gav92] See, e.g., *Atoms in Intense Laser Fields*, edited by M. Gavrilu, (Academic Press, Boston, 1992).
- [Gis99] S. J. A. van Gisbergen, P. R. T. Schipper, O. V. Gritsenko, E. J. Baerends, J. G. Snijders, B. Champagne, and B. Kirtman, *Phys. Rev. Lett.* **83**, 694 (1999).
- [Gör93] A. Görling and M. Levy, *Phys. Rev. B* **47**, 13105 (1993).
- [Gör94] A. Görling and M. Levy, *Phys. Rev. A* **50**, 196 (1994).
- [Gör96] A. Görling, *Phys. Rev. A* **54**, 3912 (1996).
- [Gör97] A. Görling, *Phys. Rev. A* **55**, 2630 (1997).
- [Gör99] A. Görling, *Phys. Rev. Lett.* **83**, 5459 (1999).
- [Gra94] S. K. Gray, D. W. Noid, and B. G. Sumpter, *J. Chem. Phys.* **101**, 4062 (1994).
- [Gra00] T. Grabo, T. Kreibich, S. Kurth, and E. K. U. Gross, in *Strong Coulomb Correlation in Electronic Structure*, edited by V. Anisimov, (Gordon & Breach, Tokyo, 2000).
- [Gra02] I. Grabowski, S. Hirata, S. Ivanov, and R. J. Bartlett, *J. Chem. Phys.* **116**, 4415 (2002).
- [Gre97] A. Greenbaum, *Iterative Methods for Solving Linear Systems*, (SIAM, Philadelphia, 1997).
- [Gri00] O. V. Gritsenko, S. J. A. van Gisbergen, A. Görling, and E. J. Baerends, *J. Chem. Phys.* **113**, 8478 (2000).
- [Gro95] *Density Functional Theory*, Vol. 337 of *NATO Advanced Study Institute Series B: Physics*, edited by E. K. U. Gross and R. M. Dreizler (Plenum Press, New York, 1995).
- [Gro96] E. K. U. Gross, J. F. Dobson, and M. Petersilka, in *Density Functional Theory*, Vol. 181 of *Topics in Current Chemistry*, edited by R. F. Nalewajski (Springer, Berlin 1996).

- [Häk04] H. Häkkinen, M. Moseler, O. Kostko, N. Morgner, M. A. Hoffmann, and B. v. Issendorff, *Phys. Rev. Lett.* **93**, 093401 (2004).
- [Ham02] S. Hamel, M. E. Casida, and D. R. Salahub, *J. Chem. Phys.* **116**, 8276 (2002).
- [Hes99] P. Hessler, J. Park, and K. Burke, *Phys. Rev. Lett.* **82**, 378 (1999).
- [Hey05] J. van Heys, M. Lindenblatt, and E. Pehlke, *Phase Transit.* **78**, 773 (2005).
- [Hir01] S. Hirata, S. Ivanov, I. Grabowski, R. J. Bartlett, K. Burke, and J. Talman, *J. Chem. Phys.* **115**, 1635 (2001).
- [Hoh64] P. Hohenberg and W. Kohn, *Phys. Rev.* **136**, B864 (1964).
- [Iva99] S. Ivanov, S. Hirata, and R. J. Bartlett, *Phys. Rev. Lett.* **83**, 5455 (1999).
- [Jav88] J. Javanainen, J. H. Eberly, and Q. Su, *Phys. Rev. A* **38**, 3430 (1988).
- [Jel03] J. Jellinek and P. H. Acioli, *J. Chem. Phys.* **118**, 7783 (2003).
- [Jin94] X. Jing, N. Troullier, D. Dean, N. Binggeli, J. R. Chelikowsky, K. Wu, and Y. Saad, *Phys. Rev. B* **50**, 12234 (1994).
- [Kan94] D. R. Kanis, M. A. Ratner, and T. J. Marks, *Chem. Rev.* **94**, 195 (1994).
- [Kel65] L. V. Keldysh, *Sov. Phys. JETP* **20**, 1018 (1965).
- [Kha01] S. N. Khanna, M. Beltran, P. Jena, *Phys. Rev. B* **64** 235419 (2001).
- [Kie96] H. Kietzmann, J. Morenzin, P. S. Bechthold, G. Ganteför, W. Eberhardt, D. S. Yang, P. A. Hackett, R. Fournier, T. Pang, and C. F. Chen, *Phys. Rev. Lett.* **77**, 4528 (1996).
- [Kni84] W. D. Knight, K. Clemenger, W. A. de Heer, W. A. Saunders, M. Y. Chou, and M. L. Cohen, *Phys. Rev. Lett.* **52**, 2141 (1984).
- [Koh65] W. Kohn and L. J. Sham, *Phys. Rev.* **140**, A1133 (1965).
- [Koh99] W. Kohn, *Rev. Mod. Phys.* **71**, 1253 (1999).
- [Kör06] T. Körzdörfer, Diploma thesis, University of Bayreuth (2006).
- [Kos07] O. Kostko, B. Huber, M. Moseler, and B. von Issendorff, *Phys. Rev. Lett.* **98**, 043401 (2007).
- [Kot94] T. Kotani, *Phys. Rev. B* **50**, 14816 (1994).
- [Ko95a] T. Kotani, *Phys. Rev. Lett.* **74**, 2989 (1995).
- [Ko95b] T. Kotani and H. Akai, *Phys. Rev. B* **52**, 17153 (1995).

- [Kot96] T. Kotani and H. Akai, *Phys. Rev. B* **54**, 16502 (1996).
- [Kr92a] J. B. Krieger, Y. Li, and G. J. Iafrate, *Phys. Rev. A* **45**, 101 (1992).
- [Kr92b] J. B. Krieger, Y. Li, and G. J. Iafrate, *Phys. Rev. A* **46**, 5453 (1992).
- [Kro00] L. Kronik, I. Vasiliev, and J. R. Chelikowsky, *Phys. Rev. B* **62**, 9992 (2000).
- [Kro02] L. Kronik, R. Fromherz, E. Ko, G. Ganteför, and J. R. Chelikowsky, *Nat. Mater.* **1**, 49 (2002).
- [Kro06] L. Kronik, A. Makmal, M. L. Tiago, M. M. G. Alemany, M. Jain, X. Huang, Y. Saad, and J. R. Chelikowsky, *Phys. Stat. Sol. (b)* **243**, 1063 (2006).
- [Küm98] S. Kümmel, M. Brack, and P.-G. Reinhard, *Phys. Rev. B* **58**, R1774 (1998).
- [Kü00a] S. Kümmel, M. Brack, and P.-G. Reinhard, *Phys. Rev. B* **62**, 7602 (2000); **63**, 129902(E) (2001).
- [Kü00b] S. Kümmel, J. Akola, and M. Manninen, *Phys. Rev. Lett.* **84**, 3827 (2000).
- [Kü00c] S. Kümmel, Ph. D. thesis, University of Regensburg (2000).
- [Küm01] S. Kümmel, K. Andrae, and P.-G. Reinhard, *Appl. Phys. B* **73**, 293 (2001).
- [Kü03a] S. Kümmel and J. P. Perdew, *Phys. Rev. Lett.* **90**, 043004 (2003).
- [Kü03b] S. Kümmel and J. P. Perdew, *Phys. Rev. B* **68**, 035103 (2003).
- [Kü04a] S. Kümmel, L. Kronik, and J. P. Perdew, *Phys. Rev. Lett.* **93**, 213002 (2004).
- [Kü04b] S. Kümmel, *J. Comput. Phys.* **201**, 333 (2004).
- [Kun03] T. Kunert and R. Schmidt, *Eur. Phys. J. D* **25**, 15 (2003).
- [Lee88] C. Lee, W. Yang, and R. G. Parr, *Phys. Rev. B* **37**, 785 (1988).
- [Lee96] R. van Leeuwen, *Phys. Rev. Lett.* **76**, 3610 (1996).
- [Lee98] R. van Leeuwen, *Phys. Rev. Lett.* **80**, 1280 (1998).
- [Lee99] R. van Leeuwen, *Phys. Rev. Lett.* **82**, 3863 (1999).
- [Lee01] R. van Leeuwen, *Int. J. Mod. Phys. B* **15**, 1969 (2001).
- [Lee03] R. van Leeuwen, *Adv. Quantum Chem.* **43**, 25 (2003).
- [Lee05] R. van Leeuwen, N. E. Dahlen, G. Stefanucci, C.-O. Almbladh, and U. von Barth, LANL preprint cond-mat 0506130 (2005).
- [Lei05] M. Lein and S. Kümmel, *Phys. Rev. Lett.* **94**, 143003 (2005).

- [Lev79] M. Levy, Proc. Natl. Acad. Sci. U.S.A. **76**, 6062 (1979).
- [Lev84] M. Levy, J. P. Perdew, and V. Sahni, Phys. Rev. A **30**, 2745 (1984).
- [Li85] T. C. Li and P. Q. Tong, Phys. Rev. A **31**, 1950 (1985).
- [Li93] Y. Li, J. B. Krieger, and G. J. Iafrate, Phys. Rev. A **47**, 165 (1993).
- [Lou82] S. G. Louie, S. Froyen, and M. L. Cohen, Phys. Rev. B **26**, 1738 (1982).
- [Löw72] P.-O. Löwdin and P. K. Mukherjee, Chem. Phys. Lett. **14**, 1 (1972).
- [Ma02a] N. T. Maitra, K. Burke, and C. Woodward, Phys. Rev. Lett. **89**, 023002 (2002).
- [Ma02b] N. T. Maitra, K. Burke, H. Appel, E. K. U. Gross, and R. van Leeuwen, in *Reviews in Modern Quantum Chemistry: A celebration of the contributions of Robert Parr*, edited by K. D. Sen (World Scientific, Singapore 2002).
- [Mai04] N. T. Maitra, F. Zhang, R. J. Cave, and K. Burke, J. Chem. Phys. **120**, 5932 (2004).
- [Man04] K. Manninen, H. Häkkinen, and M. Manninen, Phys. Rev. A **70**, 023203 (2004).
- [Mar01] M. A. L. Marques, A. Castro, and A. Rubio, J. Chem. Phys. **115**, 3006 (2001).
- [Ma03a] M. A. L. Marques, X. Lopéz, D. Varsano, A. Castro, and A. Rubio, Phys. Rev. Lett. **90**, 258101 (2003).
- [Ma03b] M. A. L. Marques, A. Castro, G. F. Bertsch, and A. Rubio, Comput. Phys. Commun. **151**, 60 (2003).
- [Mer65] N. D. Mermin, Phys. Rev. **137**, A1441 (1965).
- [Mos01] M. Moseler, H. Häkkinen, and U. Landman, Phys. Rev. Lett. **87**, 053401 (2001).
- [Mos03] M. Moseler, B. Huber, H. Häkkinen, U. Landman, G. Wrigge, M. A. Hoffmann, and B. v. Issendorff, Phys. Rev. B **68**, 165413 (2003).
- [Mun05] M. Mundt and S. Kümmel, Phys. Rev. Lett. **95**, 203004 (2005).
- [Mu06a] M. Mundt and S. Kümmel, Phys. Rev. A **74**, 022511 (2006).
- [Mu06b] M. Mundt, S. Kümmel, B. Huber, and M. Moseler, Phys. Rev. B **73**, 205407 (2006).
- [Mu07a] M. Mundt, S. Kümmel, R. van Leeuwen, and P.-G. Reinhard, Phys. Rev. A **75**, 050501(R) (2007).
- [Mu07b] M. Mundt and S. Kümmel, Phys. Rev. B **76**, 035413 (2007).

- [Ngu04] H. S. Nguyen, A. D. Bandrauk, and C. A. Ullrich, *Phys. Rev. A* **69**, 063415 (2004).
- [OuY90] H. Ou-Yang and M. Levy, *Phys. Rev. Lett.* **65**, 1036 (1990), in particular above Eq. (24).
- [Per81] J. P. Perdew and A. Zunger, *Phys. Rev. B* **23**, 5048 (1981).
- [Pe82a] J. P. Perdew, R. G. Parr, M. Levy, and J. L. Balduz, *Phys. Rev. Lett.* **49**, 1691 (1982). The first half of the last sentence of the abstract should be qualified with the phrase ‘for open-shell systems’ [Pe85b].
- [Pe82b] J. P. Perdew and M. R. Norman, *Phys. Rev. B* **26**, 5445 (1982).
- [Per83] J. P. Perdew and M. Levy, *Phys. Rev. Lett.* **51**, 1884 (1983).
- [Pe85a] J. P. Perdew, *Phys. Rev. Lett.* **55**, 1665 (1985).
- [Pe85b] J. P. Perdew, in *Density Functional Methods in Physics*, Vol. 123 of *NATO Advanced Study Institute Series B: Physics*, edited by R. M. Dreizler and J. da Providencia (Plenum, New York, 1985).
- [Per92] J. P. Perdew, J. A. Chevary, S. H. Vosko, K. A. Jackson, M. R. Pederson, D. J. Singh, and C. Fiolhais, *Phys. Rev. B* **46**, 6671 (1992).
- [Per96] J. P. Perdew, K. Burke, and M. Ernzerhof, *Phys. Rev. Lett.* **77**, 3865 (1996).
- [Per97] J. P. Perdew and M. Levy, *Phys. Rev. B* **56**, 16021 (1997).
- [Per98] J. P. Perdew and S. Kurth, in *Density Functionals: Theory and Applications*, Vol. 500 of *Lecture Notes in Physics*, edited by D. P. Joubert (Springer, Berlin, 1998).
- [Pet96] M. Petersilka, U. J. Gossmann, and E. K. U. Gross, *Phys. Rev. Lett.* **76**, 1212 (1996).
- [Pet99] M. Petersilka and E. K. U. Gross, *Laser Phys.* **9**, 105 (1999).
- [Peu78] V. Peuckert, *J. Phys. C* **11**, 4945 (1978).
- [Phi59] J. C. Phillips and L. Kleinman, *Phys. Rev.* **116**, 287 (1959).
- [Poh03] A. R. Pohl, Ph. D. thesis, Friedrich-Alexander-Universität Erlangen-Nürnberg (2003).
- [Pre92] W. H. Press, S. A. Teukolsky, W. T. Vetterling, and B. P. Flannery, *Numerical Recipes in FORTRAN*, (Cambridge University Press, Cambridge, England, 1992).

- [Rei82] P.-G. Reinhard and R. Y. Cusson, Nucl. Phys. A **378**, 418 (1982).
- [Rei03] P.-G. Reinhard and E. Suraud, *Introduction to Cluster Dynamics*, (Wiley, Berlin, 2003).
- [Rei06] P.-G. Reinhard, P. D. Stevenson, D. Almeded, J. A. Maruhn, and M. R. Strayer, Phys. Rev. E **73**, 036709 (2006).
- [Run84] E. Runge and E. K. U. Gross, Phys. Rev. Lett. **52**, 997 (1984).
- [Saa96] U. Saalman and R. Schmidt, Z. Phys. D: At. Mol. Clusters **38**, 153 (1996).
- [Sch93] F. Schwabl, *Quantenmechanik*, (Springer, Berlin, 1993). The Heitler-London ansatz is used to estimate the ground-state energy of H₂. However, the generalization to the case of two different atoms is straightforward.
- [Ser05] I. Serban, J. Werschnik, and E. K. U. Gross, Phys. Rev. A **71**, 053810 (2005).
- [Sha53] R. T. Sharp and G. K. Horton, Phys. Rev. **90**, 317 (1953).
- [Sha80] R. Shankar, *Principles of Quantum Mechanics*, (Plenum Press, New York, 1980).
- [Sha93] V. R. Shaginyan, Phys. Rev. A **47**, 1507 (1993).
- [Sha83] L. J. Sham and M. Schlüter, Phys. Rev. Lett. **51**, 1888 (1983).
- [Stä97] M. Städele, J. A. Majewski, P. Vogl, and A. Görling, Phys. Rev. Lett. **79**, 2089 (1997).
- [Stä99] M. Städele, M. Moukara, J. A. Majewski, P. Vogl, and A. Görling, Phys. Rev. B **59**, 10031 (1999).
- [Sva90] A. Svane and O. Gunnarsson, Phys. Rev. Lett. **65**, 1148 (1990).
- [Tal76] J. D. Talman and W. F. Shadwick, Phys. Rev. A **14**, 36 (1976).
- [Ton98] X. M. Tong and Shih-I Chu, Phys. Rev. A **57**, 452 (1998).
- [Ton01] X. M. Tong and Shih-I Chu, Phys. Rev. A **64**, 013417 (2001).
- [Toz03] D. J Tozer, J. Chem. Phys. **119**, 12697 (2003).
- [Tro91] N. Troullier and J. L. Martins, Phys. Rev. B **43**, 1993 (1991).
- [Tve98] A. Tveito and R. Winther, *Introduction to Partial Differential Equations*, (Springer, New York, 1998).
- [Ull95] C. A. Ullrich, U. J. Gossmann, and E. K. U. Gross, Phys. Rev. Lett. **74**, 872 (1995).

- [Ull97] C. A. Ullrich, P.-G. Reinhard, and E. Suraud, *J. Phys. B* **30**, 5043 (1997).
- [UI98a] C. A. Ullrich, P.-G. Reinhard, and E. Suraud, *J. Phys. B* **31**, 1871 (1998).
- [UI98b] C. A. Ullrich, P.-G. Reinhard, and E. Suraud, *Phys. Rev. A* **57**, 1938 (1998).
- [Ull00] C. A. Ullrich, P.-G. Reinhard, and E. Suraud, *Phys. Rev. A* **62**, 053202 (2000).
- [Val80] S. M. Valone, *J. Chem. Phys.* **73**, 4653 (1980).
- [Vén01] V. Véniard, R. Taïeb, and A. Maquet, *Phys. Rev. A* **65**, 013202 (2001).
- [Vig95] G. Vignale, *Phys. Rev. Lett.* **74**, 3233 (1995).
- [Wri02] G. Wrigge, M. Astruc Hoffmann, and B. v. Issendorff, *Phys. Rev. A* **65**, 063201 (2002).
- [Yab96] K. Yabana and G. F. Bertsch, *Phys. Rev. B* **54**, 4484 (1996).
- [Yan02] W. Yang and Q. Wu, *Phys. Rev. Lett.* **89**, 143002 (2002).
- [Zah04] F. E. Zahariev and Y. A. Wang, *Phys. Rev. A* **70**, 042503 (2004).
- [Zan80] A. Zangwill and P. Soven, *Phys. Rev. A* **21**, 1561 (1980).

Publications

Publications in direct relation to this work:

1. *Derivative Discontinuities in Time-Dependent Density-Functional Theory*
M. Mundt and S. Kümmel, Phys. Rev. Lett. **95**, 203004 (2005).
2. *Zeitabhängige Dichtefunktionaltheorie und der elektrische Response molekularer Ketten*
M. Mundt and S. Kümmel, 26. EAS-Bericht (2005).
3. *Photoelectron spectra of sodium clusters: The problem of interpreting Kohn-Sham eigenvalues*
M. Mundt, S. Kümmel, B. Huber, and M. Moseler, Phys. Rev. B **73**, 205407 (2006).
4. *Optimized effective potential in real time: Problems and prospects in time-dependent density-functional theory*
M. Mundt and S. Kümmel, Phys. Rev. A **74**, 022511 (2006).
5. *Violation of the ‘Zero-Force Theorem’ in the time-dependent Krieger-Li-Iafrate approximation*
M. Mundt, S. Kümmel, R. van Leeuwen, and P.-G. Reinhard, Phys. Rev. A **75**, 050501(R) (2007).
6. *Photoelectron spectra of anionic sodium clusters from time-dependent density-functional theory in real-time*
M. Mundt and S. Kümmel, Phys. Rev. B **76**, 035413 (2007).

Other publications:

7. *Modeling Na clusters in Ar matrices*
F. Fehrer, M. Mundt, P.-G. Reinhard and E. Suraud, Ann. Phys. (Leipzig) **14**, 411 (2005).
8. *Electric response of molecular systems: the power of self-interaction corrected Kohn-Sham theory*
T. Körzdörfer, M. Mundt, and S. Kümmel, in preparation.
9. *Ionization dynamics and high-harmonic generation in time-dependent density-functional theory*
M. Mundt, in preparation.

Acknowledgment

- First and foremost, I would like to thank Dr. S. Kümmel for his continuous support, his patience, and for all discussions concerning physical and non-physical subjects. I have greatly benefitted from his physical understanding and knowledge.
- Dr. P.-G. Reinhard I would like to thank for encouraging me to join the group of Dr. S. Kümmel at the Max Planck Institute for the Physics of Complex Systems in Dresden. In addition, I would like to thank him for his continuous interest in my work and many useful discussions in this context.
- A big thank you to Dr. R. van Leeuwen for sharing his understanding of DFT with me. His comments and mails have influenced the present work considerably.
- The Max Planck Institute for the Physics of Complex Systems, in particular Dr. J.-M. Rost, I would like to thank for the kind hospitality.
- Many thanks to T. Körzdörfer for the nice time in the office. The physics discussions as well as the other discussions have always been a special pleasure.
- I would also like to thank the ‘Finite Systems’ group, in particular C. Ates, Dr. M. de Menech, C. Gnodtke, Dr. A. Kenfack, G. Makolies, Dr. T. Pattard, Dr. T. Pohl, Dr. U. Saalmann, and Dr. B. Zimmermann, for making the time in Dresden unforgettable.
- All members of the Physics Institute at the University of Bayreuth, in particular Dr. R. Armiento and M. Thiele, I would like to thank for many serious and many funny discussions about physics and other things.
- My parents, my sister, and my two brothers I would like to thank for all their support, understanding, and advice. I am deeply grateful to them for making this work possible.
- Finally, I would like to thank Francisca Waldinger for her advice, her encouraging words in harder times, and for putting many things into the right perspective. Her optimism has always been a great help. Without her this work would not be the same.

Erklärung

Hiermit erkläre ich, dass ich die vorliegende Arbeit nur unter Zuhilfenahme der angegebenen Quellen und keiner weiteren Hilfsmittel angefertigt habe. Die Arbeit wurde in gleicher oder ähnlicher Form keiner anderen Prüfungsbehörde zur Erlangung eines akademischen Grades vorgelegt. Desweiteren erkläre ich hiermit, dass ich bisher keinen Promotionsversuch unternommen habe.

Bayreuth, den 23. Mai 2007